Impact of ionizing radiation on human embryonic stem cells

Einfluss ionisierender Strahlung auf humane embryonale Stammzellen

Vom Fachbereich Biologie der Technischen Universität Darmstadt zur Erlangung des akademischen Grades eines Doctor rerum naturalium genehmigte Dissertation von Dipl.-Biol. Sabine Luft aus Darmstadt

1. Referent: Prof. Dr. Marco Durante
2. Referent: Prof. Dr. Paul G. Layer

Tag der Einreichung: 24.2.2015; Tag der mündlichen Prüfung: 30.6.2015; Darmstadt 2015; D 17

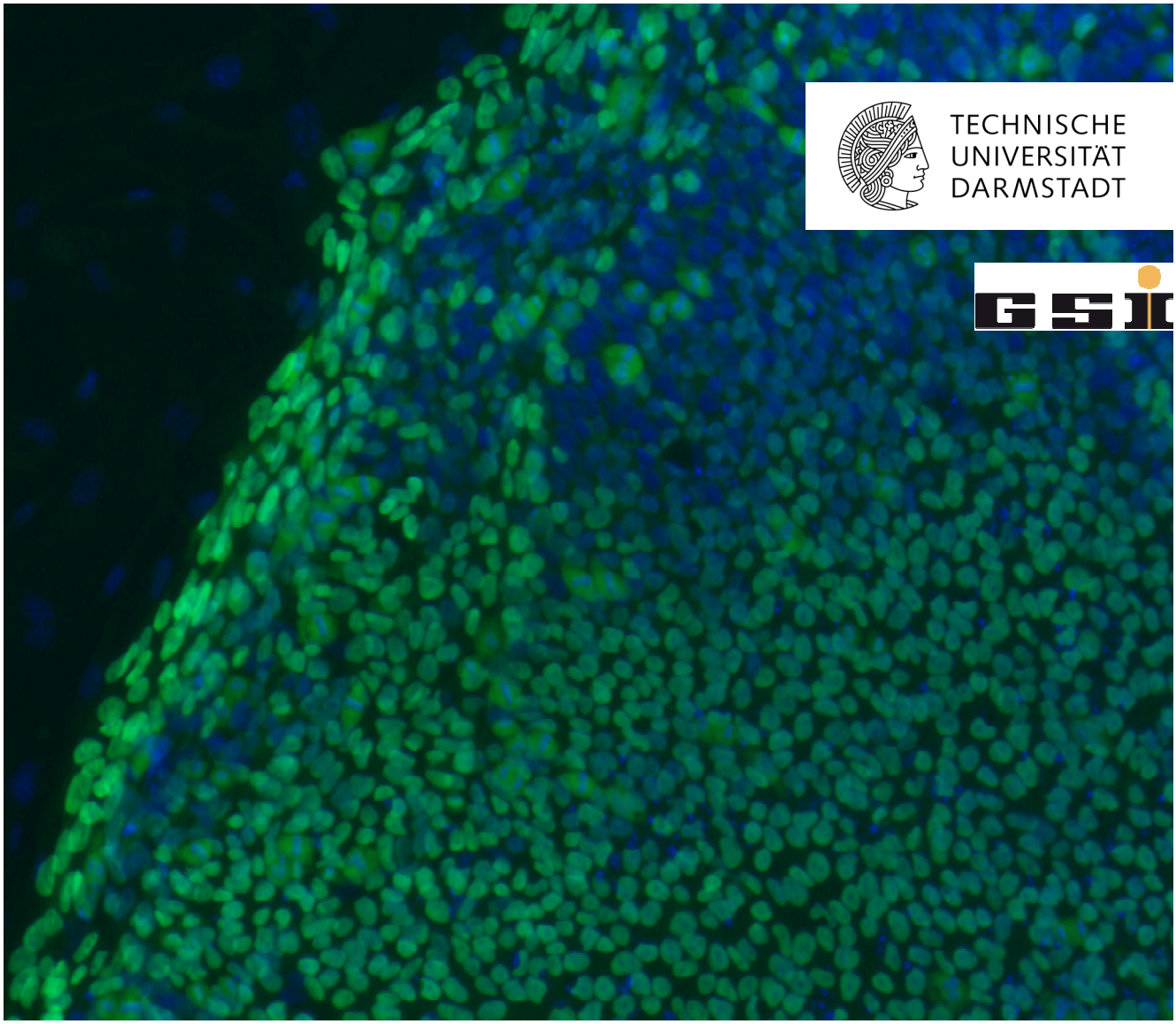

Impact of ionizing radiation on human embryonic stem cells
Einfluss ionisierender Strahlung auf humane embryonale Stammzellen

1. Referent: Prof. Dr. Marco Durante
2. Referent: Prof. Dr. Paul G. Layer

Darmstadt 2015
D 17

The picture on the title page shows an immunocytochemical labeling of the pluripotency marker OCT4A (Alexa Fluor®488, green) in hESCs (H9) counterstained with Hoechst 33 342 (blue).

Abstract

The radiosensitivity of the early developing human embryo is not well characterized. Radiation protection guidelines in case of an *in utero* exposure are mainly based on animal experiments and on epidemiological data. The mechanisms behind a radiation response of the embryo especially of high LET radiation is not completely understood. Therefore, there is a need to elucidate the effects of low and high LET ionizing radiation on early embryonic development. To contribute to a better understanding of this topic, H9 human embryonic stem cells were used as an *in vitro* tool to investigate the early blastocyst-like stage of the human embryonic development. As the latter give rise to an entire functional organism, maintaining their structural and genomic integrity is mandatory to avoid passing DNA damage on to the progeny. In the literature, it is reported that embryonic stem cells indeed exhibit a lower mutation frequency and that they show a higher apoptotic activity upon DNA damage, compared to differentiated somatic cells. A previous study on mouse embryonic stem cells performed at GSI indicates that even though eighth generation daughter cells still harbor chromosomal aberrations after exposure to high LET radiation, they are capable to maintain a pluripotent cell population.

This study elucidates the capacity of human embryonic stem cells to efficiently eliminate damaged cells upon ionizing radiation exposure and to proceed normally into endoderm differentiation. Thus, human embryonic stem cells were exposed to 1 and 3 Gy of X-rays, as well as to 1 Gy and 3 Gy of high LET radiation i.e. C, Ca, Ni and Ti ions. Human embryonic stem cells were observed up to 14 days after exposure in pluripotency maintaining culture conditions, and up to 11 days in conditions promoting differentiation into definitive endoderm. Endpoints such as cell cycle block, apoptosis, chromosomal aberrations, and gene expression related to embryonic signaling pathways and pluripotency as well as differentiation were investigated. It was found that isodoses of high LET radiation were more effective than X-rays in inducing apoptosis and chromosomal aberrations in human embryonic stem cells. After a radiation induced G2 block, a fraction of cells undergoes apoptosis. However, few stable chromosomal aberrations are still found in the progeny of exposed human embryonic stem cells. Gene expression studies of embryonic signaling pathways showed a majority of downregulated genes related to WNT, FGF, Hedgehog, TGFβ and Notch signaling pathways. These signaling alterations presumably cause the observed downregulation of core pluripotency markers like OCT4A and NANOG. Consequently, differentiation capability into definitive endoderm was impaired.

Together, the results reported in this work might indicate several consequences for the early embryo in case of an *in utero* exposure, like implantation failure due to cell cycle arrest and apoptosis, or malformations due to alterations in cell signaling and differentiation processes.

Zusammenfassung

Die Empfindlichkeit des frühen Embryos auf ionisierende Strahlung ist nicht ausreichend charakterisiert. Richtlinien des Strahlenschutzes bezüglich einer *in utero* Bestrahlung basieren hauptsächlich auf Tierexperimenten sowie epidemiologischen Studien. Die Mechanismen, die einer Strahlenantwort des Embryos zu Grunde liegen, sind besonders im Fall von Hoch-LET Strahlung nicht vollständig geklärt. Um zu einem besseren Verständnis über die Wirkung ionisierender Strahlung auf die frühe embryonale Entwicklung beizutragen, wurden H9 embryonale Stammzellen als *in vitro* Modell für das Blastozysten-Stadium des frühen Embryos eingesetzt. Da die embryonalen Stammzellen in diesem Entwicklungsstadium die Grundlage für einen vollständig funktionalen Organismus darstellen, und um zu verhindern, dass mögliche DNA Schäden an Tochterzellen weitergegeben werden, ist eine Aufrechterhaltung der genomischen Integrität notwendig. Tatsächlich wurde in der Literatur bereits eine geringere Mutationsrate in embryonalen Stammzellen sowie eine hohe Apoptoserate in Folge von DNA Schäden im Vergleich zu differenzierten Zellen beschrieben. In einer zuvor an der GSI durchgeführten Studie konnte beobachtet werden, dass Nachkommen von Hoch-LET bestrahlten embryonalen Stammzellen der Maus Chromosomenaberrationen aufweisen. Die Ergebnisse in Bezug auf das Pluripotenzstadium weisen aber darauf hin, dass die Zellen in der Lage sind, dieses aufrechtzuerhalten.

In dieser Arbeit wurde die Fähigkeit von humanen embryonalen Stammzellen untersucht, durch ionisierende Strahlung geschädigte Zellen von der pluripotenten Population zu entfernen um somit die Differenzierungseigenschaften in definitives Entoderm aufrechterhalten zu können. Dazu wurden Bestrahlungsexperimente mit 1 und 3 Gy Röntgenstrahlen, als auch mit 1 und 3 Gy Schwerionen-Strahlung (C, Ca, Ni und Ti Ionen) durchgeführt. Die Zellen wurden zum einen unter Pluripotenz-erhaltenden Bedingungen bis zu 14 Tage, als auch 11 Tage lang unter Bedingungen, die die Differenzierung in definitives Entoderm fördern, beobachtet. Dabei wurden Endpunkte wie Zellzyklus-Arrest, Apoptose, chromosomale Aberrationen und Genexpression in Bezug auf embryonale Signalwege, Pluripotenz und Differenzierung untersucht. Die Ergebnisse der Apoptose-Messung sowie der Untersuchung von chromosomalen Aberrationen zeigten eine höhere biologische Wirksamkeit von Hoch-LET im Vergleich zu Niedrig-LET Strahlung in humanen embryonalen Stammzellen. Es wurde zudem ein strahleninduzierter G2 Zellzyklus-Arrest beobachtet. Obwohl ein Teil der geschädigten Zellen in Apoptose ging, traten auch in den Tochterzellen noch chromosomale Aberrationen auf. Untersuchungen der Genexpression infolge von Bestrahlung zeigten eine Herabregulation von embryonalen Signalwegen wie WNT, FGF, Hedgehog, TGFβ und Notch, was vermutlich auch für die beobachtete Herabregulation der Expression von Pluripotenzmarkern wie OCT4A und NANOG verantwortlich ist. In der Folge war auch die Differenzierung zu definitivem Entoderm im Vergleich zu unbestrahlten Zellen beeinträchtigt.

Zusammenfassend weisen die Ergebnisse dieser Arbeit im Falle einer *in utero* Bestrahlung darauf hin, dass es auf Grund von Zellzyklus-Arrest und Apoptose zu einer Nidationsstörung und Frühabort kommen kann, und dass auf Grund von Veränderungen in Signalwegen und Differenzierungsprozessen Missbildungen möglich sind.

Contents

Abbreviations

a.u.	Arbitrary units
CT	Cycle threshold
d	Days
DAPI	4’,6-Diamidino-2-phenylindole
DDR	DNA damage response
DE	Definitive endoderm
DNA	Desoxyribonucelic acid
DSB	Double strand break
EdU	5-Ethynyl-2’-deoxyuridine
EMT	Epithelial-mesenchymal transition
FCS	Fetal calf serum
GSI	GSI Helmholtzzentrum für Schwerionenforschung GmbH
Gy	Gray
h	Hours
hESCs	Human embryonic stem cells
HR	Homologous recombination
ICM	Inner cell mass
ICRP	The International Commission on Radiological Protection
iPSCs	Induced pluripotent stem cells
IR	Ionizing radiation
LET	Linear energy transfer
MEF	Mouse embryonic fibroblasts
mFISH	Multicolor Fluorescence In Situ Hybridization
mRNA	Messenger ribonucleic acid
NCRP	National Council on Radiation Protection and Measurements
NHEJ	Non homologous end joining
PCR	Polymerase chain reaction
ROS	Reactive oxygen species
RBE	Relative biolgical effectiveness
RNA	Ribonucelic acid
RT	Room temperature
SD	Standard deviation
SOBP	Spread out Bragg peak
SSB	Singel strand breaks
StZG	Stammzellgesetz (stem cell act)
Sv	Sievert

1 Introduction

1.1 Human exposure to ionizing radiation

Human beings, like every other living organism on earth, are constantly exposed to ionizing radiation (IR) with a mean dose of 4 mSv/year (reviewed in [1]). This background radiation results from natural sources, e.g. cosmic radiation (0.3 mSv/year) or to a greater extend from the decay of inhalated radon gas (0.4 mSv/year), and from man-made sources that mainly comprise diagnostic and therapeutic medical procedures (1,9 mSv/year). Furthermore, accidents in atomic power plants or radio-terrorism could be conceivable scenarios, in which a person absorbs an additional dose of IR. These exposure scenarios can as well affect the unborn embryo (see also section 1.7), even though law and security guidelines restrict the medical and occupational exposure of an expectant mother. These laws and guidelines can only work effectively if the pregnancy is already noted. However, especially in the very early phase of gestation, the mother-to-be is often not yet aware of being pregnant. Possible scenarios of an *in utero* exposure comprise occupational exposures like pregnant aircraft personnel being exposed to cosmic radiation, diagnostic imaging techniques like computer assisted tomography (CT), or ion radiotherapy. The dose of a medical procedure using IR depends on many factors like the region of interest, the size of the patient, or the number of scans performed. The number of medical imaging procedures pregnant patients undergo has increased by 121 % from 1997 to 2006 [2]. For instance, for an abdominal CT scan an average dose of 10 mSv for the patient [3] and 25 mGy for the conceptus [4] is estimated. An example for a therapeutic exposure of a pregnant woman is reported in a case study about a patient who's skull-base chordoma was treated with carbon ion therapy at GSI, Darmstadt [5]. The patient got aware of the pregnancy after six fractions of a total treatment of 60 GyE (isoeffective photon dose) to the tumor in 20 fractions. Expecting a low dose to the uterus based on water phantom calculations, the treatment was continued. Additional active and passive dosimetry was used to monitor the dose received by the pelvis, revealing a total dose of 82 µSv. The dose in the uterus was estimated as <0.2 mSV. The child was born without any malformations and normal development was recorded up to the age of one year.

Besides the medical scenarios, a better understanding of the effect of IR on the embryonic development is also important for determining correct occupational dose limits for pregnant workers. In Germany, the dose limit for the embryo during the entire gestation period (from the moment when the women officially declares being pregnant to delivery) is 1 mSv according to §55 of the Radiation Protection Ordinance [6]. Risk estimates and dose limits are mainly derived based on epidemiological data from atomic bomb survivors, and often supported by animal studies. Consequences from IR exposure for the embryo range from deterministic effects (meaning an effect bearing a threshold dose) like embryonic death, congenital malformations, low birth weight, neurobehavioral effects to stochastic effects (no threshold dose) namely childhood cancer (see figure 1.1; reviewed in [2]). The risk of a certain consequence depends on the gestation period. The pre-implantation phase (up to two weeks post conception) is also known as the all-or-nothing-phase of gestation. In this early phase, the embryo either survives without any other defects or the exposure results in embryonic death depending on whether adjacent

cells are able to replace the IR affected cells or not. In this period, the threshold dose of 0.1 Gy for embryonic death is fairly low and increases with the duration of the pregnancy. During organogenesis (two to seven weeks), IR affected cells are not replaced as easily anymore as in earlier developmental periods. Therefore, the most likely results are congenital malformations and growth retardations with a threshold dose of 0.3 Gy. From week 8 to week 15, data from atomic bomb survivors being exposed *in utero* show that neurobehavioral effects occurring with a threshold dose of 0.3 Gy are the most frequent consequences in this developmental phase. These effects include microcephaly and a loss of approximately 30 points of IQ per Gy. Furthermore, a correlation between childhood cancer and *in utero* exposure exists, but the sensitivity during the gestation period is controversially discussed. For example, none of the atomic bomb survivors exposed *in utero* developed leukemia [7]. The recommendation of the NCRP [8] and the ICRP [9] state that there is no increased probability for non-cancerous effects below a dose of 0.05 Gy, which is below the dose of most diagnostic medical procedures.

Still, the effects of IR on the early embryonic development raise many questions related to the radiation risk, consequences of exposure and the underlying biological mechanisms, that also depend on the physical characteristics of IR (overview in [10] and [11]).

Figure 1.1: Consequences resulting from IR exposure *in utero*. Three dose ranges (<0.05 Gy, 0.05 to 0.5 Gy and >0.5 Gy) are evaluated over the three developmental periods, i.e. blastogenesis (also known as pre-implantation phase), organogenesis and fetogenesis. From [2].

	Embryonic/fetal developmental stage				
			Fetogenesis		
Acute radiation dose*	Blastogenesis (up to 2 weeks postconception)	Organogenesis (2 to 7 weeks postconception)	8 to 15 weeks postconception	16 to 25 weeks postconception	26 to 38 weeks postconception
< 0.05 Gy (5 rad)†	Noncancer health effects not detectable				
0.05 to 0.50 Gy (5 to 50 rad)	Incidence of failure to implant may increase slightly, but surviving embryos probably will not have substantial noncancer health effects	Incidence of major malformations may increase slightly; growth restriction possible	Growth restriction possible; IQ reduction possible (≤ 15 points)‡; incidence of severe mental retardation ≤ 20%‡	Noncancer health effects unlikely	
> 0.50 Gy§	Incidence of failure to implant is likely large‡‖, but surviving embryos probably will not have substantial noncancer health effects	Incidence of miscarriage may increase‡; substantial risk of major malformations (e.g., neurologic and motor deficiencies); growth restriction likely	Incidence of miscarriage probably will increase‡; growth restriction likely; IQ reduction (> 15 points)‡; incidence of severe mental retardation > 20%‡; incidence of major malformations probably will increase	Incidence of miscarriage may increase‡; growth restriction, IQ reduction, and severe mental retardation possible‡; incidence of major malformations may increase	Incidence of miscarriage and neonatal death may increase‡¶

*—Acute dose is delivered in a short time (usually minutes), whereas fractionated or chronic doses are delivered over time. The health effects to the fetus may differ for fractionated or chronic doses.

†—The gray (Gy) and the rad are units of absorbed dose and ref ect the amount of energy deposited into a mass of tissue. The absorbed dose is the dose received by the fetus (whole-body fetal dose). Absorbed dose levels are assumed to be from beta, gamma, or x-ray radiation. Neutron or proton radiation produces many of the health effects described at lower absorbed dose levels.

‡—Effect is dose dependent.

§—Pregnant women may experience acute radiation syndrome in this range, depending on the whole-body dose.

‖—A fetal dose of 1 Gy (100 rad) will likely kill 50% of embryos. The dose necessary to kill 100% of human embryos before 18 weeks' gestation is about 5 Gy (500 rad).

¶—For adults, the LD50/60 (i.e., the dose necessary to kill 50% of the exposed population in 60 days) is about 3 to 5 Gy (300 to 500 rad), and the LD100 (i.e., the dose necessary to kill 100% of the exposed population) is about 10 Gy (1,000 rad).

Adapted from Centers for Disease Control and Prevention. Radiation and pregnancy: a fact sheet for clinicians. http://www.bt.cdc.gov/radiation/prenatalphysician.asp. Accessed January 19, 2010.

1.2 Physical characteristics of ionizing radiation

Radiation is termed ionizing, if its energy exceeds the amount needed to eject a single electron from and therefore ionize a target atom. For accelerated particles, the energy exceeds this threshold (see also table 2.1 for energies used in this work). The dose (D) delivered by IR in a target is defined as the energy absorbed (ΔE) per mass unit (m) in Gray (Gy):

$$D = \frac{\Delta E}{m} \tag{1.1}$$

The absorbed dose multiplied with a radiation weighting factor (W_R) is defined as the radiation weighted dose or equivalent dose (H) in Sievert (Sv):

$$H = D \cdot W_R \tag{1.2}$$

A microscopic view on the process of dose deposition in the target reveals different ways of interaction of IR with matter. X-rays and γ-rays are called sparsely IR. They interact mainly via Compton and photoelectric processes. Particles like heavy ions are densely ionizing and mainly interact via Compton and nuclear interactions. Thus, the resulting dose distribution pattern of sparsely IR is rather homogeneous, while densely IR reveals a heterogeneous dose distribution pattern (see figure 1.2A). The shown pattern of carbon ions for instance exhibits local dose maxima and areas without any dose deposited. As a result, few cells might receive a fairly high dose, while other cells in the same target sample do not receive any dose at all. With increasing energy of the particle radiation, the number of local dose maxima (as well as the particle range, see figure 1.2B) increases. The different microscopic dose distribution patterns eventually lead to a different biological effect when comparing isodoses of different radiation qualities. For example, an exposure to 2 Gy carbon ions results in a much stronger biological effect than an exposure to 2 Gy X-rays. As a measure for this difference, the Relative Biological Effectiveness (RBE) is defined as the ratio of the dose of a reference exposure (D_{ref}) to the dose of a certain exposure (D_{test}) for the same effect, also expressed as:

$$RBE = \frac{D_{ref}}{D_{test}} \tag{1.3}$$

With increasing mass of the particle and with decreasing velocity, the number of ionization events along the particle track, and accordingly the energy deposited along the particle track increases. The energy transferred to the target (dE) per unit length of the track (dx) is defined as the linear energy transfer (LET):

$$LET = \frac{\mathrm{d}E}{\mathrm{d}x} \tag{1.4}$$

A macroscopic view of the interactions of IR is shown in figure 1.2B, where the dose deposition is illustrated as a function of the depth. The dose deposited by photons shows an initial maximum caused by the buildup effect, which then continuously declines with increasing depth. In contrast, particles show an inverted dose profile, meaning that its dose deposition is very low in the beginning and exhibits a sharp peak (also known as Bragg peak) near the end of its penetration depth. This is an important characteristic for heavy ion therapy, where the normal tissue surrounding a tumor is spared owing to the physical characteristics of particles resulting in the inverted dose profile. By changing the energy of the particles, the range of the particles can be adapted to a certain position in the tissue.

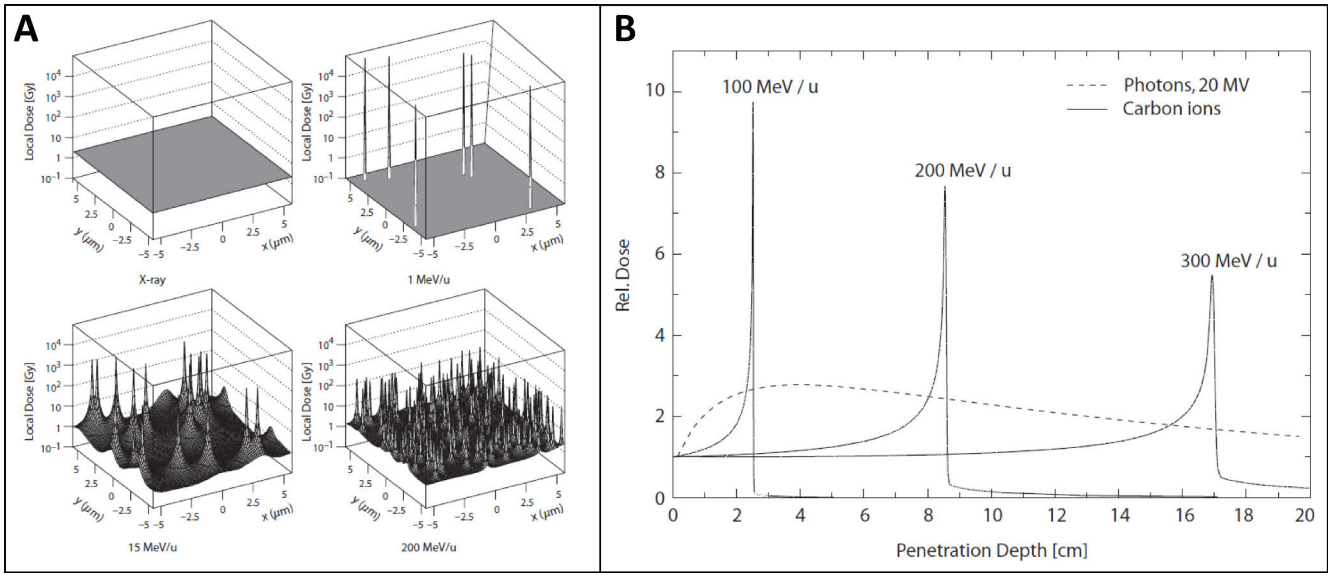

Figure 1.2: A: Dose deposition pattern of sparsely ionizing X-rays (upper left panel) and of densely ionizing particle radiation with three different energies, ranging from 1 MeV/u (upper right panel) to 15 MeV/u (lower left panel) and 200 MeV/u (lower right panel). While X-rays deposit a homogeneous dose in the target, densely ionizing particles show a heterogeneous dose deposition pattern with local dose maxima. The higher the energy of the particle, the lower the local dose of a single dose maximum (corresponding to the height of a local dose peak). Consequently, more local dose maxima with a lower local dose in case of 200 MeV/u result in the same total dose of 2 Gy as do fewer local dose maxima with higher local dose in case of 15 MeV/u. B: Depth dose profile of sparsely ionizing photons and of densely ionizing carbon ions with three different energies (100 MeV/u, 200 MeV/u and 300 MeV/u). While the dose of photons first exhibits a buildup region and then continuously decreases with depth, the dose of particle radiation shows the typical Bragg peak, describing a dose peak at a certain penetration depth that depends on the energy of the particle. A and B both from [11].

1.3 DNA damage and its relation to the cell cycle

Revisiting the microscopic view, the most radiosensitive target in the cell is the DNA. It can be damaged directly or indirectly by IR (reviewed in [11]). For example, an atom in the DNA molecule can be directly hit and ionized, which most likely happens in case of high LET radiation. Low LET IR is more likely to first hit another molecule like water, therefore producing a secondary electron (also known as delta electrons), which in turn hits the DNA. These events can lead to different types of DNA damage such as single strand breaks (SSBs) or double strand breaks (DSBs). SSBs can be repaired more easily, while the consequences of DSBs are more severe. In case of high LET IR, clustered DSBs and SSBs occur more likely compared to low LET IR due to the high local ionization density. This complex DNA damage is even more difficult to repair, and can lead to cell death, mutations and genetic instability.
Not only the radiosensitivity but also the resulting consequences of radiation induced DSBs are directly connected with the cell cycle phases [12]. Normally, the cell is cycling through a growing phase named G1, a DNA synthesis phase named S, and a second growing phase named G2 followed by mitosis (also known as M phase). Once the DNA damage is induced, the cell can arrest at different cell cycle checkpoints in order to repair the damage (for more details on the cell cycle in pluripotent stem cells, refer to section 1.5.3 and 1.5.4) before continuing with proliferation. Cells in S phase are the least radiosensitive ones due to the open chromatin structure during replication that is easily accessible for repair proteins, followed by cells in G1 phase. The most radiosensitive cell cycle phases are the G2 and the M phase, due to the double amount of the most sensitive target for radiation, the DNA, and due to its very compact state. Also, which DNA repair mechanism is chosen depends on cell cycle phases. In G1 phase, the error prone non-homologous end joining (NHEJ) is the most prominent repair mechanism, while in G2 phase, the homologous sister chromatid can be used to repair damage via the high fidelity homologous recombination (HR) in addition to NHEJ [13].

1.4 Chromosome aberrations

Depending on their severity, lesions are not necessarily repaired completely. Instead, DNA can be rejoined, stay unrejoined or even rejoin incorrectly. Different chromosome staining techniques were developed like G-banding, Giemsa staining, multicolor Fluorescence In Situ Hybridization (mFISH) etc. to detect such lesions and their resulting chromosome aberrations and each technique contains its advantages and disadvantages. They differ in the resolution of detectable chromosomal changes and in their potential of revealing different types of aberrations. For example, reciprocal translocations can be detected in mFISH, but not with Giemsa staining. The classification of mFISH stained chromosome and chromatid aberrations used in this study is based on the, even though much more complex, classifications defined by M. N. Cornforth [14]. Chromatid aberrations do result from breaks that are produced when already two sister chromatids are present like in G2 phase, while chromosome aberrations result from breaks induced when only one chromatid is present and the damage can be replicated, like in G1 phase. Based on the number of breaks induced, on the number of chromosomes involved, and on the type of rejoining (symmetrically or asymmetrically), one can define further classifications of aberrations (see figure 1.3). Transmissible aberrations like reciprocal translocations are considered to be potentially carcinogenic or lead to genomic instability. Non-transmissible aberrations like rings and dicentrics often lead to anaphase bridges during mitosis, and truncated chromosomes with acentric fragments lead to intolerable genetic loss. Complex aberrations are non-transmissible if they

comprise a ring or a dicentric. The spectrum of radiation induced aberrations depends on the radiation quality. For example, complex chromosome aberrations can be observed more likely in cells exposed to densely IR than exposed to sparsely IR due to their different microscopic dose distribution patterns. The quantity of radiation induced chromosome aberrations depends on the absorbed dose in a linear-quadratic manner, as well as on the radiation quality. Therefore, chromosome aberrations such as easily detectable dicentrics are often used for biological dosimetry [15].

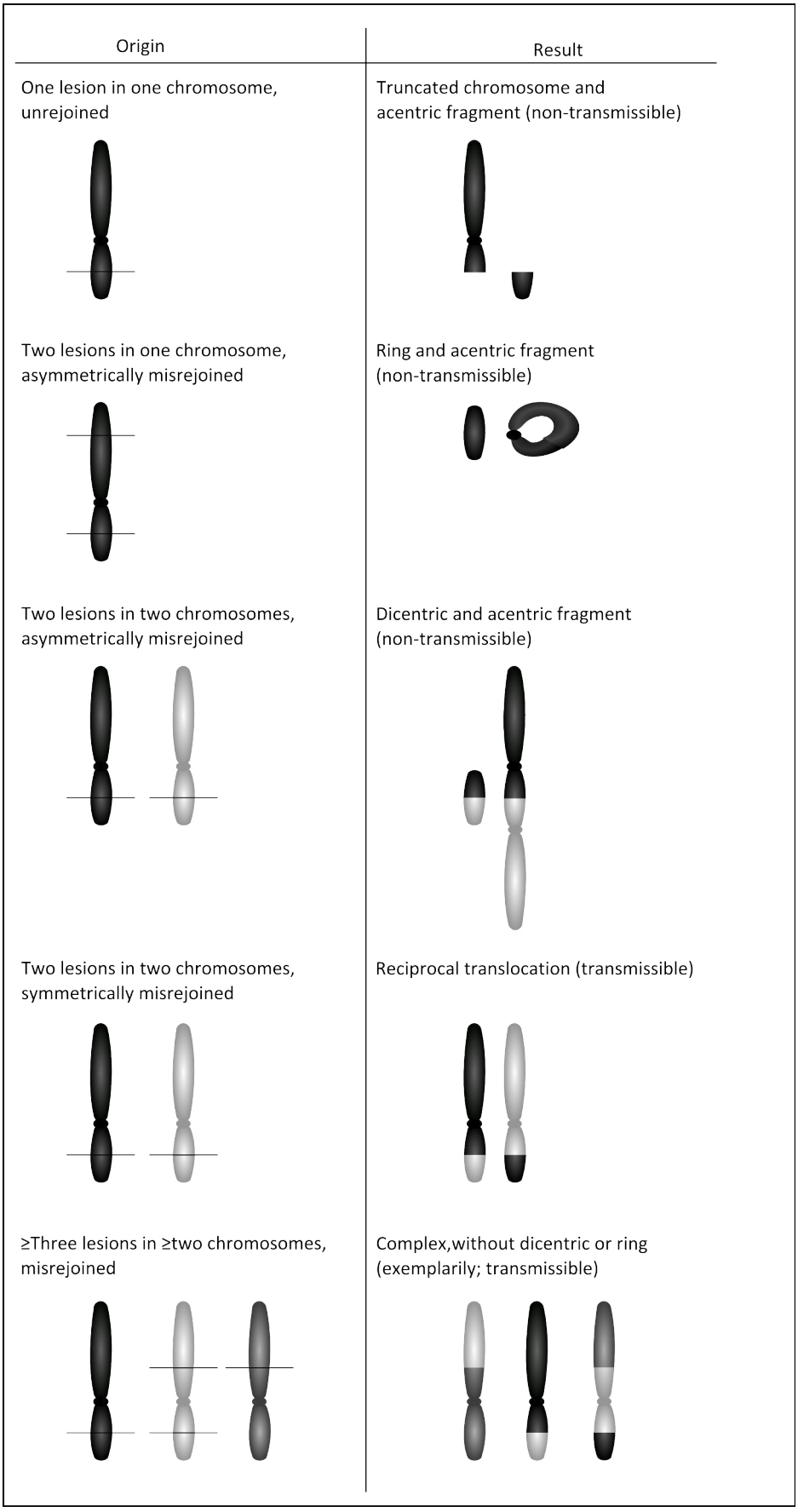

Figure 1.3: Classification of chromosome aberrations, showing the origin of DNA lesions with lines indicating the lesion, and the involved chromosomes (left) as well as the resulting aberrations (right).

1.5 Stem cells

The term “stem cells” first appeared in scientific literature in 1886. It was the German scientist Ernst Haeckel who used this term to describe a fertilized egg from which the three germ layers originate [16, 17]. Only a few years after, A. Weismann published his work in which he found that neither acquired characteristics can be inherited, nor are characteristics inherited by somatic cells, but by germ cells [18, 19]. At the same time, H. Driesch, a former student of Haeckel and Weismann, studied the embryonic development in sea urchins. He found that, when separated at the four-cell-stage, each single cell was able to develop an entire larvae. This finding was remarkable, because he expected that only the corresponding quarter of the larvae would develop. With this experiments, he found the concept of totipotency, the ability of a single cell to develop an entire organism. The first embryonic stem cells (ESCs) cultured *in vitro* were isolated from mouse blastocysts in 1981 by M. J. Evans (who won the Nobel Prize for Physiology and Medicine in 2007 [20]) and M. H. Kaufman [21], and in parallel by G. R. Martin [22]. Such cells are capable to form all cell types of the embryo. But as they lack the capacity to form tissue arising from the trophoblast, no living individual can develop from these cells, which are termed pluripotent (see also section 1.5.1). In 1998, James A. Thomson for the first time succeeded in deriving human embryonic stem cells (hESCs) and culturing them *in vitro* [23]. However, isolating hESCs requires the destruction of embryos, which in case of human embryos is a subject of ethical debate (see also section1.5.1). Therefore, it was an important step to resolve this issue when in 2007 Shinya Yamanaka published that it is possible to reprogram adult human fibroblasts into pluripotent cells [24]. Today we know that there are still important differences between these induced pluripotent stem cells (iPSCs) and ESCs like epigenetic background or genetic stability [25]. However, this finding was of tremendous importance, because it changed the dogma of unidirectional differentiation, and it provided the basis for investigating diseases in patient derived iPSC. Eventually, Yamanaka together with John B. Gurdon received the Nobel Prize in 2012 “for the discovery that mature cells can be reprogrammed to become pluripotent” [26].

Besides pluripotent stem cells, different levels of cell potency are known. The zygote for example is described as being totipotent, meaning that it can still generate a whole organism including all extraembryonic tissues needed for its complete development. An example for multipotent adult stem cells are hematopoietic stem cells. They are more restricted in their differentiation potential than pluripotent stem cells, since they can give rise only to a subgroup of cells, like the different blood cell types. A much lower level in cell potency can be described by unipotent cells, which are able to differentiate only into one cell type (reviewed in [27]).

1.5.1 Embryonic stem cells

The two main characteristics of ESCs are their potential to differentiate into every cell type of an organism also known as pluripotency, as well as their ability for infinite self-renewal. Thanks to these special traits, hESCs represent the most suited *in vitro* tool available to understand early mechanisms of human embryonic development [28]. hESCs are derived from the inner cell mass (ICM) of blastocysts. These are about five days old pre-implantation embryos that consist of an outer cell layer named trophoblast, which later will give rise to extraembryonic tissues, and the ICM from which the organism will originate (for more information on embryogenesis, see section 1.6). By isolating cells from the ICM and culturing them *in vitro*, hESC lines can be established. However, it is discussed in literature that hESCs isolated from the ICM are

considered primed pluripotent instead of naive pluripotent, since hESCs resemble more mouse epiblast stem cells than mouse ESCs [29]. It is suggested that from the isolation of the ICM to the establishment of the hESC cell line, the cells might continue some developmental steps and might thus more closely resemble the epiblast [30].
The fact that hESCs are derived from early human embryos automatically introduces ethical concerns. The potential implications of hESCs for regenerative medicine, toxicity testing, and studies of the early embryonic development etc, have to be weighted up against the inevitable destruction of the embryo during hESC derivation. In Germany, the Stem Cell Act of June 14, 2008 (StzG) [31] together with the Act for Protection of Embryos of October 23, 2001 (ESchG) [32] provide the legal basis for the research on hESCs. To prevent that human embryos are created for any other reason than reproduction, the act allows research on hESCs only in very limited cases. The research must be of high interest for basic research or for potential medical use and it must be justified that this research cannot be performed with any other means, for example mouse ESCs or iPSCs. Furthermore, it is only allowed to import hESCs, that are established before May 1, 2007. An application for the import and the use of hESCs has to be submitted to the Robert-Koch-Institute, that further asks the Central Ethics Commission on Stem Cell Research for its opinion and eventually approves or rejects the application. To date, 99 applications are granted for the scientific use of hESCs in Germany (www.rki.de/DE/Content/Gesund/Stammzellen/Register/register_node.html, as of January 2015).

1.5.2 Pluripotency network in hESCs

Our understanding of pluripotency is mainly based on studies in mouse ESCs. However, since pluripotency differs in its mechanisms between mouse and human ESCs [33], I want to emphasize that this section mainly deals with the mechanisms responsible for pluripotency in human ESCs as long as species-specific data is available. Pluripotency is established and maintained by a huge interactive network comprising many different players, for example embryonic signaling pathways that process mainly external signals, miRNAs inhibiting the translation of proteins involved in differentiation, chromatin structure and its remodeling factors, epigenetic modifications and the core transcription factors namely OCT4, NANOG and SOX2 (reviewed in [34]). All these many players not only act autonomously, but interact in a complex manner with each other. Additionally, many interactions, targets or effects are not yet elucidated, and those mechanisms investigated for a certain hESC line are not necessarily acting in the same manner in another hESC line. Thus, understanding the pluripotency network is still a challenging subject in ESC research. Due to the experimental focus of this work, the main signaling pathways like TGFβ signaling, FGF signaling, WNT signaling as well as the core transcription factors and their mechanisms will be explained in the following sections.

TGFβ signaling

Besides the TGFβ superfamily members like TGFβ, NODAL, GDFs and BMPs, Activin is the mostly used TGFβ receptor ligand to maintain the pluripotent state of hESCs *in vitro*. Binding of Activin (see figure 1.4A) leads to the formation of a heterotetramer composed of two type I and two type II serin/threonin kinase receptors. Downstream of the canonical Activin signaling, SMAD2 and SMAD3 are phosphorylated and then act together with SMAD4 as a transcription factor complex activating the expression of *NANOG*. At the same time, Activin signaling also leads to an inhibition of BMP4, which otherwise would activate SMAD1, SMAD5 and

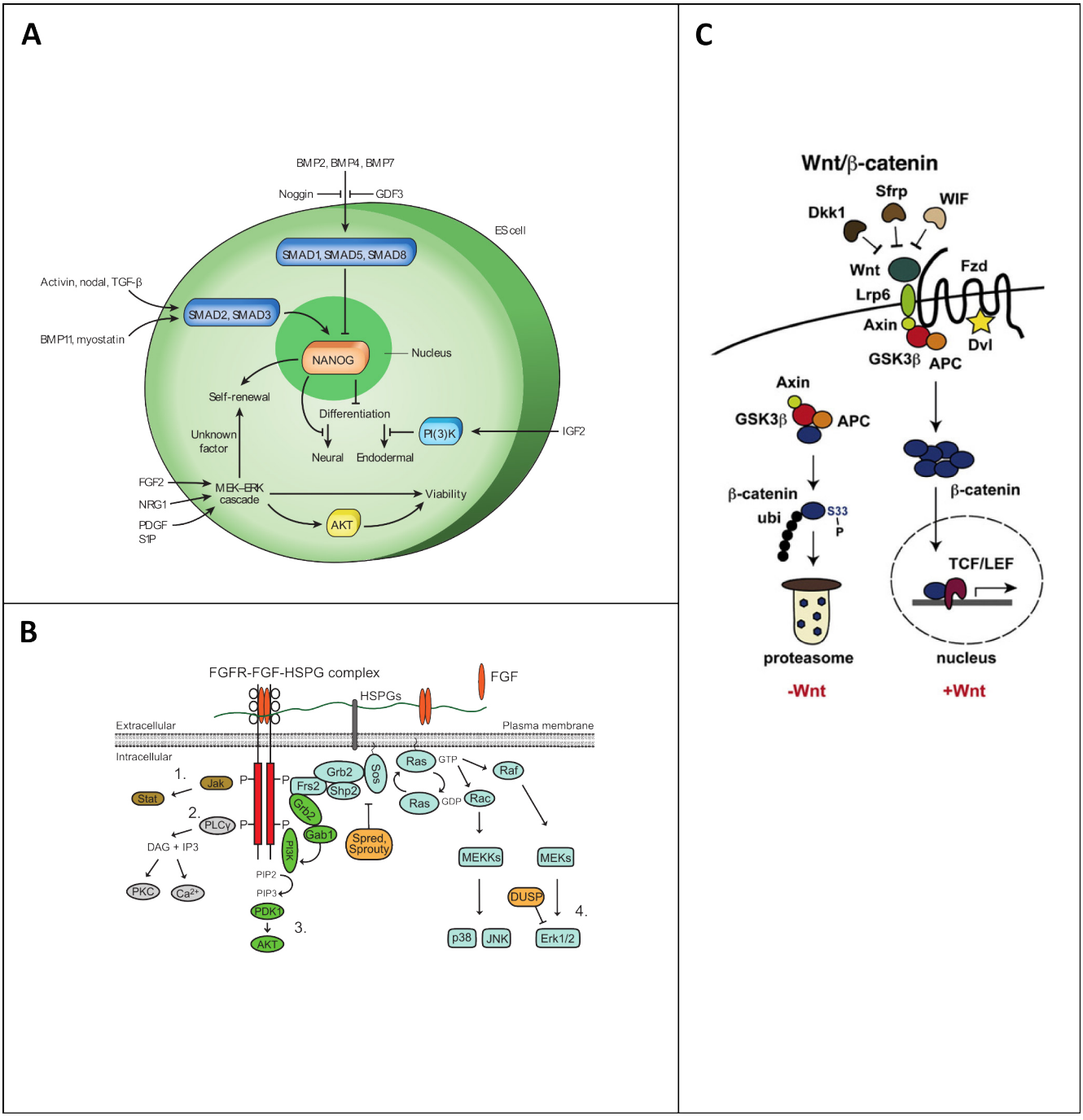

Figure 1.4: The pluripotency network as described in section 1.5.2 is composed of many interacting pathways. A shows the TGFβ signaling pathway adapted from [35], B shows the FGF signaling pathway with its four downstream pathways JAK/STAT, PLCγ, PI3K and the MEK/ERK from [36], and C shows the canonical WNT signaling pathway adapted from [37].

SMAD8 and therefore inhibit the expression of *NANOG*. In short, Activin signaling preserves the pluripotent state of the cell and simultaneously inhibits the expression of factors leading to differentiation (overview in [35, 38]). The effect of Activin on hESCs is concentration dependent. Lower concentrations of Activin, such as 5 to 10 ng/ml, are sufficient to maintain pluripotency [39]. In contrast, increasing the dose of Activin to 100 ng/ml in the culture medium induces differentiation into definitive endoderm [40, 41].

FGF signaling

Even though it is known that the main ligand of FGF signaling for the *in vitro* culture of hESCs, FGF2, plays a major role in the maintenance of pluripotency [42], the exact mechanisms are still not understood in detail. However, it is widely accepted that FGF2 acts via several intracellular and indirect extracellular mechanisms (see figure 1.4B). The latter comprises the induction of feeder cells secreting TGFβ and Activin A. These in turn lead to the activation of *NANOG* expression in hESCs via intracellular SMAD2/3 signaling. The direct intracellular mechanisms of FGF2 all require its binding to one of the four FGF receptor isoforms (FGFR1-4). For the binding, heparan sulfate proteoglycans are important due to their co-receptor function, but they are also necessary for the regulation of the FGF2 bio-availability. As a consequence, FGFRs dimerize and four possible downstream pathways can be activated. These comprise the JAK/STAT, PLCγ, PI3K and the MEK/ERK pathway [36]. Additionally, these downstream signaling pathways do also perform a complicate crosstalk among each other. However, the JAK/STAT pathway plays a bigger role for pluripotency in mouse than in human ESCs. The PLCγ pathway leads to the activation of protein kinase Cδ as well as to Ca^{2+} release from intracellular storages. The PI3K pathway leads to the inhibition of differentiation via Akt, as well as together with Activin/SMAD to a maintenance of pluripotency and self renewal [43, 44]. This pathway is also adressed by Knockout Serum Replacement [45], a common medium component in hESC culture. The most important MEK/ERK pathway acts via H-RAS and eventually leads to the activation of ERK2 and ELK1, which as transcription factors inhibit the expression of genes involved in differentiation and support pluripotency and self-renewal [46]. In addition to these four classical signaling pathways, it was also found that FGF2 has an anti-apoptotic function in which it prevents caspase-mediated anoikis, a subtype of apoptosis induced by the detachment of the cell from its extracellular matrix [47].

WNT signaling

WNT signaling (reviewed in [48, 37]) can occur via different pathways. Thus, this section will focus on the canonical WNT/β-catenin signaling pathway (see figure 1.4C). In the absence of the WNT ligand, β-catenin located in the cytosol of the hESC forms a complex with Axin, GSK3β and APC. β-catenin is then phosphorylated and polyubiquinated and can therefore be recognized to be degraded by proteasomes. In contrast, if WNT ligand is present, it interacts with its receptor Frizzled as well as the co-receptor LRP5/6 whereby three different pathways can be activated. These comprise WNT/JAK, WNT/Ca2+ and the canonical WNT/β-Catenin, the latter being described as the most important for hESC maintenance among the three pathways (see also figure 1.4C). Subsequently, the protein Dishevelled is phosphorylated and translocates to Frizelled, where LRP5/6 is phosphorylated by CK1 and GSK3β. Then, Axin is recruited by LRP5/6 disrupting the degradation of β-Catenin. As a consequence, β-Catenin accumulates in the cytoplasm and enters the nucleus where it can interact with members of the TCF/LEF family (LEF1, TCF1, TCF3 and TCF4), especially with TCF3. Consequently, the effect of TCF3 is

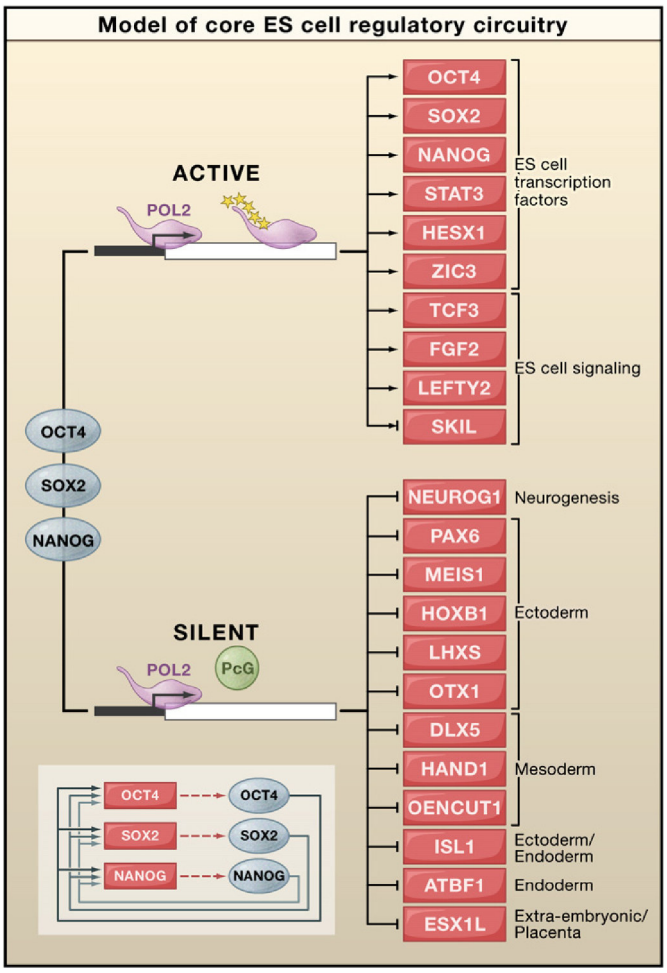

Figure 1.5: The core pluripotency transcription factors OCT4, SOX2 and NANOG can either activate or silence many target genes that either support pluripotency or differentiation, respectively. The lower left panel shows the autoregulatory feedback loop between OCT4, SOX2 and NANOG. For more details see section 1.5.2. From [27].

annihilated and its targets like *SOX2*, *NANOG* and *POU5F1* as well as many common targets of OCT4 are not repressed anymore. In short, β-Catenin is degraded in the absence of WNT, while it accumulates and then targets gene regulatory regions together with TCF3 in the presence of WNT. However, the effect of WNT signaling depends on the interplay with other extrinsic factors. In the presence of FGF2 and Activin, WNT signaling supports self-renewal, while in the absence of FGF2 and Activin, WNT signaling supports differentiation towards endo- and mesoderm [49].

Core pluripotency transcription factors: OCT4, SOX2 and NANOG

The main transcription factors associated with pluripotency like OCT4, SOX2, NANOG are known as core transcription factors of pluripotency (reviewed in [50–52]).

The Octamer binding transcription factor 4 (also known as OCT3, OCT4 or OCT3/4) belongs to the class V POU family of transcription factors and is encoded by the *POU5F1* gene. It consists of a POU-specific domain POU_S and a POU homeodomain POU_{HD} connected with a linker region, both of them operating as DNA-binding motives. In hESCs, three different isoforms of OCT4 are known, among which OCT4A is related to pluripotency, and OCT4B and OCT4B1 are related to cell stress response [53]. OCT4A does not only function as a transcription factor but also interacts with chromatin remodeling factors or factors involved in DNA replication and repair (reviewed in [50]).

NANOG, another homeobox domain protein, occurs in two isoforms. It consists of three domains being an N-terminal domain, a homeodomain and C-terminal domain, which is functionally the

most dominant. It can directly be bound and upregulated by SMAD2 and SMAD3 [54].
OCT4, NANOG and SOX2 (SRY (sex determining region Y)-box 2) are all highly conserved within their protein families, as well as evolutionary conserved in mammals. They are found in the pre-implantation embryo as well as in many cancers. They bind not only as a single transcription factor to many downstream target genes, but also act co-operatively as transcription factor complexes. In ChIP-Chip studies, Boyer and colleagues found that OCT4, NANOG and SOX2 occupied 404 genes simultaneously [55]. It is further known that the three factors not only regulate downstream targets, but form auto regulatory positive and negative feedback loops to regulate their own expressions (see figure 1.5). Furthermore, besides promoting the expression of genes that are important for the pluripotent state, they are also found to occupy genes that are important for differentiation, thus silencing them in cooperation with the repressive function of PcG proteins [50]. OCT4 for example was found to inhibit definitive endoderm differentiation. Already slight variations in their protein concentration can change their function from maintaining pluripotency and subsequently leading to differentiation. OCT4, NANOG and SOX2 also play an important role in reprogramming of somatic cells into iPSCs. Different approaches of cell reprogramming involve the increase of expression of various sets of genes. For example, Yamanaka and colleagues used the four transcription factors OCT4, SOX2, C-MYC, and KLF4, also known as the Yamanka factors, to reprogram mouse embryonic fibroblasts into induced pluripotent stem cells [56].

1.5.3 Unique properties of hESCs

Besides pluripotency and infinite self-renewal, hESCs possess additional properties in which they differ from adult somatic cells. All these properties comprise a network that ensures the maintenance of the pluripotent state and genomic integrity.

Anaerobic metabolism

In the pre-implantation embryo, no mitochondrial biogenesis takes place in the anyway hypoxic environment (1,5-9 % *in vivo* [57]), leading to a very low number of immature mitochondria [58]. Consequently, the main metabolic pathway used in hESCs is anaerobic glycolysis, which is independent of mitochondria, shifting towards oxidative phosphorylation when differentiating (reviewed in [59]). The low number of mitochondria implies a low production of reactive oxygen species (ROS), and additionally hESCs posses the capacity to remove ROS by high levels of antioxidant enzymes. Since ROS are known to induce endogenous DNA damage and enhance differentiation of ESCs, the metabolic characteristics of hESCs help to protect their genomic integrity and pluripotent state. hESCs also exhibit a high metabolism rate, which causes a high uptake rate of medium components and the need for daily medium exchanges in *in vitro* cell cultures.

Abbreviated cell cycle

hESCs cultured *in vitro* possess a relatively short cell cycle with a duration of approximately 16-20 h, of which 65 % are attributed to S phase and only 15 % each are attributed to the very short gap phases [60, 61]. The relatively long S phase implicates a long period that hESCs spend to replicate their DNA, making them more prone to replication-induced DSBs compared to differentiated somatic cells [62]. However, the duration of the cell cycle can vary by 25 % depending on the passage number [63]. The G1 phase is especially interesting in relation to pluripotency. That part of the cell cycle is characteristically short in ESCs compared to differ-

entiated somatic cells, due to mitogen-independent proliferation. The transition through the different cell cycle phases is controlled by a system of cyclin dependent kinases (CDKs) and cyclines. CDK2 plays a crucial role in G1/S- transition, and it has been shown that downregulation of CDK2, for example as a consequence of DNA damage, induces cell cycle arrest and apoptosis, interferes with DNA replication and repair, and leads to differentiation [64, 65]. CDKs and cyclins are also regulated by transcription factors like OCT4, SOX2 and NANOG, connecting the pluripotency network directly with cell cycle progression. The exact mechanisms behind the abbreviated G1 phase and its connection to pluripotency are not yet elucidated. However, reprogrammed iPSCs also show an abbreviated G1 phase, and differentiation of pluripotent cells is initiated in G1 phase [66]. A short G1 phase limits the time frame for receiving differentiation signals and therefore supports the pluripotency state [67].

Maintenance of genetic stability

Even though it is reported that early embryos in the cleavage state exhibit a high rate in aneuploidy and genome instability [68], *in vitro* cultured hESCs mostly reveal a normal diploid karyotype. Compared to differentiated somatic cells, ESCs even show a lower mutation frequency [69]. Studies that are reporting karyotypic abnormalities in hESCs are mostly related to culture conditions like enzymatic or manual passaging, the number of freezing cycles and the passage number, the media composition, the mouse embryonic fibroblast (MEF) feeder line as well as the oxygen pressure (reviewed in [70]). The biggest consensus in this highly debated field of karyotypic abnormalities is its correlation with culture conditions and passaging number. It is also the most likely factor given that most karyotypic alterations appear due to a growth advantage of a cell harboring a certain abnormality, that can overgrow the culture with time and increasing passage numbers.

A study by the International Stem Cell Initiative investigated genetic changes in hESC lines from world wide laboratories, and they found abnormal karyotypes in 34 % of the 125 cell lines investigated [61]. These aberrations mostly comprise gains of the total chromosomes or duplication of segments of 1, 12, 17, 20 (20q11.21 being the most prominent) or X [70], or losses of chromosome segments 10p13-pter, 18q21-qter and 22q13-qter. A significantly higher fraction of long-term cultures (33 %) showed karyotypic alterations in comparison to early passages (14 %). Also, they found a correlation of abnormal karyotypes and passaging technique, namely a significant higher fraction of karyotypic alterations in cells passaged enzymatically than in cells passaged manually. The reasons of specific, recurrent karyotypic alterations are not understood in detail. However, the loci of genes that might be responsible for a growth advantage were located among the set of chromosomes commonly observed as trisomies or duplicated segments. For example, a potential explanation for a correlation of a growth advantage and the gain of chromosome 20 is the location of genes for the BCL2L1, DNMT3B, ID1 [70] and miR-1825 on this particular chromosome in segment 20q11.21. The product of BCL2L1 has an anti-apoptotic function, DNMT3B is pluripotency-associated, the expression of ID1 is self-renewal promoting, and miR-1825 is discussed to potentially inhibit more than 400 targets that could be involved in suppression of apoptosis and in cell growth [71]. Furthermore, the gene for self-renewal promoting NANOG as well as its pseudogene *NANOGP1* that might act as competing miRNA targets is located on chromosome 12, giving a hint to explain the growth advantage in case of trisomy 12 or gain of chromosome 12 [61]. Noteworthy, hESC specific karyotypic alterations are also observed in cancer cells, raising the question whether hESCs might harbor a tumorigenic potential [71].

Facilitated cell death

To further protect their genome, hESCs are capable to undergo apoptosis more easily and rapidly than differentiated somatic cells [72]. A study performed by Dumitru and colleagues revealed a mechanism based on constitutively active BAX that is responsible for the facilitated apoptosis in hESCs [73]. In differentiated somatic cells, BAX exists in complex with KU70, which keeps it in its inactive form. Upon apoptotic stimuli, KU70 becomes acetylated, and BAX becomes activated, translocates into the mitochondria where it induces Cytochrome C release and consequently activation of Caspase cascades. In contrast, KU70 in hESCs is already acetylated under normal circumstances, and BAX is constitutively available in its active form. Upon apoptotic stimuli, it can easily translocate in a p53 dependent manner to the mitochondria [74]. Thus, apoptosis is induced much faster than in differentiated somatic cells. These findings are supported by a study of Liu and colleagues, in which they report that hESCs are in a mitochondrial primed state, which predisposes them to apoptosis [75]. More detailed, they found elevated mRNA levels of pro-apoptotic PUMA and lowered mRNA levels of the anti-apoptotic BCL2 in hESCs compared to differentiated somatic cells. Furthermore, Wang et al. found that adherent hESCs undergo a subtype of apoptosis, namely anoikis, to balance cell density in *in vitro* cultures [47]. Anoikis is a form of programmed cell death induced by detachment of the cell from its extracellular matrix [76].

1.5.4 Response of hESCs to IR: state of the art

IR induced DNA damage response (DDR) of hESCs has been investigated in the past years mainly with a focus on sparsely IR like X-rays and γ-rays [77–80].

Most studies investigating the influence of IR on cell cycle progression report that hESCs do not undergo a cell cycle checkpoint in G1 phase, but in G2 phase [79, 78, 66]. A G1/S checkpoint was only observed in few studies investigating the effect of non-ionizing radiation like ultraviolet C light [63, 65]. It is further shown that even though p21 mRNA is expressed in hESCs, functional p21 protein is not translated upon IR, presumably leading to a nonfunctional G1/S checkpoint [79]. Consequently, hESCs revealing DNA damage can easily progress into S phase, where the damage is amplified due to DNA replication, which might lead to apoptosis. This could be part of a suicide strategy, by which cells with DNA damage might undergo apoptosis more efficiently instead of risking any misrepair that might be propagated to the daughter cells [69].

hESCs also show special DNA repair characteristics compared to differentiated somatic cells (reviewed in [62]). On the one hand, they are more sensitive to DNA damage, but on the other hand they repair DNA damage with faster kinetics and more accurately [81]. This might at first seem counter intuitive, however this strategy enables hESCs to exclude damaged cells from the population by facilitated apoptosis and to maintain their genomic integrity efficiently. Going more into detail, hESCs exhibit an elevated level of proteins involved in DNA repair [82]. While differentiated somatic cells rely mainly on NHEJ as a DNA repair mechanism, hESCs exhibit an ATM dependent HR as their preferentially used repair pathway. Additionally, it was found that they also rely on NHEJ. However, this pathway might not necessarily resemble the classical error-prone NHEJ used by differentiated somatic cells. Instead, Adams and colleagues found that the NHEJ mechanism used in hESCs is independent of the typical cNHEJ protein DNA-PK, as well as of PARP and ATM, and that it shows high fidelity instead of error prone characteristics [83]. Another study by Bogomazova and colleagues revealed DNA-PK dependent NHEJ acting

in late G2 phase, leading to chromatid exchanges [84]. The different results of these studies show that there is still a need to elucidate the characteristic DDR of hESCs.

Massive cell death has been observed in hESC cultures using H9 cells exposed to sparsely IR. Based on Annexin-V assay, Wilson and colleagues found a dose-dependent decrease of viable cells 48 h after exposure to γ-rays, with a control level of 73 % viable cells that drops to 32 % after only 0.4 Gy, reaching a plateau of 5 % viable cells after 2 and 4 Gy, respectively. The exposure to 2 and 4 Gy resulted in holes and patchy regions in hESC colonies [80]. This patchy morphology of exposed hESC colonies has also been observed by Momcilovic and colleagues, who reported an increase in cleaved Caspase-3 positive cells at 4 h after 2 Gy of γ-radiation [78]. Sokolov and colleagues reported no effect for 0.2 Gy up to 65 h after γ-radiation. However, when they increased the dose to 1 Gy, viability dropped to 72 % at 65 h after exposure (compared to 86-94 % in controls) [85]. A study by Zou and colleagues report a loss of 99 % of living cells after 10 Gy X-rays already after 5-7 h [86]. However, drawing a common conclusion from these studies is difficult due to the different experimental approaches.

Studies on the effect of sparsely IR on alterations in gene expressions were mainly performed by the groups of Wilson [80] and Sokolov [77]. Wilson and colleagues used microarray analyses to investigate transcript levels of hESCs (H9) 48 h after 0.4, 2 and 4 Gy of γ-radiation. They report that VDR/retinoid X response (RXR) activation, p53 signaling, and aryl hydrocarbon signaling pathways as well as cancer, cell death, cell cycle, growth and proliferation, and embryonic development functions are mainly affected. They also observed a coclustering of gene expression patterns in the sham irradiated samples and in the samples exposed to 0.4 Gy, as well as a coclustering of the samples exposed to 2 and 4 Gy. Expression of pluripotency markers was not significantly different compared to unexposed samples. Sokolov and colleagues also used microarrays to investigate gene expression in exposed hESCs (H9). However they used a dose of 1 Gy γ-rays and analyzed the samples at earlier time points, namely 2 h and 16 h post irradiation. Just 2 h after exposure, they found only 30 genes that were upregulated, mainly involving p53 related and pro-apoptotic genes. 16 h after irradiation, they found 354 upregulated genes that were involved in pro-survival pathways. Their results concerning no differential expression of pluripotency markers after IR exposure is in accordance with the study by Wilson [85, 87]. However, Sokolov also found that there can be large variations in gene expression among different hESC lines [88]. This variability of IR response among hESC lines has to be kept in mind when interpreting results obtained with only one hESC line.

Non-targeted effects also known as bystander effects of IR have not been observed in hESCs [89]. After transferring conditioned medium from hESCs exposed to 10 Gy X-rays on unexposed hESCs, Sokolov and colleagues neither observed an increase in apoptotic cells nor a significant increase of radiation induced foci.

1.6 Early embryogenesis and *in vitro* differentiation towards definitive endoderm

hESCs are the closest *in vitro* model available for the early human embryogensis. In this work, hESCs themselves (resembling cells from the epiblast) as well as their development into definitive endoderm are investigated with respect to the influence of IR. An overview of the embryonic development described in this section is given in [90] (see also figure 1.6A). *In vivo*, the embryonic development starts with the fertilized egg, the totipotent zygote. While it migrates down the oviduct, it undergoes its first cell divisions called cleavages, during which the embryo does not increase in size. Unlike other species, these initial cell divisions occur asynchronously (rotational holoblastic) every 12 to 24 h and the embryo is independent of the maternal genome very

quickly (at the two cell stage in mice). After three to four days, the human conceptus reaches the 16-cell stadium and is now called morula. The morula undergoes a process called compaction, that prepares the embryo for the next developmental stage. During compaction, the cells form gap junctions and tight junctions that bind the former loose cell aggregate together to a more compact and tight array. The cells now start to secrete fluid inside the morula, creating a cavity that ensures proper nutrition of cells positioned inside the growing embryo, namely the ICM. The outer cell layer surrounding the blastocoel and the ICM is called the trophoblast. It will give rise to extraembryonic tissues like the chorion thus providing the fetal part of the placenta. At this stage, around five days after conception, the embryo is called a blastocyst. When arrived at the uterus, the embryo hatches from the zona pellucida, the membrane that prevented its implantation while migrating down the oviduct. It can now connect with the endometrium and implant in the uterus around day seven to day eight. While the blastocyst buries itself deeper into the endometrium, the ICM develops into a bilaminar embryo consisting of an upper cell layer, the epiblast, and a lower cell layer, the hypoblast also known as primitive endoderm. The cells of the latter are going to line the blastocoel below the hypoblast and form the inner lining of the yolk sac. Above the epiblast, the amnionic cavity develops. The epiblast itself will give rise to the actual organism. As a next hallmark of early embryogenesis, the gastrulation starts, characterized by massive cell migration and resulting in the formation of the three germ layers (definitive) endoderm, mesoderm and ectoderm. Between 14 and 16 days post conception, a structure forms at the posterior end of the epiblast called the primitive node and the primitive streak. Cells of the epiblast lose cell-cell contacts due to E-cadherin repression, undergo epithelial to mesenchymal transition (EMT), migrate anterior together with the expanding primitive streak and invade through the streak (also known as invagination). These cells displace the hypoblast and form the definitive endoderm (DE) that will give rise to the epithelial lining of the primitive gut tube that is the origin of the gastrointestinal tract, liver, pancreas and other associated visceral organs. Before going more into detail concerning the development of endoderm (overview in [91]), the classification of the various terms of endoderm will be explained. Besides the endoderm of the actual organism namely the DE, several extraembryonic endodermal tissues exist. The hypoblast is equivalent to the primitive endoderm, the lower part of the bilayered embryo in the blastocyst. A proportion of the cells of the primitive endoderm differentiates into visceral endoderm, while another proportion undergoes EMT and differentiates into parietal endoderm. This work concentrates more on DE than on extraembryonic endoderm and I will therefore now focus on the DE. For further understanding of the endodermal development, we have to rely on studies that were performed mainly in the frog (Xenopus laevis), the chicken (Gallus gallus) and the mouse (Mus musculus). Even though many crucial steps in endoderm development are evolutionary conserved, one has to be careful when extrapolating the knowledge from one species to another. When migrating through the primitive streak, endoderm progenitors are exposed to temporally and spatially varying levels of signaling molecules from the adjacent tissue. These varying signals allow the endoderm progenitors to differentiate in a certain pattern aligned to the anterior posterior axis. The signals are mainly originating from two areas, the primitive node and the anterior visceral endoderm. In between the epiblast and endoderm stage, there is an intermediate cell type that expresses markers for both endo- and mesoderm. These cells are called mesendoderm and are located in the anterior primitive streak. The development of DE is mainly controlled by TGFβ signaling and canonical WNT signaling (see figure 1.6B), as well as by other factors like SOX17 etc. NODAL (a member from the TGFβ signaling pathway) expressed in the node is a crucial player in the DE development.

When translated as a protein precursor ProNodal, it can be cleaved and activated by Furin and PACE4, both secreted from the trophectoderm. NODAL can now act via different ways. It can stimulate WNT signaling in the anterior primitive streak via BMP4 signaling. WNT signaling acts on the promoter PEE, which promotes NODAL expression, therefore forming a positive feedback loop. Furthermore, NODAL can stimulate its own expression via the promoter ASE. Additionally, NODAL can stimulate the expression of Lefty2, which eventually inihibits NODAL, therefore forming a negative feedback loop. Eomesodermin expressed in the trophectoderm is also discussed to participate in a feedback loop of NODAL. The expression of NODAL in the node eventually creates a protein gradient that leads in case of high levels to endoderm formation and in case of lower levels to mesoderm formation. Besides NODAL, GDF1 and GDF3 are also expressed in the node. They can interact with NODAL and increase its activity in a way that enables long-range signaling of NODAL [92]. Not only NODAL, but also the expression of SOX17 seems to be dependent on canonical WNT signaling [93], and SOX17 itself plays an important role in DE development. It has been shown in mice that SOX17-null mutant embryos are deficient in developing a DE lining of the embryonic gut [94]. The authors conclude that SOX17 is important for the maintenance of endoderm as well as for further endodermal cell fate decisions. However, the mechanism governed by SOX17 is not yet revealed.
Despite this complex signaling network, it is possible to recapitulate the DE development *in vitro*. D'Amour and colleagues developed a protocol that leads to an efficient differentiation of hESCs into cells of the DE [40] (see also section 2.4). First of all, the pluripotent culture needs to be depleted of conditions that would maintain their pluripotency and prevent differentiation. Therefore, hESCs are adapted to feeder-free conditions on matrigel. Then, hESCs are cultured for 24 h in medium containing WNT3A and Activin A. As Activin A acts as a surrogate for NODAL, this conditions mimic the situation described in figure 1.6B. After these first 24 h, cells are incubated in medium including serum and Activin A. The serum inhibits PI3K signaling, which would otherwise prevent efficient DE differentiation [95]. Cells of the DE can already be observed three days after initiation of differentiation.

Figure 1.6: A: Early embryogenesis showing the fertilization of the zygote, the migration of the embryo down the oviduct, undergoing cleavages that lead to the morula and after compaction to the blasytocyst. After hatching from the zona pellucida, the blastocyst consisting of trophoblast (outer cell layer, yellow), epiblast (orange) and hypoblast (green) implants into the endometrium of the uterus. From [96]. B: Signaling network resulting in the development of DE. NODAL is regulated via positive and negative feedback loops including signals from cells of the trophectoderm and the anterior primitive streak. Cells migrating through the streak that are exposed to high concentrations and/or long exposure time of NODAL develop into endoderm, whereas exposure to lower concentrations and/or shorter duration leads to mesoderm development. From [91].

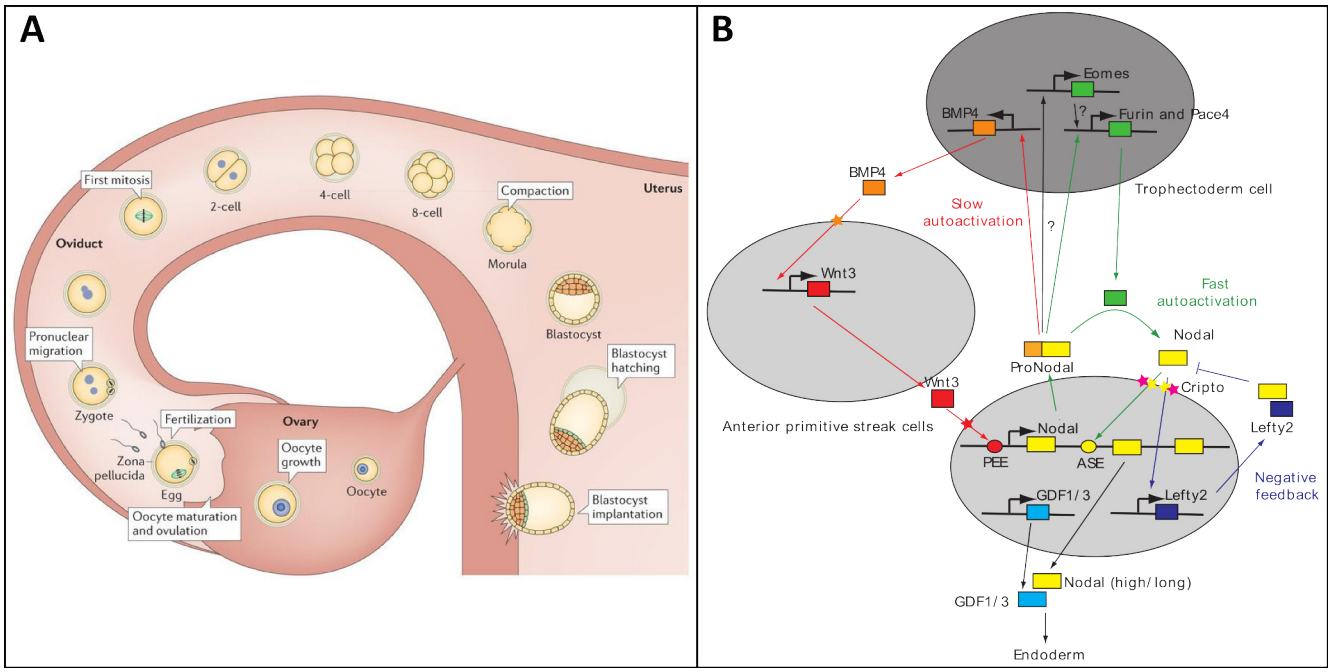

1.7 Motivation and objective

A need to further understand the effects of IR on the human embryonic development exists. As a model system, hESCs can be exploited to elucidate the mechanisms behind the effects of IR on the early human embryonic development, since they have the potential to recapitulate these early developmental processes *in vitro* [28]. As discussed in section 1.5.3, hESCs comprise unique properties to protect their genome in order to give rise to an intact and fully developed organism. Based on studies of Stambrook, Dumitru, Nagaria and colleagues [69, 73, 62], we hypothesize that hESCs exposed to IR exclude cells with induced DNA damage from the population either by facilitated apoptosis, or high fidelity DSB repair that leads to a low frequency of chromosome aberrations. As a consequence of these unique properties, hESCs surviving IR exposure should be able to maintain their pluripotency. This hypothesis is supported by our previous studies that revealed that mouse ESCs surviving the exposure to X-rays or C ions may carry chromosomal aberrations, however, they are still able to maintain pluripotency [97]. To test our hypothesis, hESCs were exposed to different radiation qualities in order to investigate their IR induced DNA damage response. The hESC line H9 was used to overcome species specific differences between mouse and human cells. Furthermore, H9 cells are frequently used in radiation investigating studies and this cell line is well characterized. Besides X-rays, the effect of high LET radiation like accelerated C, Ca, Ni and Ti ions was investigated. Since the physical interactions of these two radiation qualities with a target differ from each other (see 1.2), and only few studies on the effect of low LET radiation on early mammalian embryonic development were performed [98], it is of special interest to include high LET radiation in the investigations of this study. For this, it was taken advantage of the particular heavy ion accelerator facility available at GSI, Darmstadt. Doses of 1 to 3 Gy were applied. Since this is the first study at GSI investigating the radioresponse of hESCs, the labor-intensive cell culture itself as well as all methods had first to be established. In characterizing studies, the size of the cell nucleus and the cell cycle duration were measured. Various endpoints up to 14 days after exposure were analyzed. The cell cycle progression with a focus on cell cycle blocks was observed up to 7 days, and apoptosis based on cleaved Caspase-3 was observed in the first 48 h after exposure. Chromosome aberrations after mFISH were scored in surviving progeny up to 14 days after exposure. Alterations in cell potency based on pluripotency markers like OCT4 and SOX2 and underlying embryonic signaling pathways were analyzed over 48 h. Additionally, the differentiation potential into one of the three germ layers, DE, was investigated until day 11 after exposure, based on gene expression studies of the marker pair SOX17/SDF1.

2 Material and methods

2.1 Cell culture

hESCs being investigated in this work were co-cultured with mouse embryonic fibroblast (MEF) feeder cells. For the weekly passage, hESCs were either transferred enzymatically or manually into the new culture vessels. The medium composition changed depending on the passaging technique (H9-medium for enzymatic passage, see appendix table 4.2, and H9-medium for manual passage, see appendix table 4.3). Cells were incubated at 37°C with ambient oxygen and 5 % CO_2. For medium compositions, refer to appendix.

2.1.1 Human embryonic stem cells

Cells of the hESC line WA09 (H9) were obtained from WiCell Research Institute, Wisconsin, in passage number 26 and stored in liquid nitrogen. The import of hESCs (H9) as well as the utilization of the cells in this study was approved on June 21, 2011 and appended on August 8, 2013 by the Robert-Koch-Institute (approval entry number 65) in concordance with the German stem cell law (§11 StZG, [31]).

Thawing was performed according to WiCell protocols. Frozen hESCs were briefly thawed in a 37°C waterbath. Cell suspension was transferred into 9 ml H9-medium and centrifuged for 3 min at 200 g for washing. The cell pellet was carefully resuspended with MEF-conditioned medium not to break up the cell clumps into a single cell suspension. Cell clumps were plated on a preseeded MEF feeder layer in a 6-well plate, with a total of 2.5 ml MEF-conditioned medium (preparation see table2.1.3).

hESCs (H9) were passaged every six to eight days based on appearance, i.e. cell density (since overgrowing colonies start to differentiate) and morphology indicating spontaneous differentiation. For enzymatic passaging, cells were cultured in T25 culture flasks. Hence, medium was aspirated, 1 ml dispase (6 U/ml) was added and cells were incubated for 3 – 7 min at 37 °C. Detached colonies were resuspended and centrifuged for 3.5 min at 200 g. The pellet was resuspended and splitted 1:3 – 1:5 on either matrigel coated T25 culture flasks in MEF-conditioned medium or on a MEF feeder layer in new T25 culture flasks with H9-medium including 10 ng/ml FGF2.

For manual passaging, cells were grown in petri dishes (21.5 cm^2). Colonies to be passaged were chosen due to morphologic characteristics, microdissected with a scalpel under a microscope with a 100x magnification under an open laminar flow cabinet. Then, 15 dissected colonies were transferred into a new petri dish with either MEF feeder and >1 h pre-conditioned H9-medium including 10 ng/ml FGF2, or with a matrigel coated surface in MEF-conditioned medium (see section 2.1.3). The manual passaging is depicted in figure 2.1.

For the feeder-free culture on a matrigel coated surface, matrigel was thawed on ice and diluted 1:25 in cold KO-DMEM. Then, 7 µl/cm^2 diluted matrigel was used to coat the surface of the culture vessel. The coated culture vessels were incubated for at least 1 h at 37°C. Prior to use, surplus liquid was aspirated and replaced with culture medium.

A medium change was performed every 24 h with H9-medium including 10 ng/ml FGF2.

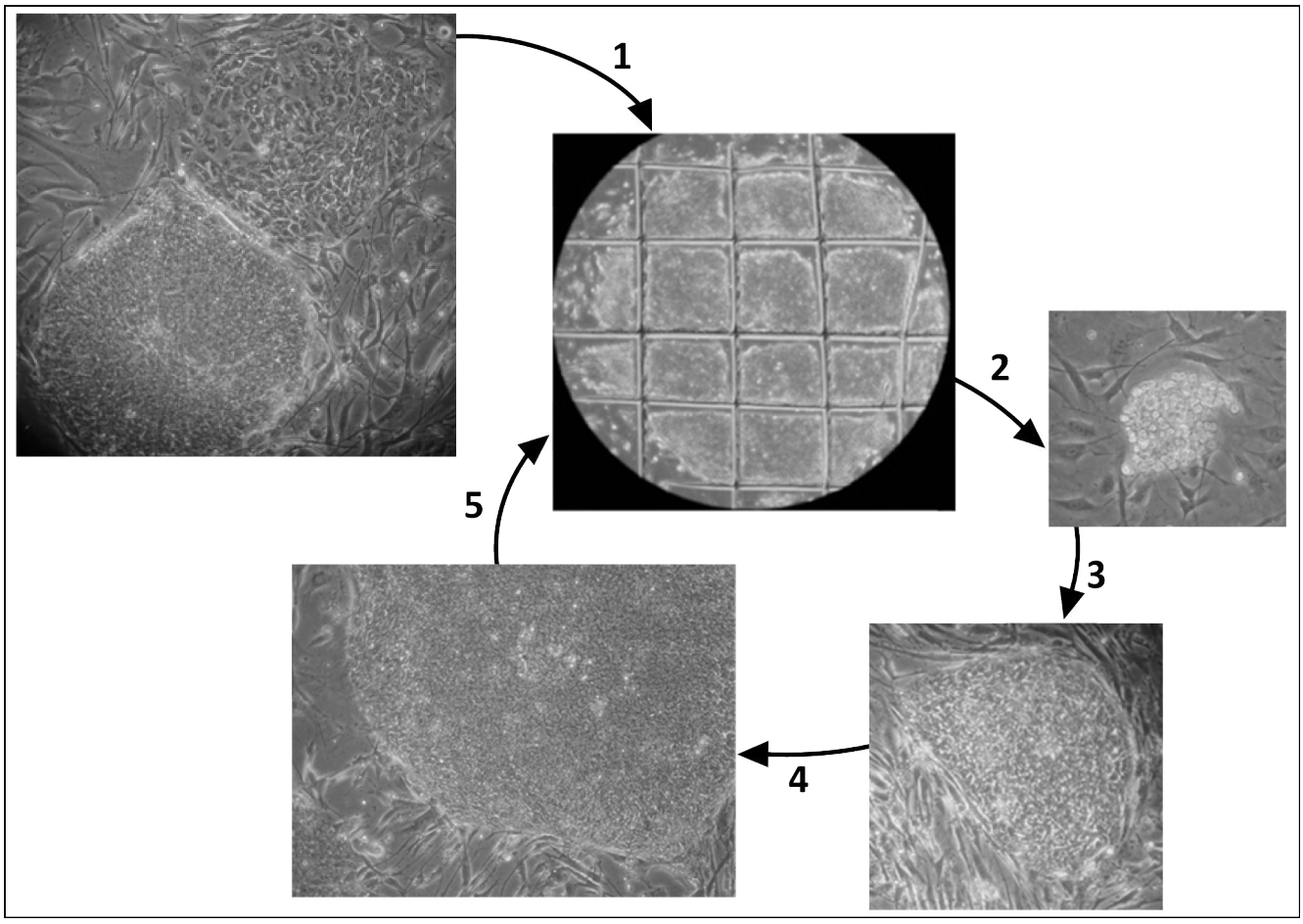

Figure 2.1: Weekly manual passaging cycle. Colonies with pluripotency indicating morphology (lower left colony in picture before step 1) are chosen, while colonies with differentiation indicating morphology (upper right colony in picture before step 1) are excluded from the passage. This selection is not possible with enzymatic passaging. Colonies are cut into squares (1) and transferred into a new culture vessel (2). The cell clumps attach and start to grow (4, at two days after passage). When the colonies reach a certain size and density in the culture vessel, a further manual passage is performed (5).

2.1.2 Mouse embryonic fibroblasts

As a feeder layer for the hESCs (H9), cells of the mouse embryonic fibroblasts line PMEF-NL were obtained from Millipore, Germany, in passage number three and stored in liquid nitrogen. MEFs were expanded on gelatinized T75 culture flaks. Therefore, the cell growth surface of T75 culture flasks was coated with 0.1 % gelatine in $PBS^{-/-}$ and incubated for at least 1 h. Then, the gelatine was aspirated and the culture flasks were prefilled with MEF-medium.
MEFs were thawed and transferred in 9 ml MEF-medium for washing. The cell suspension was centrifuged for 5 min at 200 g. The pellet was resuspended in MEF-medium and 1.5 to 2 Mio cells were plated in gelatinized T75 culture flasks in a total of 15 ml MEF-medium.
Cells were passaged at 85 to 95 % confluency and expanded up to passage 6. Therefore, adherend MEFs were washed with 5 ml $PBS^{-/-}$, and incubated in 2 ml trypsin (0.05 % trypsin/ 0.1 % EDTA in $PBS^{-/-}$ for 5 min at 37°C. Detached MEFs were flushed off the culture surface with MEF-medium and collected in 50 ml reaction tubes. The cell suspension was centrifuged for 5 min at 200 g. The pellet was resuspended in MEF-medium and 1.5 to 2 Mio cells were plated on gelatinized T75 culture flasks in a total of 15 ml MEF-medium.
In passage 6 at a confluency of 85 to 95 %, cells were enzymatically harvested as described before, collected on ice and mitotically inactivated by exposing the cells in suspension to 2 x 30 Gy X-rays. Inactivated cells were centrifuged for 5 min at 200 g and the pellet was resuspended in 1.8 ml freezing-medium per 3 Mio or 6 Mio cells. The cells were frozen at -80°C for 24 h and then stored in liquid nitrogen.
To plate the feeder layer for hESCs, inactivated MEFs were thawed >12 h prior to hESC passaging. MEFs were washed as described before and plated on gelatinized culture vessels in MEF-medium with a density of 33000 MEFs/cm^2.

2.1.3 Preparation of MEF-conditioned medium

To grow hESCs (H9) in feeder free conditions, cells were cultured in MEF-conditioned medium on matrigel coated surfaces. Therefore, H9-medium containing 10 ng/ml FGF2 was incubated 24 h on 47000 MEF/cm^2. Every 24 h, the medium was exchanged and MEF-conditioned medium was collected for four days. Prior to use, the MEF-conditioned medium was filtered through a 0.22 µm pore size filter and 4 ng/ml FGF2 were added.

2.2 Irradiation procedures

2.2.1 X-ray irradiation

For X-ray exposure, an Isovolt DS1 X-ray tube (Seifert, Ahrensberg, Germany) with settings of 250 kV voltage and 16 mA current was used. The X-ray tube is equipped with a filter system consisting of 7 mm Be, 1 mm Al and 1 mm Cu to absorb soft X-rays. The dose was measured with an SN4-dosimeter (PTW, Freiburg, Germany). Cells were exposed at RT, with dose rates of approximately 2 Gy/min. In case of hESC exposure, the duration of the total irradiation procedure including exposure and transport between the incubator and the X-ray tube was on average 30 min. For the inactivation of MEFs, the average duration of the procedure including cell harvest, exposure, transport and resuspension in freezing-medium was approximately 1 to 4 h. The positioning of the sample for X-ray irradiation is shown in figure 2.2.

Figure 2.2: X-ray irradiation. The sample is positioned horizontally below the exit window of the X-ray tube. The sensor of the dosimeter is placed as close as possible to the cells.

2.2.2 Ion irradiation

Irradiation of cells with heavy ions was performed at the heavy ion synchrotron SIS18 at GSI, Darmstadt. For 25 mm Spread Out Bragg Peak (SOBP) irradiation, the beam is first passing a 60 mm polyethylenbolus in order to adjust its energy. The pencil beam moves continuously over the target by using the raster scanning technique to ensure a defined number of particles being delivered at a certain raster point [99]. Ion species, their energies and corresponding characteristics are summarized in table 2.1. For exposure to heavy ions, cells were seeded in T25 culture flasks, that were filled up with H9-medium not containing knockout serum replacement prior to exposure. The flasks were positioned vertically and the surface with the adherent cells perpendicular to the beam exit window on a remotely controlled conveyor belt (see figure 2.3). Cells were exposed at RT. Mean duration of the total ion irradiation procedure including transport between the incubator and the synchrotron irradiation room was 45 min.

Table 2.1: Ion species, energy, LET on target and dose applied during irradiations with heavy ions

Ion species		Energy		LET on target	Dose
Carbon	106 - 147	MeV/u (SOBP)	75	keV/µm (dose averaged)	1 Gy
Calcium	1	GeV/u	89	keV/µm	1 Gy
Titanium	1	GeV/u	107	keV/µm	3 Gy
Nickel	1	GeV/u	174	keV/µm	1 Gy

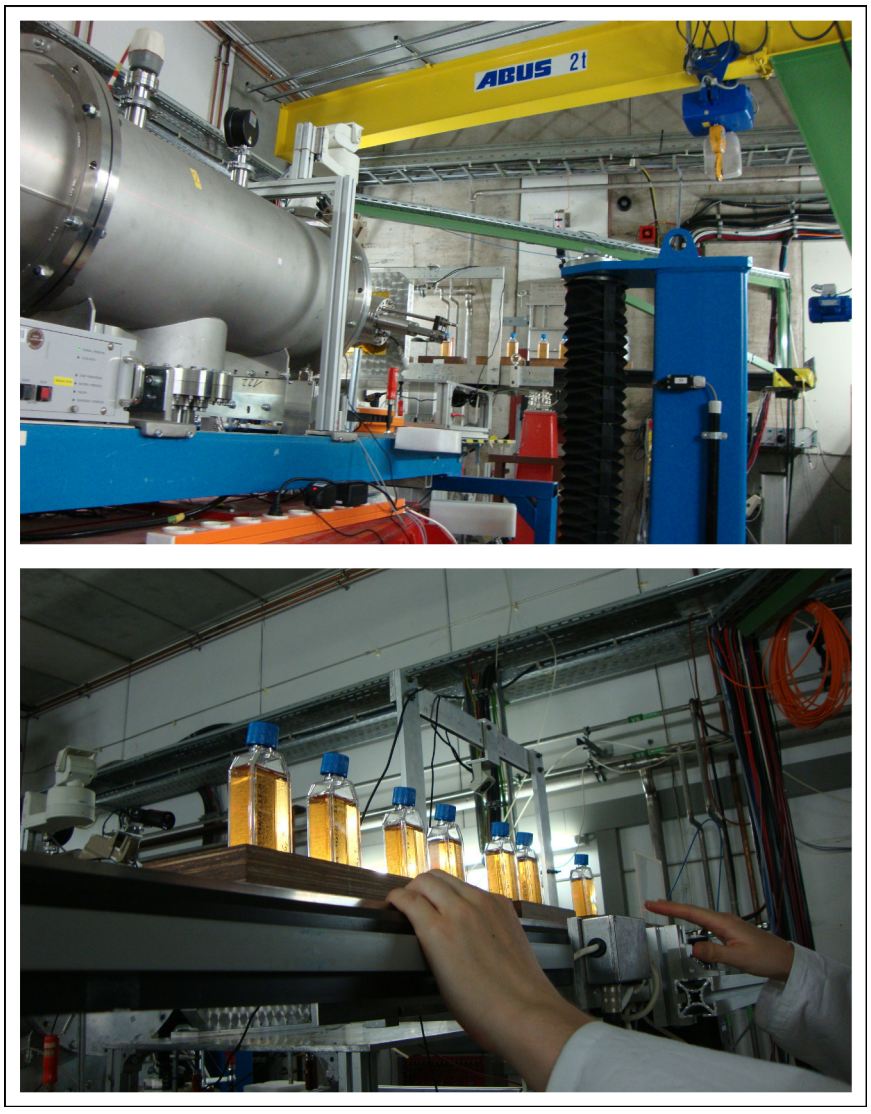

Figure 2.3: Ion irradiation. Upper picture: Beam line coming from the left, pointing at the vertically positioned culture vessels on the conveyor belt. Lower picture: Adherent hESCs (H9) in T25 culture flasks, filled up with medium. The cell growth surface is pointing into the direction of the beam.

2.3 Determination of the nuclear size and the number of particle traversals per nucleus

Knowing the cross-section of a hESC nucleus ($A_{cell\ nucleus}$) as well as the particle fluence (F), the number of particle traversals per cell nucleus can be determined.

Therefore, adherent hESCs (H9) growing on cover slips were washed with $PBS^{+/+}$ and incubated in 3.7 % PFA for 20 min at room temperature (RT) for fixation. After three washing steps with $PBS^{-/-}$, cells were stained with 5 µg/ml Hoechst 33 342. Measurement of stained cell nuclei was performed in Nikon NIS elements software by automatic object recognition.

The fluence, describing the number of particle traversal per unit area, can be calculated according to the following equation, where D is the dose in Gy, LET is the linear energy transfer in keV/µm, F is the particle fluence in cm^{-2} and ρ is the density of the target (1 cm^3/g for water):

$$D = 1.602 \cdot 10^{-9} \cdot LET \cdot F \cdot \frac{1}{\rho} \tag{2.1}$$

The number of particle traversals per cell nucleus is then calculated according to:

$$F \cdot A_{cell\ nucleus} = N_{\frac{particle\ traversals}{cell\ nucleus}} \tag{2.2}$$

2.4 Differentiation into definitive endoderm

hESCs were differentiated into DE based on a protocol from D'Amour and colleagues [40]. For this, hESCs (H9) were cultured in petri dishes on MEF under pluripotency maintaining culture conditions. Four days after the manual passage, cells were irradiated with 1 Gy X-rays or sham irradiated. Then, cells coming from two petri dishes were pooled and transferred to one matrigel-coated petri dish containing MEF-conditioned medium (day -2). After 48 h (day 0), cells were washed with $PBS^{+/+}$ and cultured in 3 ml DE-medium including 25 ng/ml Wnt3a. From day 1 to day 7, medium was exchanged daily with new DE-medium including 0.2 % FCS. A time line of this experimental procedure is shown in figure 2.4.

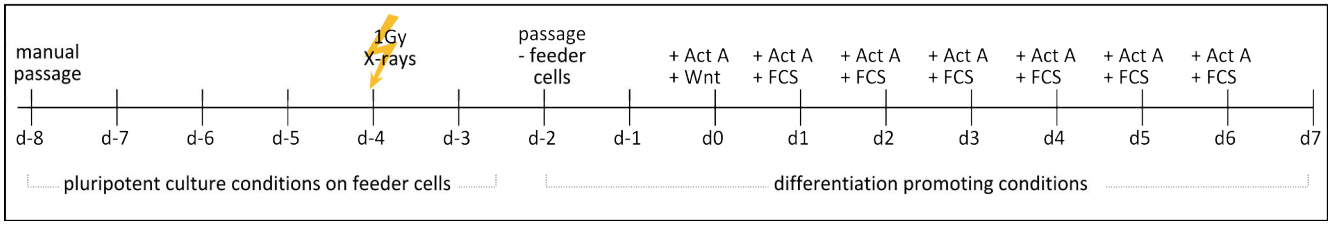

Figure 2.4: Time line of the experimental procedure for differentiation towards DE, including irradiation and directed differentiation of the cells from day -8 to day 7.

2.5 Proliferation assay

For analysis of cell cycle duration, the Click-iT® EdU Alexa Fluor® 488 Flow Cytometry Assay Kit (Invitrogen) was used. Manually passaged hESCs (H9) (passage 25) grown on MEF feeder cells in petri dishes were pulse labeled with 10 µM EdU in H9-medium for 50 min. Then, cells were washed and incubated in H9-medium and/or harvested at various timepoints (0, 12, 16, 20 and 24 h). For the fixation, permeabilisation and staining procedure, the manufacturers protocol was followed. Additionally, cells were stained with 1 µg/ml DAPI. Cells were subsequently analyzed by flow cytometry.

2.6 Apoptosis assay and simultaneous cell cycle analysis

Apoptotic cells were identified due to immunochemical staining of activated caspase-3. hESCs (H9) were cultured on matrigel to deplete MEF cells. A medium exchange was performed prior to exposure to exclude apoptotic cells not caused by irradiation. Due to the high metabolic activity of hESCs, a further medium change had to be performed after 24 h. Cells were incubated for 20 min in 1 % EDTA in $PBS^{-/-}$ to obtain a single cell suspension. For staining of active caspase-3, the FITC Active Caspase-3 Apoptosis Kit (BD) was used according to the manufacturers protocol. Stained cells were additionally incubated in 1 µg/ml DAPI to allow simultaneous cell cycle analysis. Processed samples were measured by flow cytometry. For time points >24 h, the second medium change has to be taken into account in the data analysis of apoptosis induction. Therefore, the actual fraction of apoptotic cells at more than 24 h ($A_{(>24h+mc)}$) was calculated according to equation 2.5 that was derived as follows:

$$S_{(>24h+mc)} = S_{(24h)} \cdot S_{(>24h-mc)} \tag{2.3}$$

$$1 - A_{(>24h+mc)} = (1 - A_{(24h)}) \cdot (1 - A_{(>24h-mc)}) \tag{2.4}$$

$$A_{(>24h+mc)} = 1 - (1 - A_{(24h)}) \cdot (1 - A_{(>24h-mc)}) \tag{2.5}$$

where $S_{(24h)}$ is the fraction of surviving cells observed at 24 h, $S_{(>24h-mc)}$ is the fraction of surviving cells observed at a time point later than 24 h without taking into account the medium change, and A is the fraction of apoptotic cells, respectively.

2.7 Cytogenetic analysis

To accumulate cells in metaphase, hESCs (H9) were incubated in H9-medium including 10 µg/ml colcemid for 3 h at 37°C. Then, cells were washed with $PBS^{-/-}$ and enzymatically detached with trypsin to obtain a single cell suspension. The enzyme reaction was stopped by adding 3 ml MEF medium and the cell suspension was transferred into a 15 ml reaction tube and centrifuged for 6 min at 200 g and RT. For hypotonic treatment, cells were resuspended carefully in 8 ml 37°C prewarmed KCl solution (0.075 M in H_2O) and incubated for 7 min at 37°C. Afterwards, 1.5 ml fixative (methanol:acetic acid 3:1) were added and cells were centrifuged for 10 min at 200 g and RT. The cell pellet was resuspended in 10 ml fixative, centrifuged and resuspended in ∼1 ml fixative. Cells were either stored at 4°C or subsequently dropped onto microscope slides.

Air dried metaphase spreads were hybridized with the 24xCyte Human Multicolor FISH Probe Kit (Metasystems) according to the manufacturers protocol and images of the metaphase

spreads were captured with an Axio Imager Z1 microscope (Zeiss) and Metafer software, and analyzed with ISIS software.

Structural chromosomal aberrations were scored and subdivided in the following categories, based on the classification of M. N. Cornforth [100, 14] (see also figure 1.3 for an illustration of various structural aberrations). Breaks comprise chromosomal aberrations such as truncated chromosomes with and without related acentric fragment as well as lonely acentric fragments. They result due to a terminal deletion after one break or due to an interstitial deletion due to 2 breaks in a chromosome. Simple exchanges consist of the subcategories reciprocal and non-reciprocal exchanges as well as dicentrics. Reciprocal translocations result due to a symmetric reciprocal interchange of two broken chromosomes. Non-reciprocal translocations are also known as one-way exchanges. They either represent true incomplete exchanges resulting due to an incomplete symmetric reciprocal interchange of two broken chromosomes, or they represent terminal translocations characterized by a small fragment near the telomeres of a chromosome which exceeds the resolution of the mFISH technique. Dicentric chromosomes (with and without related acentric fragment)result due to an asymmetric reciprocal interchange of two broken chromosomes. Complex aberrations result after $\geq$3 breaks in $\geq$2 chromosomes. The complexity of complex aberrations was quantified by means of the CAB system [101, 14]. This system is recording the number of chromosomes (C), the number of arms (A), and the number of breaks (B) involved in a certain complex aberration. Cells with the same aberrations, i.e. clones, were scored as only one aberrant cell.

2.8 Individual mRNA expression analysis based on quantitative RT-PCR using the standard curve method

For cell lysation, samples were washed with $PBS^{+/+}$ and lysed by adding 700 µl QIAzol lysis reagent according to the protocol of the miRNeasy Mini Kit (Qiagen). Cells were scraped of the culture vessel and the suspension was collected in a 2 ml reaction tube. After 5 min incubation at RT, cell lysates were stored at -80°C.

Simultaneous isolation of miRNA and total RNA was performed according to the miRNeasy Mini Kit protocol, using chloroform to separate RNA from DNA and proteins, and spin columns to enrich miRNA and total RNA. RNA concentration and purity were analyzed using the Colibri microvolume spectrophotometer (Titertek Berthold). If not processed immediately, isolated RNA was stored at -80°C.

In case of an RNA concentration below 1 µg/ml or bad quality of RNA absorbance spectra indicating contamination (significantly lower ratio of the absorbance at 260 nm and 280 nm), RNA was purified by adding 1/10 volume of cold 3 M sodium acetate and 1 volume of cold isopropanol. After an incubation of 3 h at -20°C, the sample was centrifuged at 20000 g for 15 min. The pellet was rinsed in 30 µl 70 % ethanol and centrifuged again at 21000 g for 2 min. The air dryed pellet was resuspended in 10 µl nuclease free water.

For the conversion of total RNA to cDNA, the RevertAid RT Kit (Thermo Fisher Scientific) with its provided protocol was used. Incubation steps were performed in a thermocycler. If not further processed, cDNA samples were stored at -20°C.

For quantitative rtPCR, 2 µl cDNA was mixed with 4 µl 5x HOT FIREPol® EvaGreen® qPCR Mix Plus (ROX), 1 µl forward and 1 µl reverse primer and 12 µl nuclease free water. For each sample, triplicates were pipetted into a 96 well plate. The plate was sealed, centrifuged and placed into the qRT-PCR instrument (StepOnePlus™Real-Time PCR System, ABI) with the following cycle

settings: 15 min at 95°C, one cycle, for initial denaturation and polymerase activation, 15 sec at 95°C followed by 1 min at 60°C, 40 cycles for denaturation, annealing and elongation. A melt curve analysis was appended to these settings.
Data analysis was performed with ABI StepOne Software v2.3, applying the relative standard curve method to relate obtained sample CT values to known concentrations of human fetal liver tissue total RNA or RNA samples from pluripotent hESCs (H9). Primers are listed in the appendix, see table 4.8.

2.9 Stem cell signaling mRNA array analysis

For cell lysation, enzymatically harvested cells were centrifuged and the cell pellet was processed according to the manufacturers protocol of the MasterPure™RNA Purification Kit (Epicentre). If not processed immediately, lysates were stored at -80°C. RNA concentration and purity were analyzed with the Colibri microvolume spectrophotometer. Using the RT^2 First Strand Kit (Qiagen), RNA was converted into cDNA according to the manufacturers protocol. cDNA and RT^2 qPCR Master Mixes (Qiagen) diluted with nuclease free water was pipetted according to the manufacturers protocol into the Human Stem Cell Signaling PCR Array (Qiagen) already including primer sets of 5 housekeeping genes as well as 84 genes of interest. The plate was sealed, centrifuged and placed into the qRT-PCR instrument with the following cycle settings: 10 min at 95°C, one cycle, for initial denaturation and polymerase activation, 15 sec at 95°C followed by 1 min at 60°C, 40 cycles for denaturation, annealing and elongation. A melt curve analysis was appended to these settings. Data analysis was performed with StepOne Software v2.3 (Applied Biosystems), applying the comparative CT method (delta delta CT). Primer sets for genes already included in the array are listed in the appendix, table 4.9.

2.10 Immunocytochemical analyses of pluripotency and differentiation markers

For fluorescence microscopy analysis of pluripotency markers, hESCs (H9) were grown and stained on cover slips. Cells were washed with $PBS^{+/+}$ and incubated in 3.7 % PFA for 20 min at RT for fixation. After three washing steps with $PBS^{-/-}$, cells were permeabilized with 1 % FCS + 0.1 % Triton-X in $PBS^{-/-}$ for 30 min at RT for intracellular staining, and blocked with 3.5 % FCS in $PBS^{-/-}$ for >30 min at RT. Then, cells were incubated in primary or directly labelled antibody dilution for 45 min at 37°C, washed 3 times in $PBS^{-/-}$ and, in case of not directly labelled antibodies, incubated in secondary antibody dilution for 30 min at 37°C. After three further washing steps in $PBS^{-/-}$, cells were stained with 5 µg/ml Hoechst 33 342. Table 2.2 summarizes applied antibodies and concentrations or dilutions.
For flow cytometric analysis of pluripotency state of hESCs, cells were incubated for 20 min in 1 % EDTA in $PBS^{-/-}$, resuspended and passed trough a 40 µm cell strainer to obtain a single cell suspension. Cell concentration was dertermined and cells were washed and centrifuged at 300 g for 5 min. The cell pellet was resuspended in $PBS^{-/-}$ and the BD Stemflow™Human and Mouse

Table 2.2: Antibodies applied for immunocytochemistry

antibody	concentration or dilution
anti-Oct3/4 (C-10)	1:100
goat anti-mouse Alexa Fluor® 488	1:400
anti-human Nanog Alexa Fluor® 488	2,5 µg/ml

Pluripotent Stem Cell Analysis Kit (BD) was used according to the manufacturers protocol. Cells were stained for the differentiation marker SSEA1 and for the pluripotency marker SSEA4.

2.11 Flow cytometry

Stained cells were measured in BD FacsCanto II flow cytometer equipped with 3 lasers (405 nm, 488 nm and 633 nm) and 8 detectors (SSC 488/10BP, FITC 530/30BP, PE 585/42BP, PerCP-Cy5.5, PerCp 670LP, PE-Cy7 780/60BP; APC 660/20BP, APC-Cy7 780/60BP; AmCyan 510/50BP, Pacific Blue 450/50BP) with the software BD FACSDiva™v7.0. For all measurements, the pulse signal of a single event passing through the laser is recorded as integrated area, indicated in histograms and dotplots as "A". Data analysis was performed with the software FlowJo V.7.6.5 for cell cycle analysis and V.10 for all other stainings.

2.12 Statistical analysis

In case of $n>2$ experiments, error bars represent the standard error of the mean. In case of $n\leq 2$ experiments, error bars were calculated according to Poisson statistics. Statistical significance was calculated based on Fisher's exact test for cytogenetic analysis and Student's *t*-test for gene expression analysis.

3 Results

3.1 Average size of hESC (H9) cell nucleus and number of particle traversals per cell nucleus

As described in section 2.3, the size of 32 adherent hESC (H9) cell nuclei in a microscopic field was measured at day 5 after seeding. The mean area ± standard deviation is 198±52 μm^2. Figure 3.1 shows an exemplary measurement of a cell nucleus.
The fluence calculated according to equation 2.1, and the number of particle traversals per nucleus calculated according to equation 2.2 is shown in table 3.1. In all ion irradiation experiments, each cell had an average of at least 12 hits per nucleus.

Table 3.1: Table describing the number of particle traversals per cell nucleus for the different ion irradiation conditions. *dose averaged LET (SOBP).

Ion species	Dose (Gy)	LET (keV/µm)	Fluence (cm^{-2})	Traversals/nucleus
C	1	75*	$8.3 \cdot 10^6$	16
Ca	1	89	$7.0 \cdot 10^6$	14
Ni	1	107	$5.8 \cdot 10^6$	12
Ti	3	174	$1.1 \cdot 10^7$	21

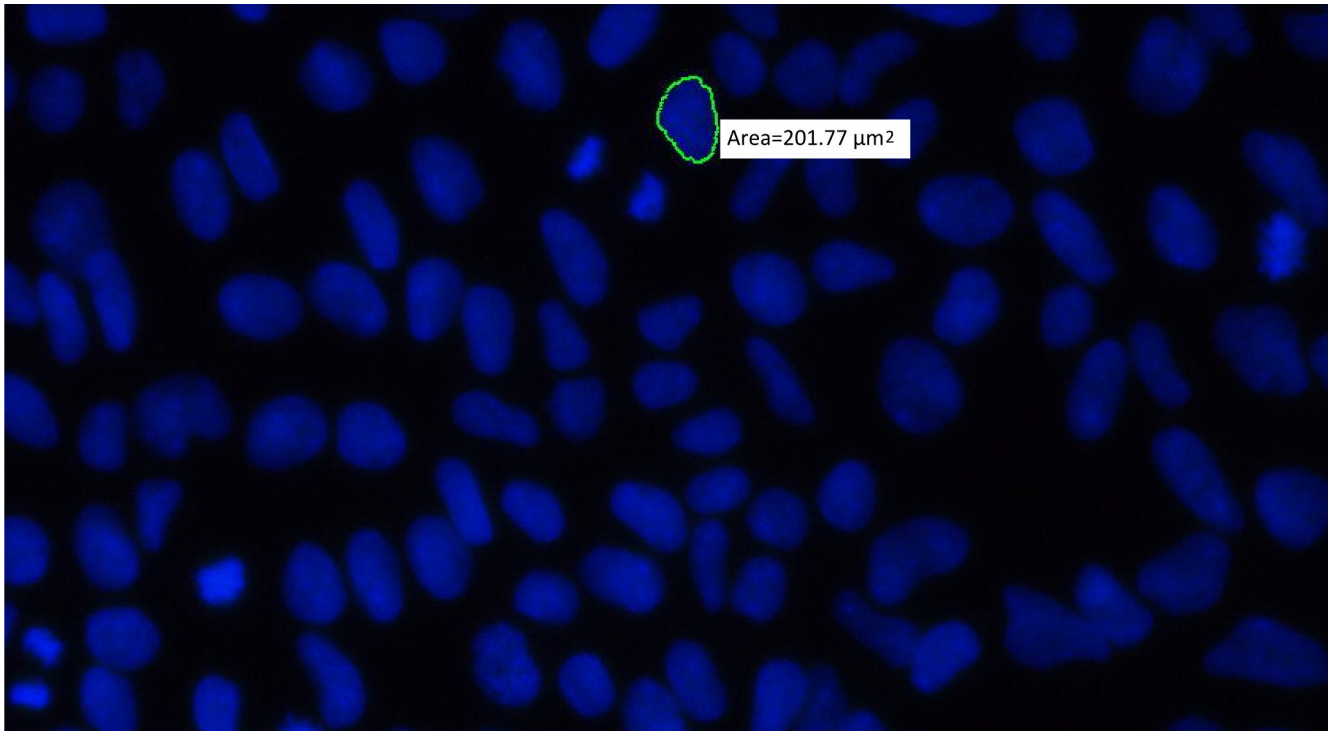

Figure 3.1: Measurement of the area of a hESC (H9) nucleus stained with Hoechst 33 342. Adherent cells were growing on cover slips. 300 x magnification.

3.2 Qualitative verification of pluripotent cell cultures

The pluripotency of the initial hESC culture used for irradiation experiments was verified based on immunocytochemistry. Figure 3.2 shows positively labeled cells and colonies of a manually passaged culture for the core pluripotency markers NANOG and OCT4A, proving their pluripotent state. Negatively labeled MEFs are indicated exemplarily with yellow arrows and automatically serve as a negative control for the specificity of the antibodies. Interestingly, the hESC colonies shown in 100-fold magnification exhibit less intense and more intense labeled areas. Furthermore, mitotic cells indicated with white arrows reveal that the localization of OCT4A is not anymore restricted to the nucleus, but is now distributed throughout the cytoplasm. In contrast, NANOG labeling seems much weaker in mitotic cells. Apoptotic cells (morphologically identified based on characteristically condensed DNA) are indicated with red arrows. Both pluripotency markers OCT4A and NANOG are not detectable in apoptotic cells.

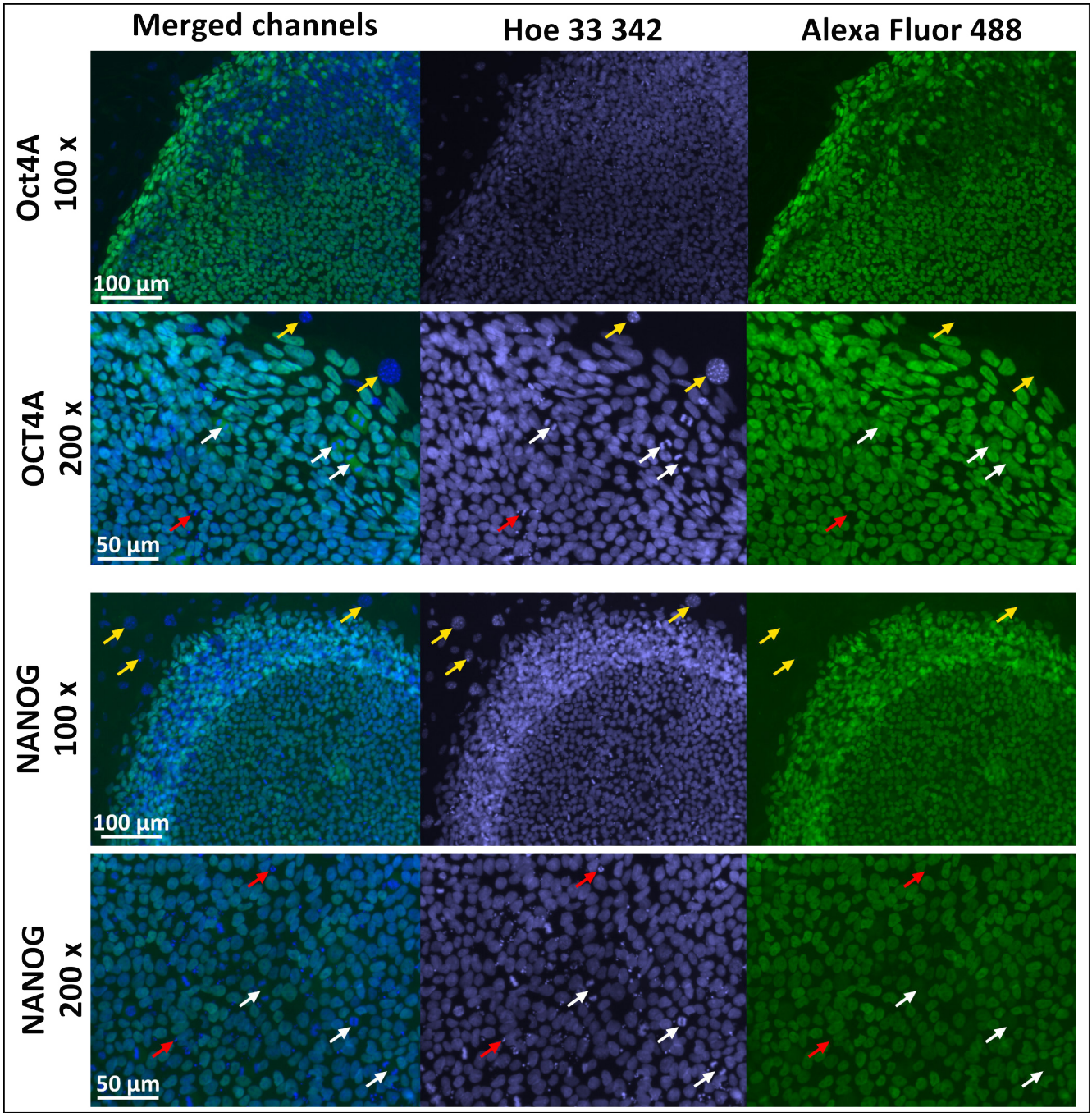

Figure 3.2: Immunocytochemical labeling of hESCs (H9) against pluripotency markers OCT4A (upper two rows) and NANOG (lower two rows) both with Alexa Fluor®488 (green), counterstained with Hoechst 33 342 (blue). White arrows exemplarily indicate mitotic cells, yellow arrows indicate MEFs, and red arrows indicate apoptotic cells.

3.3 Cell cycle duration

The cell cycle duration is a prerequisite for the experimental design of further endpoints like chromosome aberrations and for the interpretation of further results. The EdU pulse labeling assay provides a good estimate of the time the cells need to progress from one S phase to another.

First, the protocol had to be optimized in terms of adapting the EdU incorporation during DNA replication to the hESCs (H9). Therefore, three different combinations of EdU concentrations and incubation durations were tested. These are: 5 μM for 50 min, 5 μM for 2 h and 10 μM for 50 min. The best discrimination between G1, S and G2 phase cells was achieved with the protocol using 10 μM EdU for 50 min (see figure 3.3).

The determination of the cell cycle duration is shown in figure 3.4. While at 0 h only hESCs (H9) in S phase (40 %) are labeled, these cells have already progressed into G2 phase after 12 h, and further progress through mitosis into G1 phase, visible at 16 h. Between 16 and 20 h, most of the initially labeled S phase cells entered S phase again, speaking for a cell cycle duration of approximately 16-20 h.

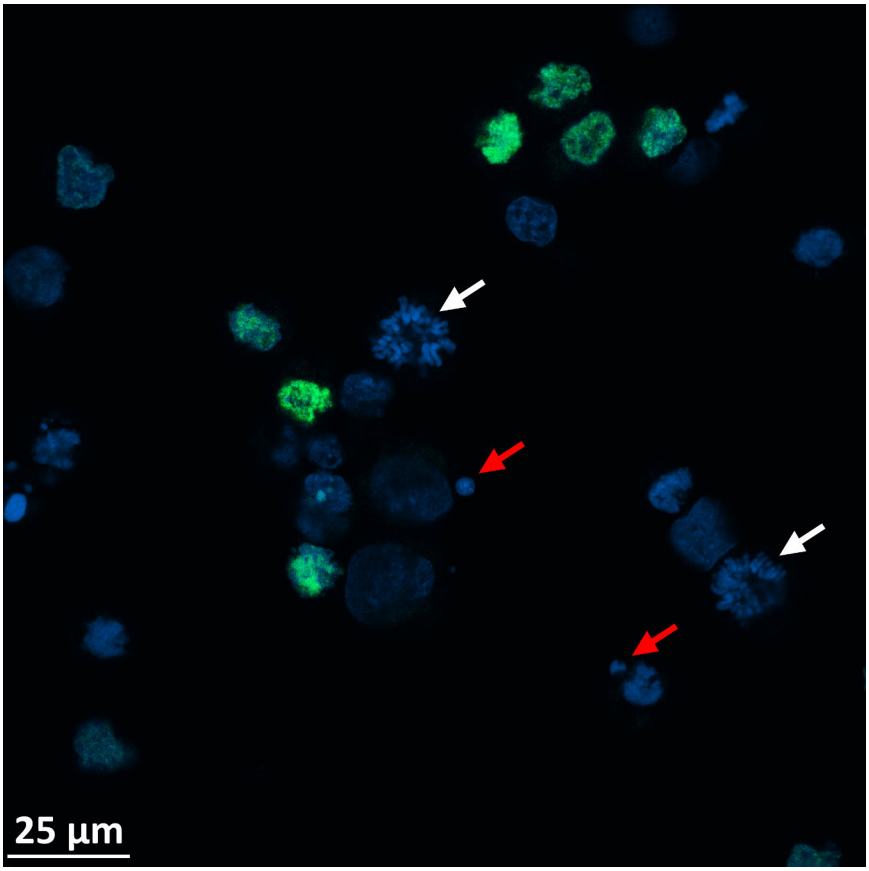

Figure 3.3: Cell suspension of hESCs (H9) incubated in 10 µM EdU for 50 min, immediately harvested for analysis. Incorporated EdU is immunocytochemically labeled with Alexa Fluor®488 (green) and DNA is stained with DAPI (blue). Cells in S phase are shown in green and blue, while cells in other cell cycle phases like mitosis (indicated with white arrows), or apoptotic cells (indicated with red arrows) did not incorporate any EdU and are shown in blue.

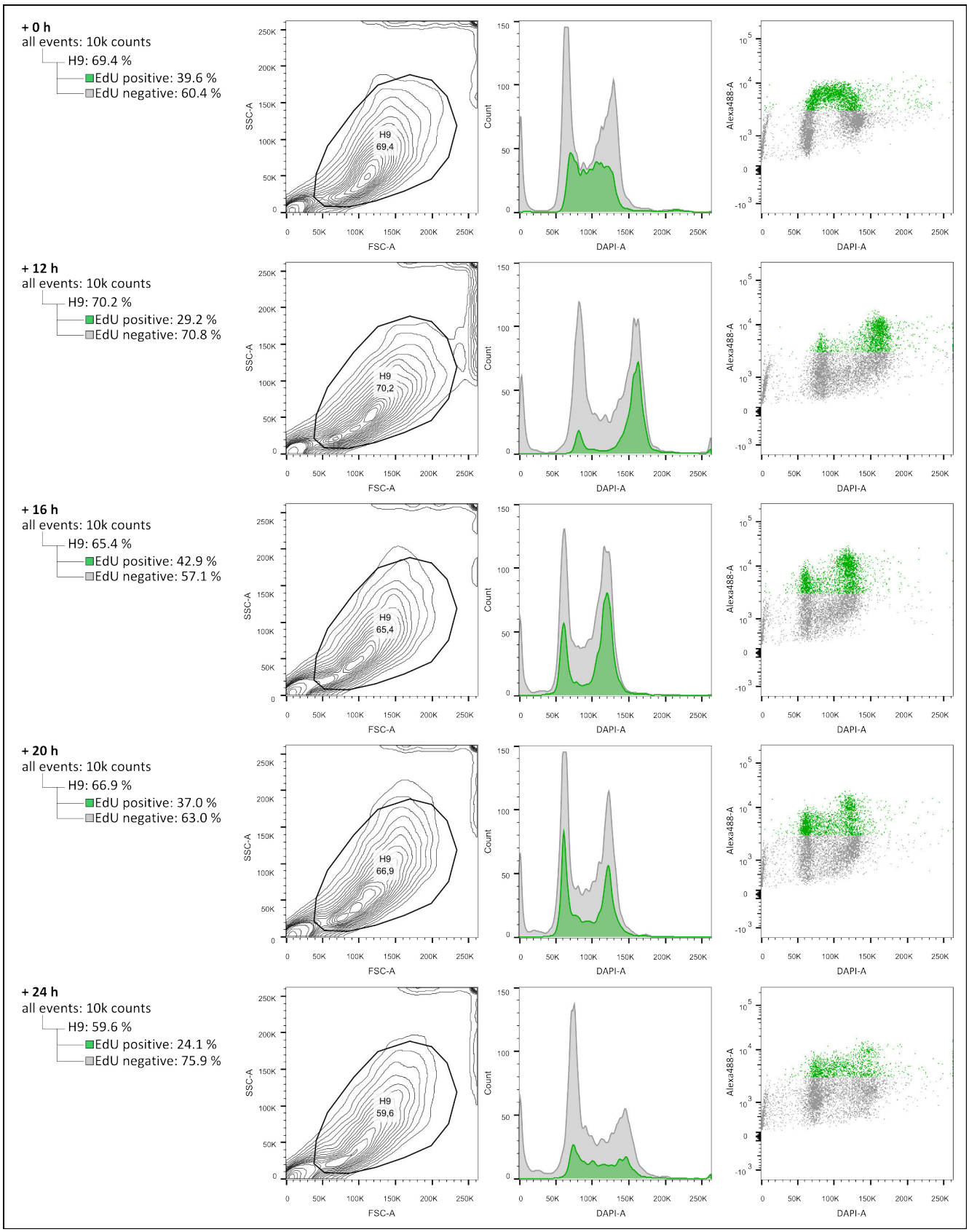

Figure 3.4: Determining the cell cycle duration of hESCs (H9). Flow cytometry measurement at 0, 12, 16, 20 and 24 h after EdU pulse labeling and counterstaining with DAPI. For every time point the gating strategy with corresponding frequencies of cells in its gated subgroup is shown together with its forward scatter versus side scatter contour plot, followed by the DNA histogram and the EdU-Alexa488-A versus DAPI-A dotplot.

3.4 Cell cycle progression

To determine the effect of IR on the cell cycle progression of hESCs (H9), cells were stained with DAPI allowing a quantification of the DNA content via flow cytometry. The resulting DNA histogram was analyzed with cell cycle fitting algorithms. The fraction of cells in G2/M phase was measured in three experiments differing with respect to the initial cell culture methods (enzymatically or manually passaged) and the radiation qualities. These three experiments are: an enzymatically passaged culture exposed to 1 Gy Ni ions, 1 Gy X-rays, and related controls (see figure 3.5A), a manually passaged culture exposed to 1 Gy X-rays and related control (see figure 3.5B), and an enzymatically passaged culture exposed to 1 Gy Ca ions, 1 Gy X-rays, and related controls (see figure 3.5C).

All controls of the three experiments have a mean fraction of 36±3 % of cells in G1 phase, 41±2 % in S phase, and 19±1 % of cells in G2/M phase (mean ± standard error of them mean). Interestingly, just like most exposed samples, also the controls show an initially elevated level of cells in G2/M phase compared to later time points after 24 h.

The main observations on the cell cycle progression in radiation exposed samples are now described separately for each of the three experiments. In the experiment with Ni and X-ray irradiation, both exposed samples show a clearly elevated fraction of cells in G2 phase at 7 h compared to the sham treated control. After 7 h, the fraction of cells in G2/M phase of both irradiated samples approaches the levels of the sham treated control (figure 3.5A). The experiment with manually passaged cells shows a lower fraction of X-ray irradiated cells compared to control after 24 h, while in the light of biological variability no conclusion regarding the statistical significance can be drawn (figure 3.5B). The third experiment with cells exposed to Ca ions and X-rays exhibits a similar G2/M phase progression in both incubator and sham treated control cells. Exposed samples show a higher fraction of cells in G2/M phase at 7 and 24 h compared to both controls (figure 3.5C).

Sample pairs with biological triplicates ($n=3$) were tested for statistical significance (Student's *t*-test; $p<0.005$). At 24 h, the fraction of G2/M cells in Ca ion exposed samples is significantly higher than the sham treated control, while the X-ray exposed sample is not significantly different (figure 3.5C).

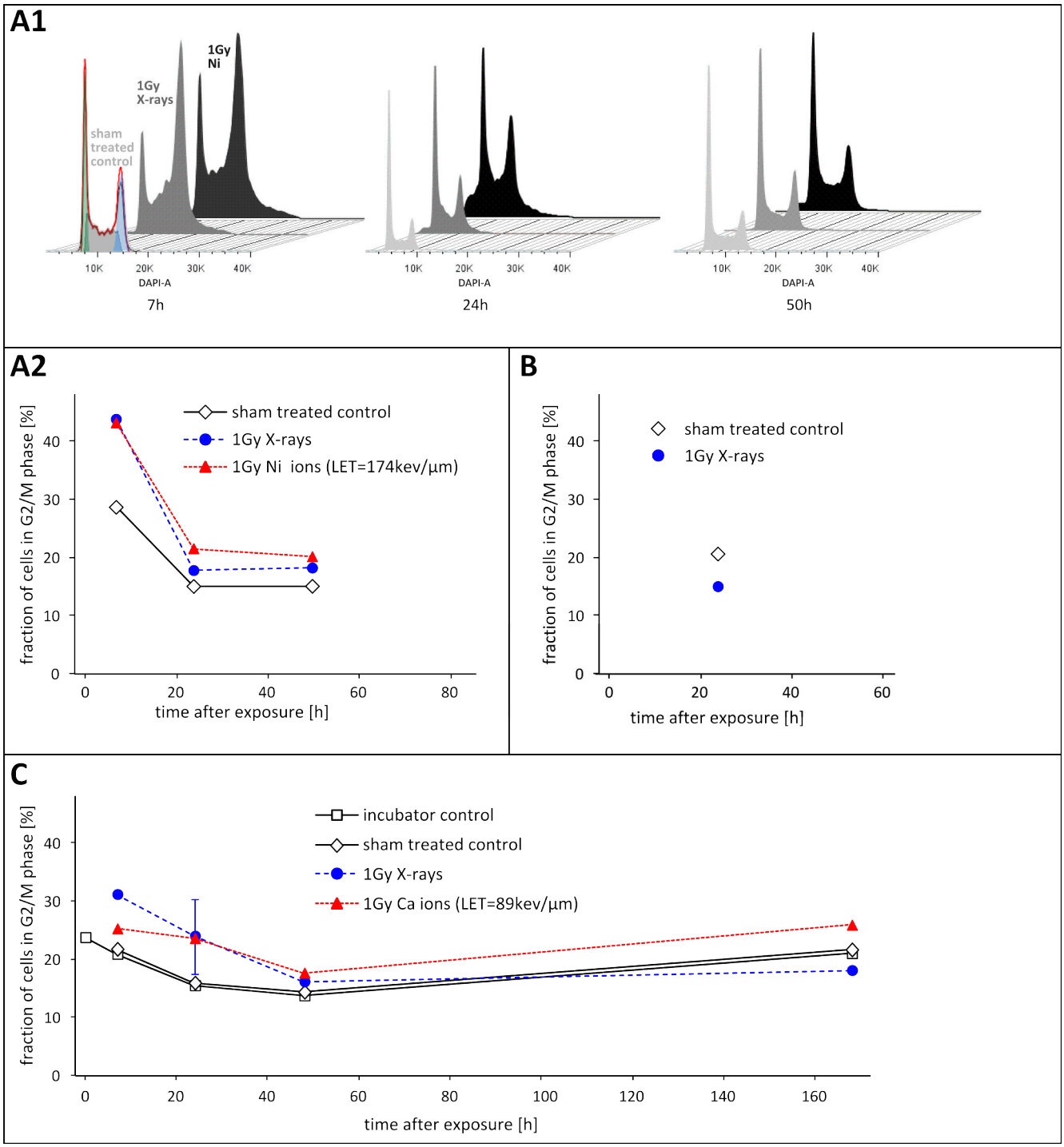

Figure 3.5: Fraction of cells in G2/M phase. A1: Cell Cycle profiles corresponding to the data shown in A2 as derived from flow cytometry. The fitting of the cell cycle is exemplarily indicated for the sham treated control sample after 7 h. Cells in G1 phase are indicated in green; cells in S phase are indicated in grey; cells in G2/M phase are indicated in blue; overall fit is indicated as red line. A2: Measurements of enzymatically passaged cultures exposed to 1 Gy Ni ions and X-rays. B: Measurements of manually passaged cultures exposed to 1 Gy X-rays. C: Measurements of enzymatically passaged cultures exposed to 1 Gy Ca ions and X-rays. Error bars in B 24 h 1 Gy X-rays, and in C 24 h sham treated control, 1 Gy X-rays, 1 Gy Ca ions represent standard error of the mean of three biologically independent samples (n=3). All other error bars represent n=1 sample and are calculated according to Poisson statistics. If absent, error bars are too small to be shown.

3.5 Cell death

The apoptosis inducing effect of IR on hESCs (H9) was investigated by an immunocytochemical staining of cleaved Caspase-3 followed by flow cytometric quantification.

A clear increase of detached cells was visible 24 h after exposure to 1 Gy X-rays, as shown in figure 3.6. While the sham treated control exhibits only few cells floating in the medium, the exposed sample shows a strong increase of detached, probably apoptotic cells, that partially obscure the colony below.

The results of three different experiments are shown in figure 3.7. These three experiments represent enzymatically passaged cultures with either Ni ions and X-ray exposed samples (A), enzymatically passaged cultures with Ca ions and X-ray exposed samples (B), and a manually passaged culture exposed to X-rays (C).

The mean fraction of apoptotic cells of all controls from the enzymatically passaged culture experiments A and B is 0.025 ± 0.005 (mean±standard error). However, the manually passaged control revealed an apoptotic fraction that was five times higher than the mean of all other enzymatically passaged controls.

The slope of ion exposed samples always exceeds that of its corresponding X-ray exposed counterpart, indicating that the fraction of apoptotic cells increases time and radiation quality dependent. An inter-experimental variability is observed when comparing the three X-ray exposed samples of experiments A, B and C at 24 h: While the lowest fraction of apoptotic cells is found in experiment A, the fraction of apoptotic cells in experiment B increases by a factor of two (and is higher than the Ni ion exposed sample of experiment A), and the fraction of apoptotic cells in experiment C increases by a factor of five compared to that in experiment A (and is higher than the Ca ion exposed sample of experiment B). The highest fraction of apoptotic cells was observed at 48 h after an exposure to 1 Gy Ca ions, that is 0.51.

Statistical significance was determined in case of $n=3$ biological triplicates (Student's *t*-test; $p<0.05$). The fractions of apoptotic cells at 24 h after exposure in sham treated control, 1 Gy X-rays, and 1 Gy Ca ions (LET=89 keV/µm) exposed samples in experiment B are all significantly different to each other. Also, the fractions of apoptotic cells at 24 h after exposure to 1 Gy X-rays in enzymatically passaged cultures (B) and in manually passaged cultures (C) are significantly different. All of those four samples are significantly different to each other with $p<0.05$.

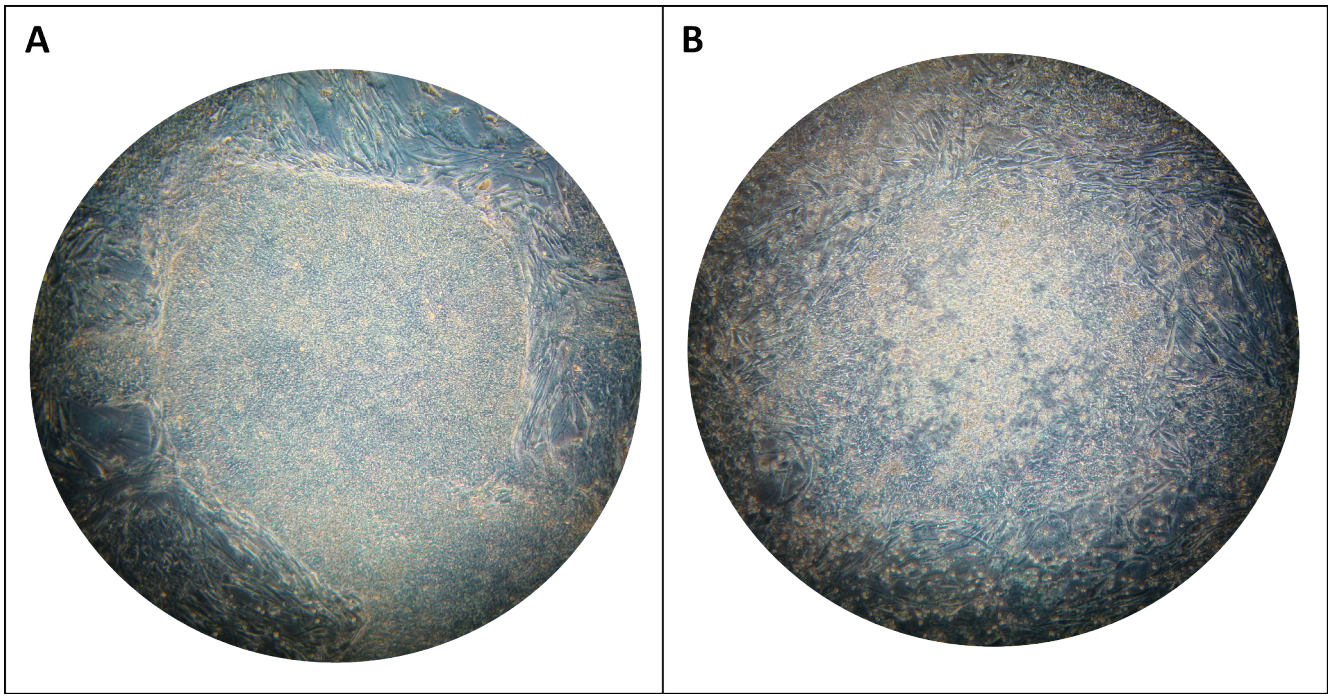

Figure 3.6: hESCs (H9) sham treated (A) and exposed to 1 Gy X-rays (B) at 24 h after exposure. Light-microscopic picture, 50x magnification. Floating cells, presumably apoptotic, appear as shiny spheres.

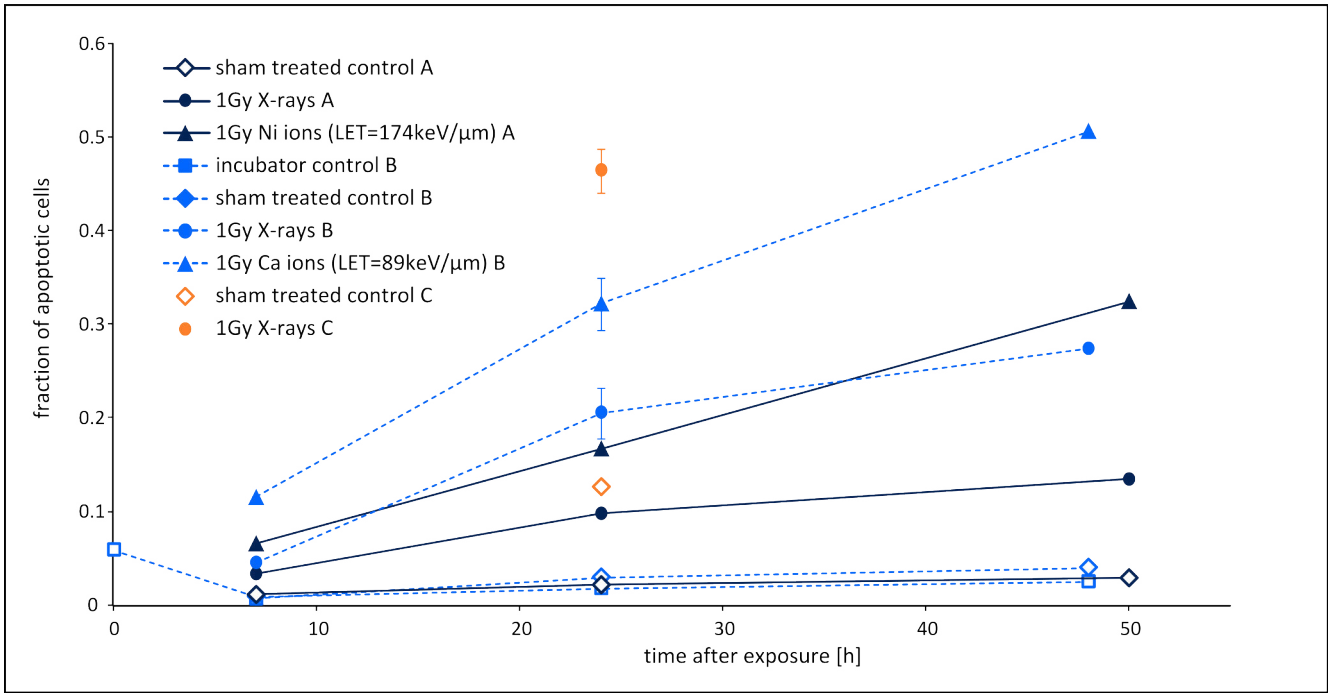

Figure 3.7: Fraction of apoptotic cells up to 50 h after exposure to heavy ion radiation or X-rays. Experiment A and B represent two independent experiments based on enzymatically passaged hESC cultures. Experiment C depicts a manually passaged culture. Error bars for the data points at 24 h of samples 1 Gy X-rays B, 1 Gy X-rays C and 1 Gy Ca ions B represent the standard error of the mean of n=3 biologically independent samples. Error bars of all other data points are calculated according to Poisson statistics. If absent, error bars are too small to be shown.

3.6 Pluripotency and differentiation marker expression in pluripotency maintaining culture conditions

To investigate the pluripotency state of irradiated hESCs (H9) cultured under pluripotency maintaining conditions, cells were stained for the pluripotency-associated surface marker SSEA4 and the differentiation-specific surface marker SSEA1 and quantified via flow cytometry.

The results are shown in figure 3.8. In panel A, the fraction of cells positive for SSEA4 is plotted 7 and 50 h after irradiation. The mean fraction of SSEA4 positive hESCs (H9) in three biologically independent control samples is 0.993 with a standard deviation of 0.008. In all irradiated samples, the fraction of SSEA4 positive cells is higher than 0.99 but within the standard deviation of the control.

Panel B shows the fraction of cells positive for the differentiation marker SSEA1. The fraction of SSEA1 positive cells in control samples is 0.087 ± 0.013 (mean of $n=3$ biological independent samples $\pm$ standard deviation). The exposed samples show a higher fraction of SSEA1 positive cells than the control samples, increasing to a maximum of 0.163. To determine a statistical significance that represents the biological variability, the sample size for exposed cells would have had to be increased, which was not feasible during the current study.

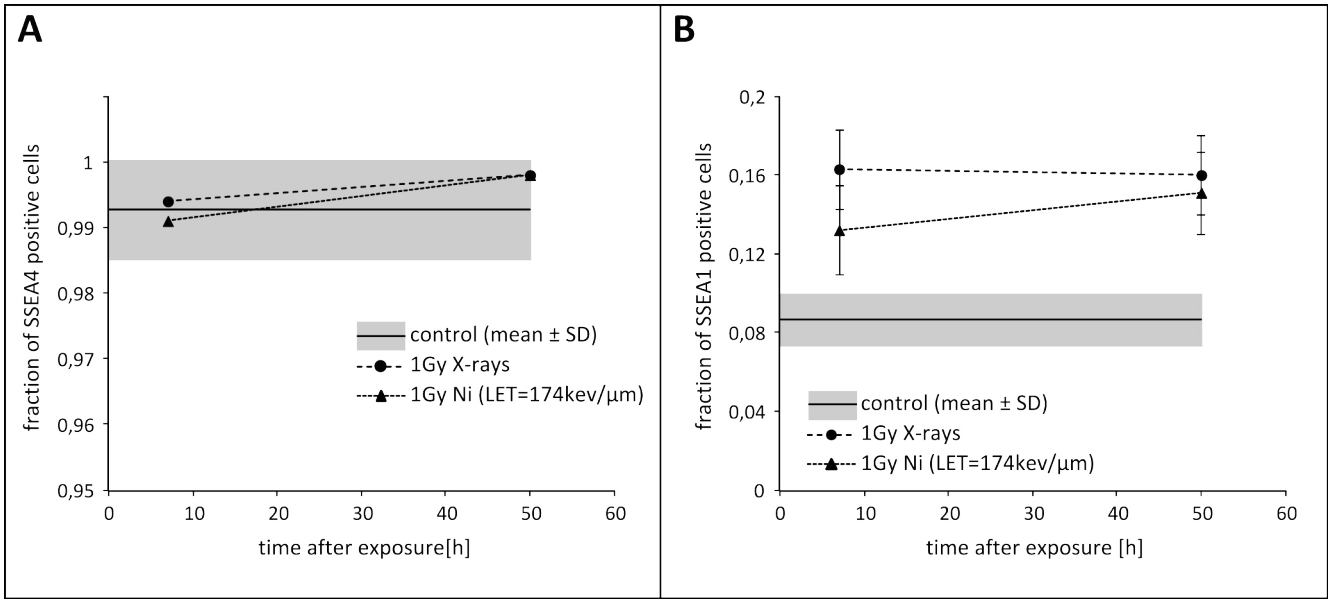

Figure 3.8: Flow cytometric quantification of pluripotency and differentiation markers in enzymatically passaged cultures exposed to 1 Gy X-rays and 1 Gy Ni ions (LET=174 keV/µm). The control represents n=3 biologically independent samples. Data points of 1 Gy X-rays and 1 Gy Ni ions represent n=1 sample with error bars calculated according to Poisson statistics. A: Fraction of cells positive for pluripotency marker SSEA4. B: Fraction of cells positive for differentiation marker SSEA1.

3.7 Chromosomal aberrations

Structural chromosomal aberrations were investigated via mFISH. Examples of karyogramms for an undamaged hESC (H9) and a damaged cell are shown in figure 3.9. Figure 3.10 summarizes the results from enzymatically and manually passaged samples, irradiated or sham treated, at three different time points. The fraction of aberrant cells increases in a radiation quality dependent manner. The lowest fraction of aberrant cells, i.e. 0 aberrant cells was only found in manually passaged samples. These comprise sham treated controls at 4 days and at 14 days as well as 1 Gy X-ray exposed cells at 14 days. The fraction of aberrant cells is highest in samples at 20 h and decreases with time. The categories of chromosomal aberrations reveal a broad spectrum in exposed samples after 20 h. After 14 days, only transmissible translocations are detected, except for a single truncated chromosome in the sample exposed to 1 Gy C ions. In cells 14 days after exposure to 1 Gy C ions, two clones were observed, and each clone was scored as one single event. One clone comprised three cells, characterized by a transmissible, reciprocal translocation involving chromosomes 6 and 7 (also depicted in figure 3.9B). The second clone comprised two cells, harboring a transmissible, reciprocal translocation involving chromosomes 1 and 19. Most non-transmissible aberrations, e.g. dicentrics, only appear in first mitotic cells at 20 h and are not detected in the progeny at later time points. Complex aberrations were only found in enzymatically passaged samples, and there is no significant difference between the frequency of complex aberrations in heavy ion irradiated and X-ray exposed samples. The complexity of all observed complex aberrations as described by the CAB number (number of involved chromosomes (C), number of involved chromosome arms (A), and number of breaks (B)) is as following:

Sample	Number of complex aberrations	C/A/B	transmissible (yes/no)
20 h 1 Gy X-rays (enz.)	3	4/4/4	no
		2/2/3	no
		5/5/5	no
20 h 1 Gy C ions (enz.)	1	3/4/4	no
4 d 1 Gy X-rays (enz.)	2	3/3/3	yes
		3/3/3	yes

The distribution of the number of aberrations per cell is broader in samples exposed to densely IR than it is in samples exposed to X-rays (data not shown). The frequency of a certain chromosome involved in aberrations is highest for chromosome 1 (involved in 11 of 53 scored aberrations in a total of 1421 analyzed metaphases) and lowest for chromosomes 20 and 22 (involved in none of all scored aberrations).

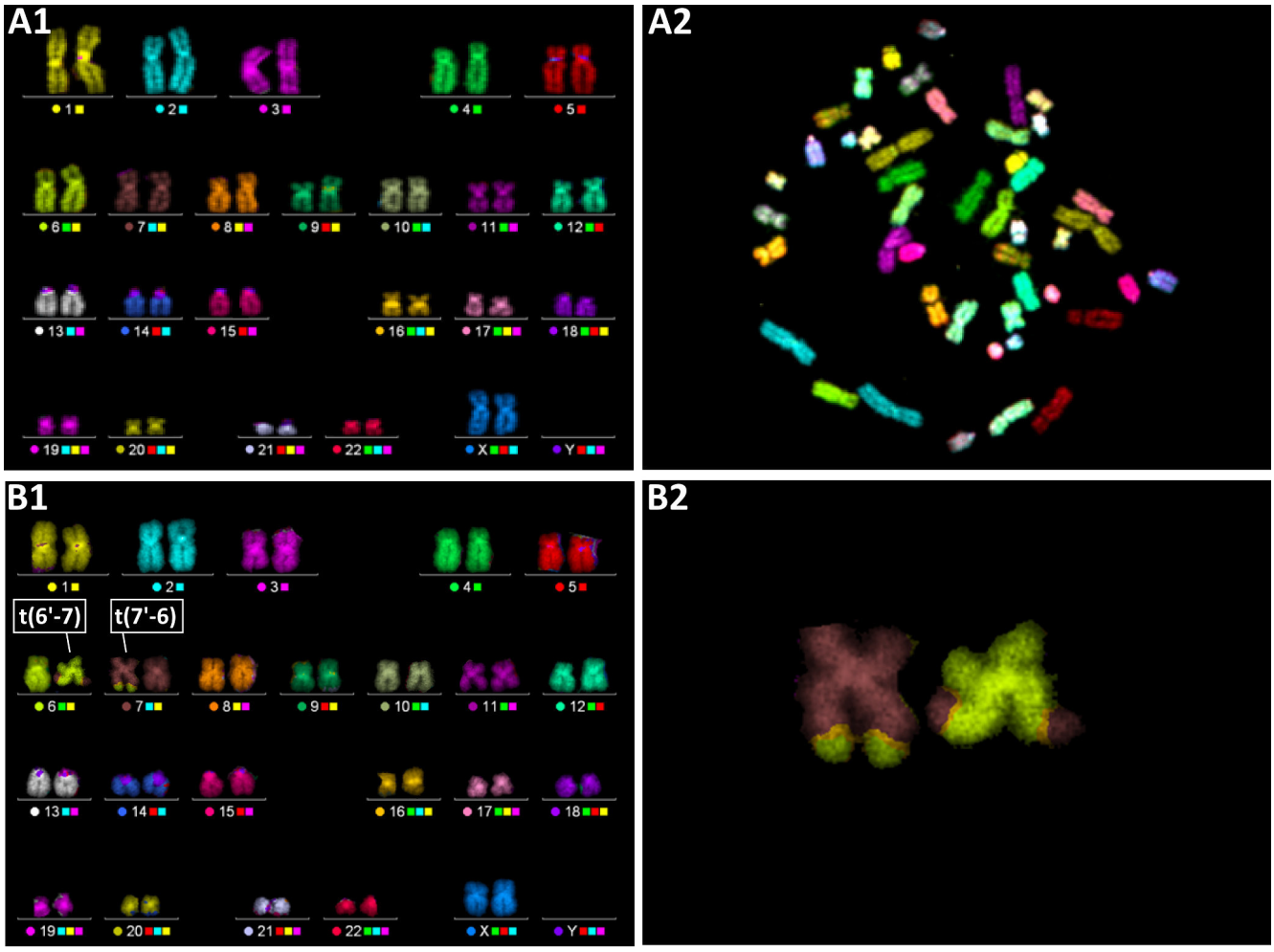

Figure 3.9: Karyotypes examplarily showing hESC (H9) chromosomes after mFISH. A: Karyogram (A1) and corresponding metaphase spread (A2) of a normal cell. B: Karyogram of a damaged cell at 14 days after exposure to 1 Gy X-rays (B1), exhibiting a reciprocal translocation between chromosomes 6 and 7 (indicated as t(6'-t) and t(7'-6)). The chromosomes involved in the reciprocal translocation are magnified in B2.

A

		Sample	Cells scored	Aberrant cells	Fraction of aberrant cells	Breaks	Simple exchanges: Reciprocal Translocations	Simple exchanges: Non-reciprocal Translocations	Simple exchanges: Dicentric chromosomes	Complex
20h	Control	enz.	269	1	0±0.004 †‡	0	0	1	0	0
20h	1Gy X-rays	enz.	105	15	0.14±0.04†	6	4	2	5	3
20h	1Gy Ca ions (LET=89kev/µm)	enz.	40	10	0.25±0.08 ‡	3	3	2	7	1
4d	Control	enz.	170	2	0.01±0.004	2	0	0	0	0
4d	Control	man.	195	0	0	0	0	0	0	0
4d	1Gy X-rays	enz.	115	3	0.03±0.02	0	1	0	0	2
4d	1Gy X-rays	man.	197	2	0.01±0.01	0	2	0	0	0
4d	1Gy Ca ions (LET=89kev/µm)	enz.	87	4	0.05±0.02	0	3	1	0	0
14d	Control	man.	114	0	0 §	0	0	0	0	0
14d	1Gy X-rays	man.	26	0	0	0	0	0	0	0
14d	1Gy C ions (LET=75 kev(µm)	man.	106	6	0.06±0.02§	1	2*	3	0	0

B

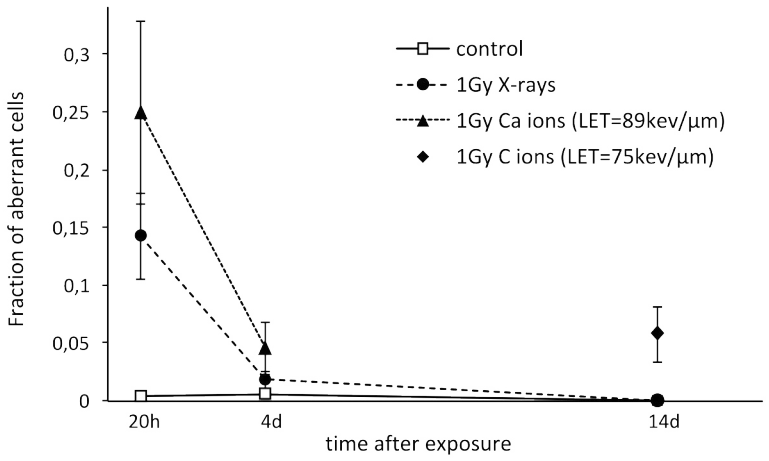

Figure 3.10: Cytogenetic analysis of hESCs (H9). A: Table illustrating the number of radiation induced aberrant cells as well as a breakdown of aberration types observed. Uncertainties of the fraction of aberrant cells were calculated according to Poisson statistics. Statistical significance ($p<0.05$) between two samples was calculated based on Fisher's exact test and is indicated by the same typographical symbol (†, ‡, §). Cells with the same aberrations, i.e. clones, were scored as only one aberrant cell. Clones appeared only in one sample, i.e. in cells 14 days after exposure to 1 Gy C ions, indicated with ∗. B: Diagram showing the fraction of aberrant cells at 20 h, 4 d and 14 d after exposure. Data from manually and enzymatically passaged controls, as well as manually and enzymatically passaged cultures exposed to 1 Gy X-rays were pooled.

3.8 Alterations in embryonic pathway signaling

To investigate alterations in stem cell signaling pathways due to IR, a qRT-PCR array already including primer sets for the detection of 89 different mRNAs was applied. As a first overview, the clustergrams of 21 enzymatically passaged samples as well as the clustergram of ten manually passaged samples are shown in figure 3.11. Expression data are clustered two dimensionally as groups of similar samples and groups of matching markers. For the samples of the enzymatically passaged culture, no radiation-specific expression pattern can be recognized. In contrast, the samples of the manually passaged culture cluster together in a related order, with two groups of genes that show one common gene expression pattern in all six controls and another common gene expression pattern in all four exposed samples. The pattern reveals 61 genes commonly expressed with a high magnitude in control samples, and expressed with a low magnitude in exposed samples. Another group consisting of 20 genes is expressed in a mostly low magnitude in the control samples and expressed in a mostly high magnitude in exposed samples. For a more detailed analysis, dotplots were calculated for those samples belonging to a group of three either biological or technical replicates (see figure 3.12). The significantly up or downregulated markers of the exposed sample group compared to their related sham treated control group are listed in the corners of the dot plots. The exposed samples that represent biological triplicates reveal more downregulated than upregulated genes compared to their related sham treated control. The largest number of significantly downregulated genes compared to control was found in the manually passaged culture 24 h after an exposure to 1 Gy X-rays.

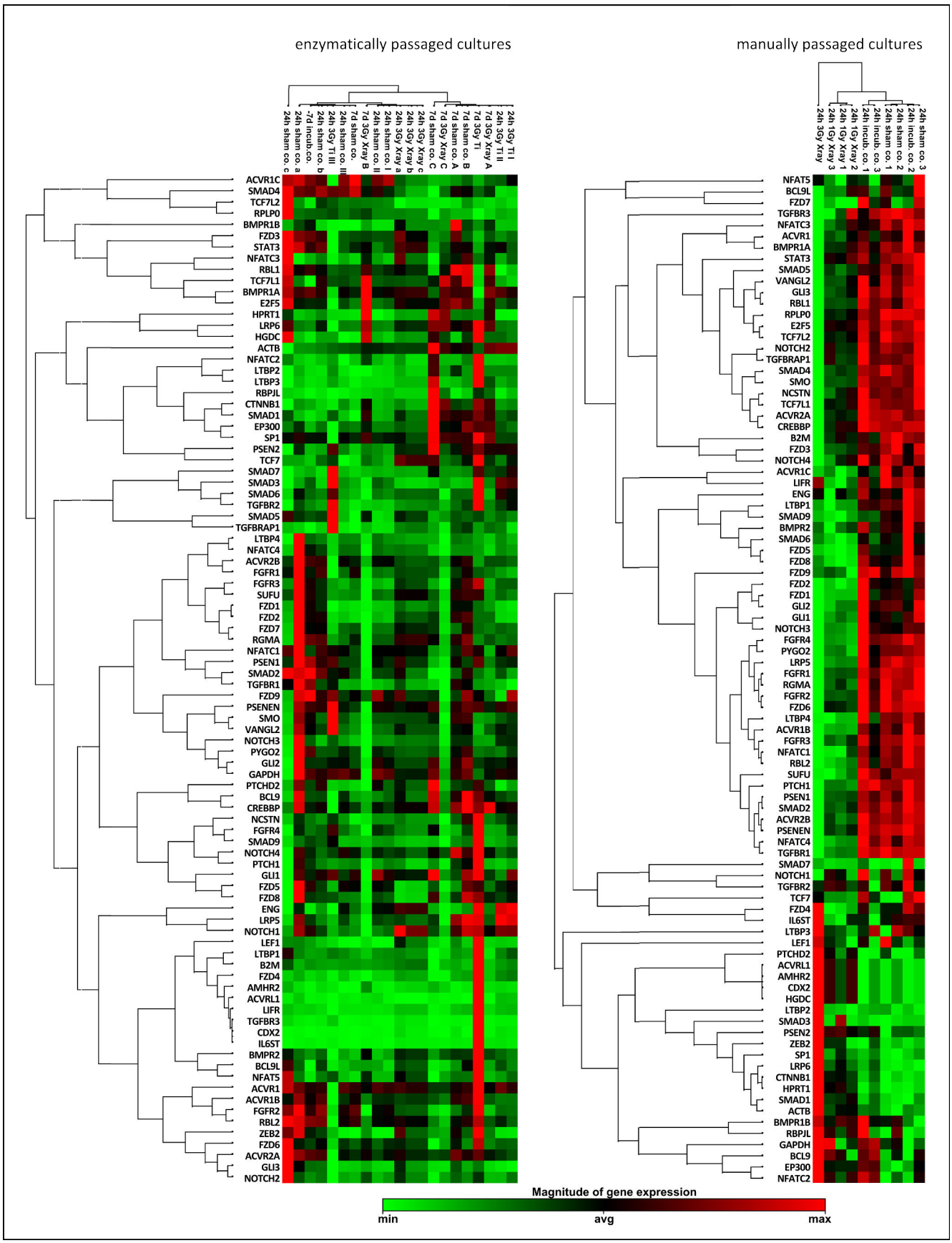

Figure 3.11: Stem cell signaling array: clustergrams. A two dimensional clustering (i.e., relation of the 89 genes and relation of the different samples) is shown for 21 different samples originating from enzymatically passaged cultures on the left, and for 10 samples stemming from manually passaged cultures on the right. The minimum magnitude of gene expression for a certain gene over all samples in one clustergram is indicated in green, while the maximum magnitude of gene expression is indicated in red.

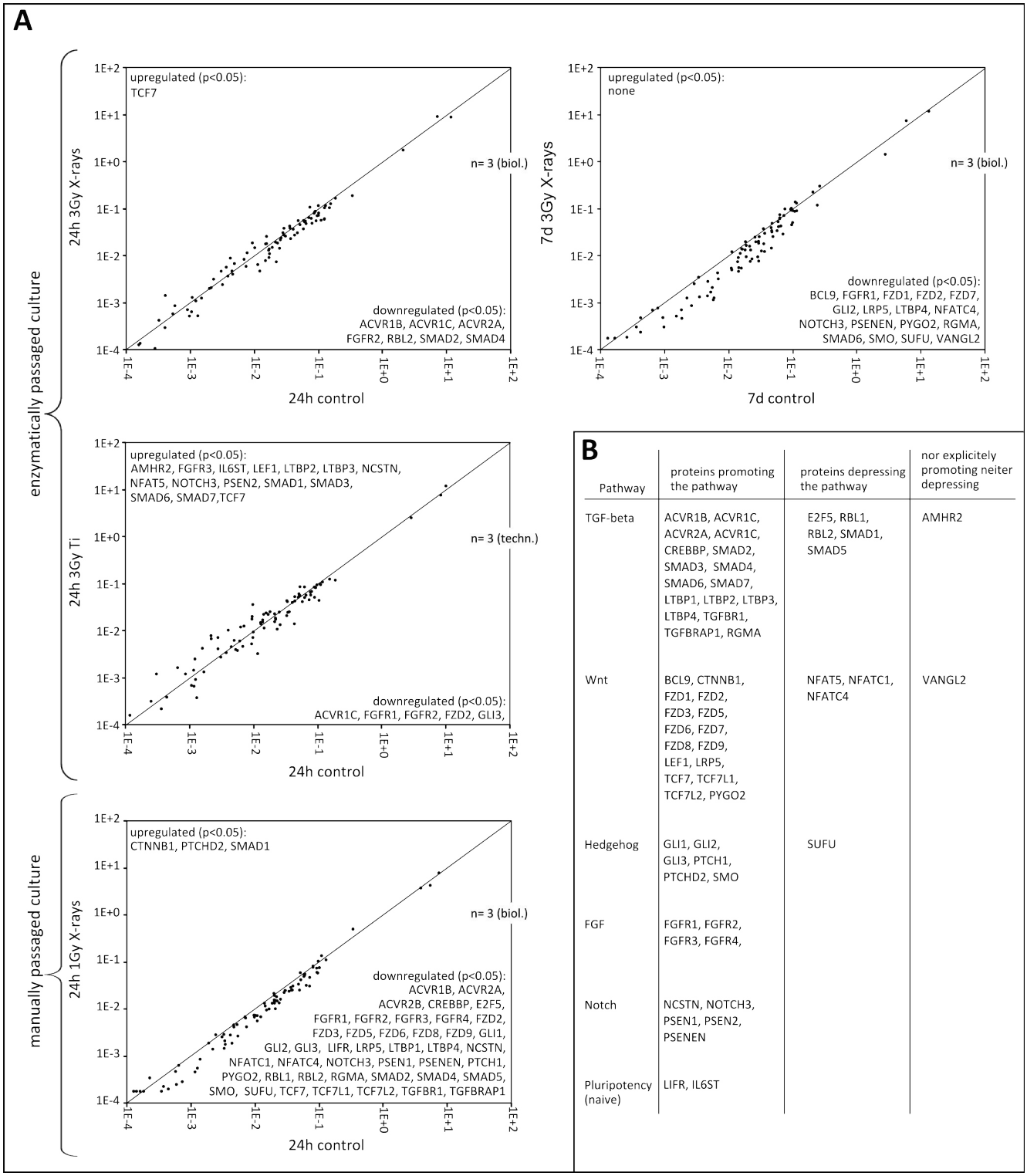

B

Pathway	proteins promoting the pathway	proteins depressing the pathway	nor explicitely promoting neiter depressing
TGF-beta	ACVR1B, ACVR1C, ACVR2A, ACVR1C, CREBBP, SMAD2, SMAD3, SMAD4, SMAD6, SMAD7, LTBP1, LTBP2, LTBP3, LTBP4, TGFBR1, TGFBRAP1, RGMA	E2F5, RBL1, RBL2, SMAD1, SMAD5	AMHR2
Wnt	BCL9, CTNNB1, FZD1, FZD2, FZD3, FZD5, FZD6, FZD7, FZD8, FZD9, LEF1, LRP5, TCF7, TCF7L1, TCF7L2, PYGO2	NFAT5, NFATC1, NFATC4	VANGL2
Hedgehog	GLI1, GLI2, GLI3, PTCH1, PTCHD2, SMO	SUFU	
FGF	FGFR1, FGFR2, FGFR3, FGFR4,		
Notch	NCSTN, NOTCH3, PSEN1, PSEN2, PSENEN		
Pluripotency (naive)	LIFR, IL6ST		

Figure 3.12: Stem cell signaling array: fold change gene expression analyses ($2^{-\Delta\Delta CT}$). Of all 21 enzymatically passaged culture samples and all 10 manually passaged culture samples, only those belonging to a group of three replicates (biological or technical) are displayed. A: Dotplots showing the fold change gene expression of exposed versus sham treated control samples. Upper three dotplots show data from enzymatically passaged cultures exposed to 3 Gy X-rays or 3 Gy Ti ions, harvested after 24 h or 7 d. The lower dotplot shows data from a manually passaged culture exposed to 1 Gy X-rays, harvested after 24 h. Significantly up or downregulated genes according to Student's *t*-test (p<0.05) are listed in the corners of the dotplots. B: Table showing the promoting or depressing effect of all listed significantly up or down regulated genes, arranged in their corresponding pathway groups.

3.9 Differentiation capability into definitive endoderm

The differentiation capability of hESCs (H9) surviving the exposure to IR was investigated by inducing directed differentiation into DE four days after exposure (see section 2.4). The differentiation efficiency was monitored by gene expression studies of the pluripotency markers OCT4A and SOX2 and of the DE marker set $SOX17_{high}$/ $SDF1_{low}$. To date a single marker for DE is not known, and SOX17 alone is also a marker for extraembryonic endoderm. Therefore, this marker is used in combination with SDF1, which is a marker for extraembryonic endoderm but absent in DE.

In figure 3.13, the different morphologies of exposed and unexposed hESCs (H9) before and after differentiation are shown exemplarily. At day -2, hESCs (H9) appear in their typical stem cell morphology: Cells are arranged in very compact colonies with a more loose structure at the growing border. It should be noted that the colonies in the exposed samples appear smaller than those in the unexposed samples, where one microscopic field only fits half of a colony. At the end of the differentiation procedure (day 7), the majority of the cells in the sham treated control show the typical, cobble-stone-like morphology of DE cells. The exposed cells, however, show a more spindle-like morphology.

The gene expression analyses are shown in figure 3.14. The trend for the pluripotency markers is similar for both OCT4A and SOX2 during the whole experiment. Before the induction of differentiation, the exposed cells show a lower mRNA level of OCT4A and SOX2 than the sham treated control cells. With ongoing differentiation starting at day 4, the sham treated control cells show a, even though not significantly, lower mRNA level of OCT4A and SOX2 than that of exposed samples. The endoderm marker SOX17 is not present in both exposed and sham treated hESC (H9) cultured in pluripotency maintaining conditions. At day 1 after the depletion of MEF cells, the mRNA level starts to increase in both samples, reaching its maximum at day 3 and decreasing again until day 7. From day 1 to the end of the experiment, the sham treated cells show a higher mRNA level of SOX17 than exposed cells. The negative marker for DE SDF1 shows lower mRNA levels in exposed cells under pluripotency maintaining conditions, and increases until it reaches its maximum at day 5. In contrast, the mRNA levels for SDF1 in sham treated cells from day 3 on are always lower than that of exposed cells. The mRNA levels of AFP, a marker for primed DE indicating differentiation into the hepatic lineage, are fluctuating without any significant differences or trends.

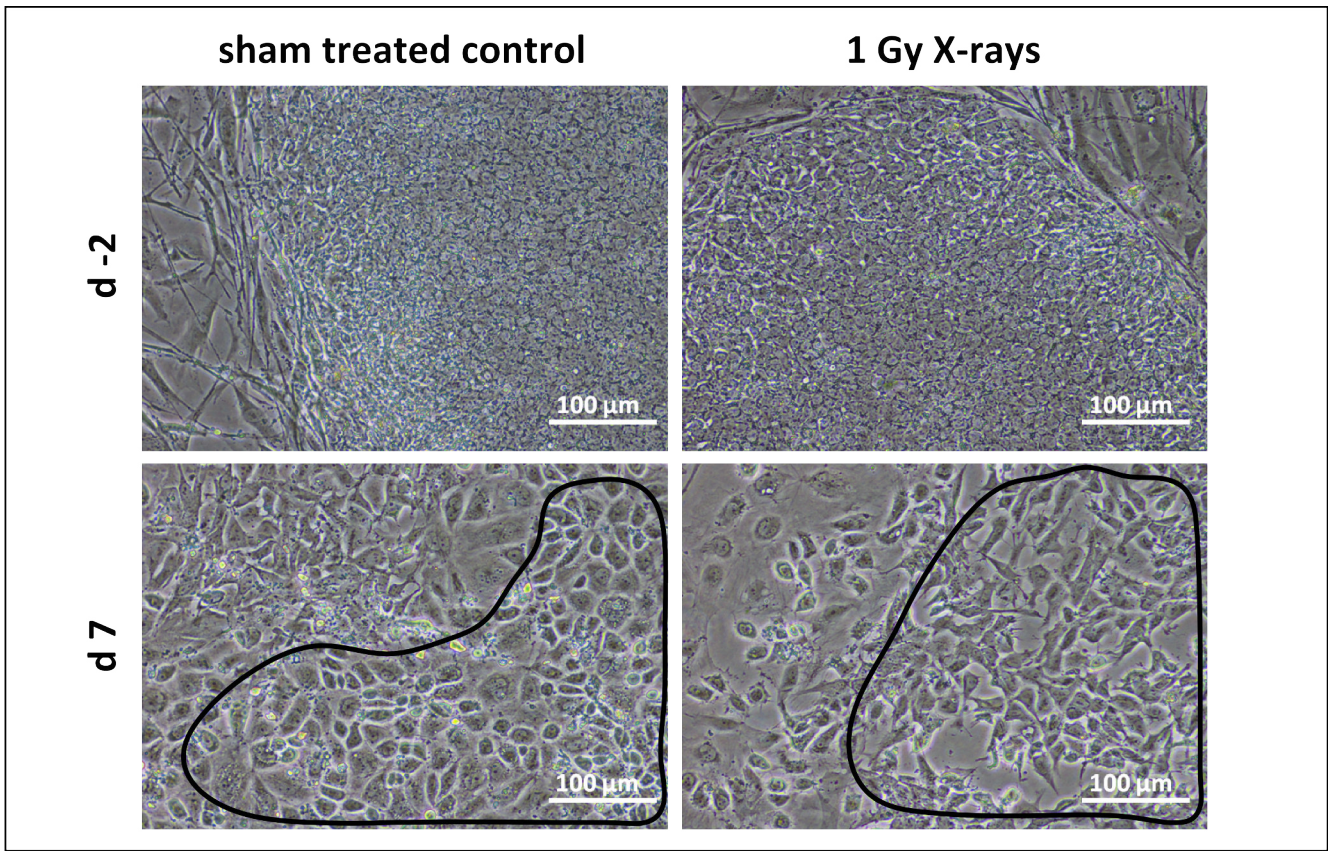

Figure 3.13: Morphology of exposed and sham treated hESCs (H9) before (d-2) and after (d7) directed differentiation into DE. The encircled area in the lower left picture indentifies differentiated cells with cobble-stone-like morphology, while the encircled area in the lower right picture identifies differentiated cells with spindle-like morphology.

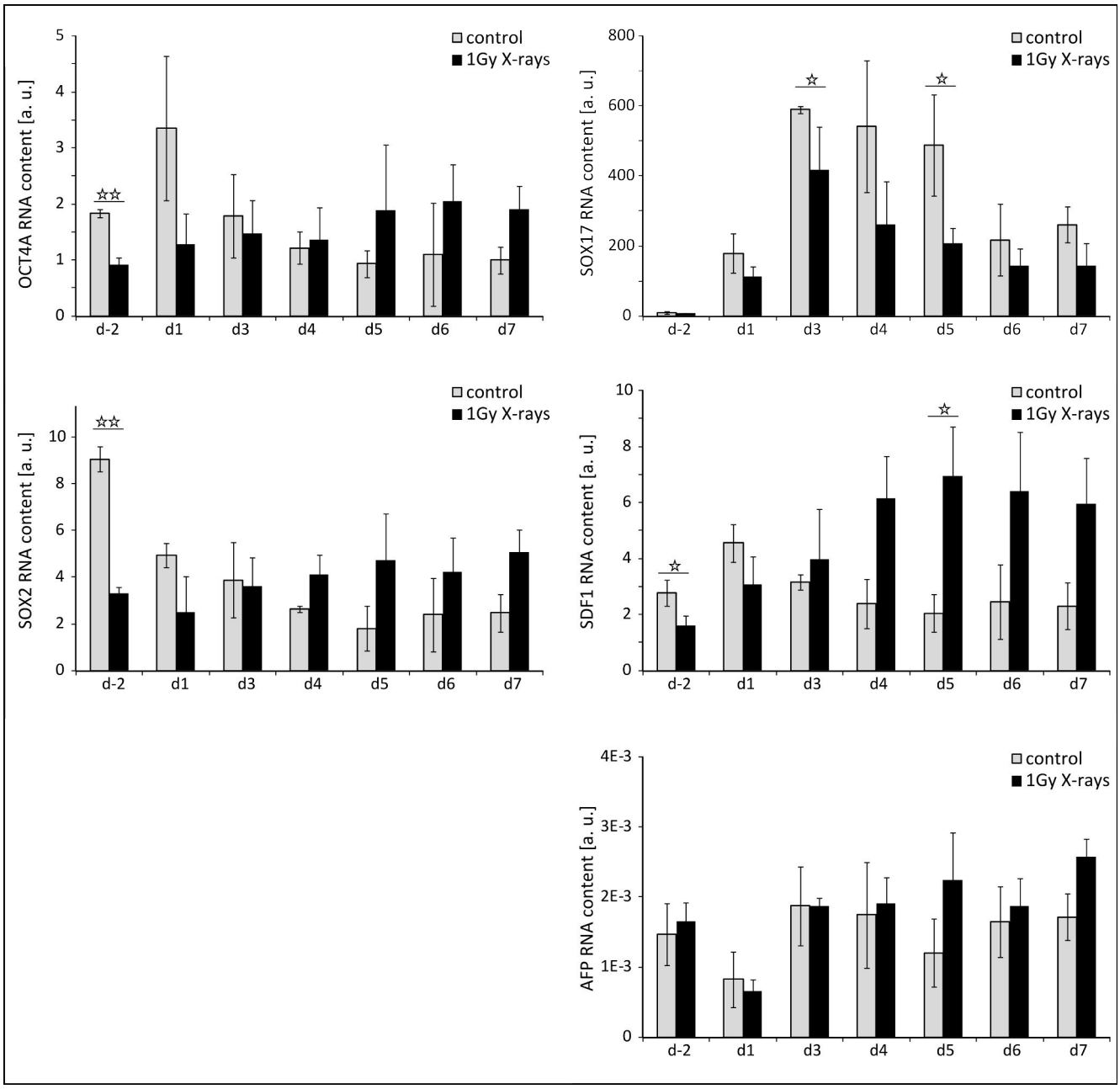

Figure 3.14: mRNA content of pluripotency markers OCT4A and SOX2 on the left side, and of differentiation markers SOX17, SDF1, and AFP on the right side. Error bars represent the standard deviation of n=3 independent biological experiments. Statistical significance according to Student's *t*-test is indicated with ⋆ for $p<0.05$ or ⋆⋆ for $p<0.01$.

4 Discussion

There exists a certain risk for the *in utero* exposure of a developing human embryo. Possible scenarios of exposure to IR comprise accidental, occupational, diagnostic or therapeutic exposures. The likelihood of unintentional exposure to IR is increased in early stages, when the pregnancy is not determined yet. Possible consequences of an *in utero* exposure are pregnancy loss, malformations, mental retardations, low birth weight and childhood cancer [2]. These consequences strongly depend on the absorbed dose, the radiation quality, and on the gestation period. Current risk estimates and recommendations for dose limits rely on animal experiments and epidemiological data [9]. The latest recommendations of the ICRP for example suggest a dose limit of 0.05 Gy for deterministic effects following an *in utero* exposure. *In vitro* studies could help to answer open questions concerning the molecular response of the early human embryo towards IR. hESCs are frequently used as a model system to investigate the very early human development. Isolated from the ICM of about five days old embryos they mimic the blastocyst stage, and they are able to recapitulate early developmental processes [102, 103]. Pluripotent stem cells are furthermore used to test the embryotoxic potential of external agents such as drugs or chemicals [104, 105]. This study investigated the effect of IR on hESCs in order to contribute to a better understanding of the IR-effects on early human embryonic development. Based on the current literature [69, 73, 62] as well as on previous studies with mouse ESCs [97], it is hypothesized that hESCs are capable to efficiently exclude IR induced damage from the population, either via apoptosis or high fidelity DNA repair. Since ESCs give rise to a whole organism, the need for a proper maintenance of an undamaged population is bigger than for differentiated somatic cells. Surviving hESCs should then be able to maintain a pluripotent state and then differentiate appropriately upon any given stimulus.

4.1 A G2 cell cycle arrest and a radiation quality dependent increase of apoptosis mark the early radiation response of hESCs.

IR is known to induce cell cycle alterations as well as cell death [10]. The level of induced apoptotic activity as well as cell cycle kinetics and a possible arrest, however, can differ among cell types. To investigate the effect of IR on cell viability and cell cycle progression, the cell cycle profile as well as apoptosis were measured after exposure.

Characterizing studies of the hESC (H9) cell cycle revealed a cell cycle duration of 16 to 20 h (see section 3.3 and figure 3.4), and a distribution of 36 % of cells in G0/G1, 41 % of cells in S and 19 % of cells in G2/M phase (see section 3.4). The cell cycle duration found in this study is in line with published data, where a cell cycle duration of 16-20 h with variations up to 25 % is reported [60, 61] (see also section 1.5.3). The cell cycle distribution for hESCs (H9) as reported by [60] comprises a smaller fraction of cells in G0/G1 phase (19 %) and a bigger fraction of cells in S phase (66 %) than what was observed in this work, while the fraction of cells in G2/M phase is very similar (16 %). The variance of cells in G1 phase might stem from spontaneous differentiation occurring in the cultures. While most differentiating colonies can be excluded during manual passaging (see figure 2.1 and 3.2), enzymatically passaged cultures might accumulate varying fractions of differentiated cells. In the study performed by

Becker et al. [60], cells were entirely passaged enzymatically, while in this study, parts of the experiments were performed using manually passaged cells. A longer duration of the G1 phase would indicate that cells have been partially differentiated as differentiated somatic cells exhibit a longer G1 phase than true pluripotent ESCs(see also section 1.5.3). Indeed, cells that were passaged manually and therefore are supposed to harbor less spontaneously differentiating cells showed a smaller fraction of cells in G1 phase of only 20 %. Interestingly, the fraction of unexposed cells in G2 phase was elevated 7 h after exposure compared to later time points. This might be due to a slight G2 block, that was induced even in control cells possibly as a consequence of temperature variations during the first medium exchange at 0 h.

Analyzing the cell cycle distribution of irradiated samples revealed an elevated fraction of cells in G2/M phase, indicating a radiation induced arrest in G2 phase. No cell cycle block at any other cell cycle check point was observed. A lack of checkpoints other than the G2 cell cycle checkpoint has already been reported by [78] in response to γ-rays, and was also observed for X-rays and heavy ions in this study. The G2 block was overcome by the majority of surviving cells after 24 h. Sokolov and colleagues [87] performed a similar experiment with hESCs (H9) exposed to 1 Gy of X-rays. The fraction of cells in G2 phase reported in their study, e.g. 29 % before exposure, 47 % at 4 h, decreasing to 36 % at 24 h after exposure, is in good accordance with the experiment of 1 Gy X-ray exposed enzymatically passaged hESCs (see figure 3.5A2) and confirms a duration of approximately 24 h for a 1 Gy X-ray induced G2 block. A dependence of the G2 block on the radiation quality was not observed, even though this is frequently reported in *in vitro* experiments, and has also been observed in previous experiments with mouse ESCs [97]. An additional time point prior to the 7 h one could elucidate a possible radiation-quality dependence for the cell cycle arrest in G2 phase.

Besides an IR induced G2 block, hESCs are known to be very sensitive to DNA damage induced apoptosis due to constitutively available active BAX and a mitochondrial primed state (see section 1.5.3). Section 3.5 describes the results of IR induced apoptosis in hESCs (H9).

The background level of apoptotic cells in enzymatically passaged control samples was five times lower than that of the manually passaged control. Even though one has to be careful with an interpretation of this high difference between enzymatically and manually passaged controls due to the low sampling numbers ($n_{enzymatically}=10$ and $n_{manually}=1$), this result might suggest that the sensitivity for radiation induced apoptosis decreases in enzymatically passaged and therefore more heterogeneous samples. This is another indication for the occurrence of differentiated cells in the enzymatically passaged culture as apoptosis is not their primary response to cell damaging impacts. Further experiments support the idea of the radio sensitivity depending on the passaging method: While enzymatically passaged hESCs were successfully cultivated up to seven days following an exposure to 3 Gy X-rays (see figure 3.12), this was not possible for manually passaged hESCs (data not shown) since most of the cells died in the first 72 h after an exposure to $\geq$2 Gy X-rays.

The experimental results shown in figure 3.7 confirm the high apoptotic rate not only for hESCs exposed to sparsely IR as already reported by [78, 80, 85, 86], but also for heavy ion radiation, which has not been demonstrated before. The facilitated cell death (see section 1.5.3) compared to differentiated somatic cells allows an efficient exclusion of damaged cells from the pluripotent population that will later give rise to a functional organism. Even though massive apoptosis was observed, i.e. >50 % in case of 1 Gy Ca ion exposed hESCs at 48 h (see also figure 3.6 showing an image of massive apoptosis in 1 Gy X-ray exposed cells after 24 h

compared to control), “patchy regions” as reported by others [80, 78] did not occur in any of the samples.

The high sensitivity for IR induced apoptosis together with an IR induced cell cycle arrest might have dramatic consequences for an *in vivo* exposure of the early, blastocyst stage embryo. Since the early embryo follows a temporally and spatially highly regulated developmental process in the peri-implantation period, a disturbance of this process could prevent an implantation of the embryo. This is also reflected in figure 1.1, in which prenatal death as a result of implantation failure as the main outcome for that developmental period after *in utero* exposure to IR is predicted.

4.2 Surviving hESCs efficiently maintain a population with hardly any chromosomal aberrations and only few transmissible translocations.

To investigate the IR sensitivity for chromosomal damage of hESCs, and their ability to maintain an aberration free population, mFISH was performed in first mitotic cells as well as in the progeny after more than 16 divisions.

The cytogenetic analysis of chromosomal aberrations in hESCs (H9) (see section 3.7) revealed an extremely low spontaneous aberration yield, i.e. an average fraction of aberrant cells in all unexposed samples of 0.004±0.002. Data from a previous study in mouse ESCs showed a spontaneous aberration yield with a fraction of aberrant cells of 0.07. According to Stambrook and colleagues, the mutation frequency according to a HPRT mutation assay is 100 fold lower in mESCs compared to MEFs [106]. In this study, the observed spontaneous aberration yield in hESCs is even lower than what was observed in mESCs (0.004 versus 0.7), speaking for a better DNA repair system and/or better DNA damage control in human ESCs compared to mouse ESCs and differentiated cells. The study by the International Stem Cell Initiative reports a significantly higher frequency of aberrant cells in enzymatically passaged cultures compared to manually passaged cultures [61] (see section 1.5.3). However, as the study does not state any passage number, the results are difficult to interpret. In our study, no difference in the fraction of aberrant cells between manually and enzymatically passaged cultures was observed.

After exposure to IR, the fraction of aberrant cells was induced in a radiation quality-dependent manner, rising up to 0.25 in 1 Gy Ca ion exposed cells and 0.14 in 1 Gy X-ray exposed cells at 20 h post exposure. At this early time point, the majority of cells was still in the first mitosis (see also section 3.3). However, it has to be kept in mind that there are three aspects that may lead to an unbalanced underestimation of the yield of aberrant cells within the samples, especially at this early time point 20 h after exposure. First, due to the asynchronous nature of the cell population a subset of cells might not reach mitosis at the time of the first chromosome harvest irrespective of the IR . Second, a large portion of the cells is eliminated via apoptosis in a radiation-quality dependent manner before the 20h time point. Third, depending in the radiation quality, some cells may stay in the abovementioned G2 cell cycle block and not reach first mitosis 20h after exposure. Using premature chromosome condensation (PCC), by which chromosomes can be harvested independent of natural mitosis, these challenges could be overcome [107]. The fraction of aberrant cells decreased with time. Four days after exposure, the majority of the cells has undergone more than four cell divisions. Therefore, henceforward no initially damaged cells but the surviving progeny was observed. At this time point, the fraction of aberrant cells in both densely and sparsely IR exposed samples converged to the level of the control, suggesting an efficient exclusion of aberrant cells from the population, which

possibly might be the result of special repair characteristics (see section 1.5.4) and an elevated apoptotic activity (see section 3.5 and figure 3.7). More than 14 days after exposure, the C ion exposed sample still exhibited a few chromosomal aberrations, that mainly consist of transmissible translocations (two reciprocal translocations and three either true non-reciprocal or small, terminal translocations). However, the frequency of aberrations in this sample was not significantly different to the Ca ion and X-ray exposed samples at 4 days, indicating that no *de novo* aberrations or genetic instability was induced. To confirm this observation and to investigate whether the densely IR induced frequency compared to controls remains elevated or further decreases at more than four days after exposure, additional time points for the same ion species and energy should be added covering an extended period of time. High LET radiation is known to induce a broader distribution of the number of aberrations per cell, and to induce more complex aberrations than sparsely IR [108, 109]. This is due to the fact that ionizing events in case of high LET radiation such as Ca or C ions cluster locally along the particle track, while in case of low LET radiation such as X-rays, ionization events are homogeneously distributed in the target sample (see also section 1.2). In hESCs (H9), a broader distribution of the number of aberrations per cell in case of heavy ion exposed cells was observed at all three time points, 20 h, 4 days and 14 days (data not shown). The number of complex aberrations is not significantly different between heavy ion irradiated and X-ray exposed samples. However, this might just be due to the fact that there were only very few complex aberrations observed in general, e.g. one complex aberration in 40 scored hESCs (H9) at 20 h after exposure to 1 Gy Ca ions. A bigger sample size would be necessary to clearly recognize the fingerprint of high LET radiation in terms of complex aberrations. The complexity of the few complex aberrations decreases in a time-dependent manner. As highly complex aberrations are mostly non-transmissible [108], they are observed only in first mitotic cells. Consequently, only transmissible complex aberrations with lower complexity compared to first mitotic cells are observed in the progeny, while at later time points after more than 16 cell divisions, no complex aberrations were found.

In a previous study with mouse ESCs, it was found that 38 additional aberrant cells per 100 cells scored were induced in first mitotic cells by 2 Gy X-rays, which decreased down to 6 aberrant cells per 100 cells scored above background level after 8 days. In contrast, only 25 aberrant cells per 100 cells scored were induced in first mitotic cells even by high LET radiation (1 Gy Ca ions), that decreased down to 5 aberrant cells per 100 cells scored only after 4 days. This comparison suggests a lower number of radiation induced aberrant cells and a faster decrease of the fraction of aberrant cells in human compared to mouse ESCs. *In vivo* studies corresponding to the ESC stage (pre-implantation embryos) are rather scarce. A study by Weissenborn and Streffer [110, 111] reports on the effect of X-ray irradiation on the chromosomal integrity of a 2-cell mouse embryo. They found a slightly higher frequency of aberrations per first mitotic cells than what was found in hESCs in this study (0.3 aberrations/cell after 0.9 Gy X-rays versus 0.2 aberrations per cell after 1 Gy X-rays in hESCs). Future experiments investigating the relation between IR induced chromosomal aberrations in blastocyst-stage embryos, mouse, and human ESCs (*in vivo* versus *in vitro*) could provide the basis to correctly extrapolate *in vitro* data to *in vivo* exposure scenarios.

Due to the technical challenges, incomplete, broken metaphases were present in all samples impeding the analysis of numerical aberrations. However, trisomies that are known to provide growth advantages in hESC cultures and that are related to cell culture techniques (like trisomy 20, see section 1.5.3) have not been observed in any of the samples, speaking for the good quality of the initial cell population.

4.3 hESCs exposed to IR exhibit alterations in key signaling pathways, leading to a downregulation of pluripotency markers and a less efficient differentiation into definitive endoderm.

To investigate IR induced gene expression alterations in embryonic signaling pathways that influence the potency of hESCs (see section 1.5.2), the mRNA content of 84 genes was analyzed using the Human Stem Cell Signaling PCR Array (see section 2.9). The two clustergrams in figure 3.11 show that in case of enzymatically passaged cultures of hESCs, neither a co-clustering of exposed samples nor of controls occurs. In contrast, manually passaged cultures cluster together depending on exposure conditions, and the number of significantly altered mRNAs is higher than in any other enzymatically passaged sample group (see figure 3.12A). This indicates that the heterogeneity in enzymatically passaged cultures, i.e. a mixture of pluripotent hESCs and spontaneously differentiating cells, leads to a high biological variability in gene expression studies and therefore a certain background noise, that masks significant differences of mRNA content between exposed and unexposed hESCs. Therefore, it is important to adapt the culture conditions of hESCs in a way that provides an initial cell culture with an absolute minimum of spontaneous differentiation that otherwise might disguise important conclusions of any given ESC study.

The following section provides a more detailed discussion of the signaling alterations observed in hESCs exposed to IR, as shown in figure 3.12A. The enzymatically passaged cultures exposed to 3 Gy X-rays and analyzed 24 h later showed eight mostly downregulated genes compared to their sham treated control. Most of these genes are involved in TGFβ signaling and indicate a downregulation of this pathway, that is normally responsible for preserving pluripotency in hESCs (see section 1.5.2). Also, an FGF receptor that is important for the maintenance of pluripotency, was significantly downregulated. Only one of 25 genes (TCF7) tested that are involved in WNT signaling showed a significantly different, i.e. higher amount of mRNA in exposed samples compared to the control. The effect of an active WNT pathway depends on other interacting factors. In the absence of downstream signals of FGF and Activin signaling, whose receptors were downregulated in the exposed samples, WNT signaling promotes differentiation instead of self renewal [49]. Taken together, enzymatically passaged hESCs (H9) analyzed 24 h after exposure to 3 Gy X-rays showed a downregulation of pluripotency maintaining pathways. However, at this time (24 h), the cell population consisted of a mixture of surviving cells, and cells that undergo apoptosis (see section 3.5). Therefore, it was of interest whether the downregulation of pluripotency supporting signaling pathways persists at a later time point, e.g. 7 days, or if this effect would be compensated after excluding damaged cells from the population via apoptosis. Seven days after exposure to 3 Gy X-rays, the surviving cells still exhibited a downregulation of TGFβ signaling, even though it is not the same genes than the ones downregulated 24 h after exposure. Also, the significantly lower mRNA content of another FGF receptor indicates a persistent downregulation of FGF signaling, and a significantly lower mRNA content of six WNT signaling-promoting genes shows a clear downregulation of the WNT pathway. Additionally, Notch signaling and Hedgehog signaling were downregulated, but there is no detailed understanding of the interaction of these two specific pathways in relation to cell potency. Taken together, these results speak for a persisting downregulation of embryonic signaling pathways in hESCs (H9) exposed to sparsely IR, predisposing them to spontaneous differentiation instead of maintaining the pluripotent state.

In enzymatically passaged hESCs exposed to densely IR (3 Gy Ti ions, LET=107 keV/µm), all six signaling pathways represented on the array were partially affected, resulting in both an up- and downregulation of genes. The majority of significantly differentially expressed genes promoted pluripotency. However, it has to be kept in mind, that the statistical significance of differentially regulated genes in the exposed sample compared to its sham treated control in this experiment is based only on technical triplicates instead of the more informative biological triplicates. Therefore, drawing a clear conclusion is difficult due to the many differentially affected pathways and might be misleading due to the unrepresented biological variability.

The largest number of significantly differentially expressed genes was found in manually passaged cultures due to the reduced heterogeneity in the initial cell culture. Since reduced heterogeneity in manually passaged cultures also results in a higher radiosensitivity (see section 4.1), the dose of 3 Gy applied in the previous X-ray experiment with enzymatically passaged hESCs had to be reduced to 1 Gy. The results captured at 24 h after exposure show that all six pathways represented on the array were downregulated. This results in an impaired maintenance of pluripotency, favoring spontaneous differentiation instead. The results of the previous X-ray experiment are confirmed.

Taken together, the investigation of IR induced embryonic signaling alterations reveals a strong and persistent downregulation of embryonic pathways like WNT, TGFβ, FGF, Notch and Hedgehog signaling in hESCs (H9) exposed to X-rays. Consequently, cells are predisposed to spontaneous differentiation at the expense of pluripotency. Assessing the reason for the downregulation of embryonic signaling pathways was not subject of this work. There are only few publications studying DNA damage induced alterations in embryonic signaling in ESCs, and these concentrate mainly on WNT signaling. A study performed by Carreras-Puigvert and colleagues reports about a cisplatin induced, p53 independent, Wnt signaling in mouse ESCs, which has a protective effect increasing the cell viability [112]. In contrast, Lee and colleagues report about an UV induced p53 dependent upregulation WNT ligands [113]. They suggest a model in which DNA damage induces active p53, which leads to differentiation or cell death in order to exclude the damaged cell from the pluripotent population. Simultaneously, p53 leads to an increased WNT secretion that leads to self renewal and maintenance of pluripotency in neighboring, undamaged cells. However, cisplatin is a crosslinks inducing chemotherapy drug, and UV light is mainly inducing thymdin dimers, which are both leading to different DDRs compared to IR. Therefore, future experiments are necessary to elucidate how IR induced DDR in hESCs can lead to a downregulation of embryonic signaling pathways.

Analyses of pluripotency and differentiation markers via flow cytometry and qPCR confirm the hypothesized consequences of the downregulated embryonic signaling pathways after exposure to IR. Figure 3.8 shows an increase of enzymatically passaged hESCs (H9) positive for the differentiation marker SSEA1 up to 50 h after exposure to 1 Gy X-rays and 1 Gy Ni ions (LET=174 keV/µm). The pluripotency marker SSEA4 does not seem to be affected though. However, SSEA4 might simply not be the right marker for investigation of IR affected pluripotency, consisting of a huge interacting network that provides many more markers with different kinetics concerning their radiation dependent expression. Indeed, the qPCR analysis of two core transcription factors in the pluripotency network of manually passaged hESCs (H9) showed a significant downregulation two days after exposure to 1 Gy X-rays: Figure 3.14 depicts a 50 % lower mRNA content of OCT4A and a 36 % lower mRNA content of SOX2 in exposed samples compared to sham treated controls. The downregulation of core pluripotency transcription fac-

tors such as NANOG and OCT4 has been reported in response to UV induced DNA damage in a p53 dependent manner [74]. As p53 is also induced in response to X-ray and ion irradiation induced DNA damage, one can assume a p53 dependent downregulation of the pluripotent circuitry in this study, including OCT4A and SOX2. Despite this crucial effect of IR on the cell potency, morphological changes of hESCs (H9) were not yet observed, except for a smaller colony size in exposed samples (see figure 3.13).

To investigate the functional consequences of the IR effect on cell potency, exposed and sham treated hESCs (H9) were directly differentiated into DE, one of the three germ layers that will give rise to the gastrointestinal tract, liver, pancreas and other associated visceral organs. In the first 24 to 48 h after exposure but before initiating directed differentiation, hESCs (H9) already showed alterations in gene expression that compromise the requirement, i.e. initial pluripotency, for an efficient differentiation into DE. As already discussed, the cells exposed to 1 Gy of X-rays showed a lower level of mRNA for pluripotency markers OCT4A and SOX2 (see figure 3.14), implying a predisposition of the cells for a spontaneous differentiation into their preferred, not necessarily DE, cell lineage. Additionally, they showed a downregulation of the five type I and type II Activin receptors (see clustergram for manually passaged cultures in figure 3.11) 24 h after exposure. The Activin receptors are necessary for a directed differentiation into DE, since a continuous supply of high concentrations of Activin A as a surrogate of NODAL (see also section 1.6 and figure 1.6) ensures that the differentiation of the cells is forced towards the DE lineage. The downregulation of the Activin receptors indicates an impaired differentiation capacity into DE. Indeed, the observation of the DE marker pair $SOX17_{high}$/ $SDF1_{low}$ during the differentiation process until day 7 showed an impaired differentiation efficiency of cells exposed to 1 Gy X-rays compared to their sham treated control. While unexposed cells showed a DE-typical pattern of high SOX17 mRNA content, especially from day 3 to day 5 and low SDF1 mRNA content, irradiated cells showed a lower SOX17 and a higher SDF1 mRNA content. Since the absence of SDF1 mRNA together with high SOx17 content accounts for DE, and the presence of SDF1 mRNA together with SOX17 mRNA accounts for extraembryonic endoderm (see also section refSec Results DE), the expression pattern of this marker pair in exposed cells might indicate a mixture of differentiating cells among which DE and extraembryonic lineages are present. Additionally, the pluripotency markers OCT4A and SOX2 were downregulated in control cells during DE differentiation as expected, but in cells exposed to IR, the downregulation of these core pluripotency markers was less efficient. Due to the irradiation, the cells have might have differentiated prematurely rendering them not responsible to the DE inducing factors. Whether the irradiation changes the differentiation preferences of ESCs has to be further elucidated. The predisposition of hESCs towards a certain cell lineage not only depends on the culture conditions, but also on the cell line itself [114]. Preliminary experiments by I. Schroeder at GSI show an increased fraction of hESCs (H9) that develop into beating cardiomyocytes after exposure to sparsely IR compared to their sham treated control. This would suggests a predisposition of irradiated hESC (H9) for the mesodermal lineage.

So far, previous studies did not detect any IR induced alteration of pluripotency in ESCs. Neither mESCs showed a differential expression of OCT4 and SOX2 17 days after 0.5 to 3 Gy X-rays and C ions [97], nor did hESCs (H9) show significant differences in OCT4, SOX2 or NANOG expression 24 h after 0.4 to 4 Gy of γ-radiation [80] or up to 65 h after 0.2 to 1 Gy γ-radiation [85] (see section 1.5.4). This is the first study that reports a profound alteration of cell potency in hESCs after exposure to X-rays.

4.4 Conclusion and outlook

It was hypothesized that hESCs that serve as a model for early human embryonic development respond to IR by either high fidelity DNA repair or by apoptosis to efficiently exclude damaged cells from the population (see section 1.7). Consequently, surviving cells should be cytogenetically healthy and able to maintain pluripotency in order to give rise to a functional organism. In this study, it was found that hESCs exposed to IR exhibit a radiation quality dependent frequency of initially damaged cells. Consequently, cells arrest in G2 phase of the cell cycle, presumably to repair the radiation induced damage. A fraction of hESCs eventually undergoes facilitated apoptosis (see also section 1.5.3), which enables them to efficiently exclude damaged cells from the population. However, surviving hESCs do harbor cytogenetic aberrations in case of high LET radiation, and show altered gene expression levels, in contrast to the initial hypothesis suggesting that surviving hESCs maintain their initial characteristics. The residual chromosomal aberrations mainly comprise transmissible translocations; IR induced cytogenetic instability was not observed. For the first time, it was shown that hESCs exhibit a loss of pluripotency after exposure to X-rays, which is in contrast to what was reported in literature up to now (see also section 4.3). Interestingly, it was found that a culture system that minimizes the events of spontaneous differentiation in the population, e.g. manually passaging, is crucial to allow the detection of effects on hESCs, that are not hidden by the heterogeneity of a poorly cultured population.

The results reported in this work might indicate several consequences for the early embryo in case of an *in utero* exposure. The radiation induced G2 block together with a high sensitivity for IR induced apoptosis might lead to a disturbance of the spatially and temporally highly regulated developmental process and to a reduction of the cell number in the pre-implantation embryo. Thus, the early embryo might fail to implant, leading to pregnancy loss. This provides a possible explanation for the predictions of *in utero* irradiation illustrated in section 1.7. Furthermore, the IR induced alterations in gene expression do influence the developmental process of the early embryo. Assuming that the effect of IR on gene expression and signaling pathways is a linear-non-threshold effect, and the dose is low enough to not disturb the implantation in the uterus, alterations in signaling pathways leading to further alterations in cell differentiation would still occur. Thus, the pregnancy would continue, but alterations in developmental processes are possible, eventually leading to severe malformations.

Future experiments could help to elucidate underlying mechanisms or the radiation response of hESCs, thereby potentially improving radiationn risk assessment for an *in utero* exposure. For example, the analysis of pluripotency markers and differentiation markers as described in section 3.6 and 3.9 was only performed with X-rays and should be repeated with hESCs exposed to densely IR, like therapy relevant C ions. As the mechanisms underlying the biological response towards sparsely and densely IR might be completely different, it is important to understand if the results observed for X-rays are different for isodoses of C ions. Also, it is of interest to clarify the mechanisms behind the signaling alterations in response to IR, that lead to the impaired potency state of hESCs. Therefore, an additional experiment could be performed, that investigates the upstream targeting contributors of embryonic signaling pathways. For example, a possible connection between upregulated DNA repair pathways or the increase of active p53 and downregulated signaling pathways represents a valuable subject of investigation. Other possible mediators that are responsible for a downregulation of embryonic signaling pathways

in hESCs could be miRNAs, that are known to inhibit the translation of other proteins. Another important experiment in addition to the differentiation capability into DE described in this study (see section 3.9) would be the effect of IR on the differentiation capability into mesodermal and ectodermal lineages. This would complete the differentiation capability studies concerning all three germ layers, and could reveal a possible predisposition of hESCs (H9) in case of spontaneous differentiation. A predisposition for spontaneous differentiation of hESC lines was already described by [114], and preliminary experiments by I. Schroeder at GSI suggest a possible predisposition for hESCs (H9) into the mesodermal lineage. For experiments focusing on special characteristics of hESCs like the facilitated apoptotsis (see section 1.5.3) or the lower mutation frequency (see section 1.5.3) compared to differentiated somatic cells, it would be interesting to additionally measure endpoints like Caspase-3 activity or chromosomal aberrations in parallel to differentiated cells originating from hESCs. A direct comparison of hESCs and an originating differentiated counterpart is important to avoid inter-experimental and inter-laboratory differences in case of a comparison with literature data as performed in this study.

Bibliography

[1] Bundesministerium für Umwelt, Naturschutz, B.u.R. *Umweltradioaktivität und Strahlenbelastung: Unterrichtung durch die Bundesregierung im Jahr 2012*. 2012.

[2] Williams, P.M. and Fletcher, S. *Health effects of prenatal radiation exposure*. Am Fam Physician, 82(5):488–493, 2010.

[3] Brenner, D.J. and Hall, E.J. *Computed tomography–an increasing source of radiation exposure*. N Engl J Med, 357(22):2277–2284, 2007.

[4] McCollough, C.H. et al. *Radiation exposure and pregnancy: When should we be concerned?* Radiographics, 27(4):909–917, 2007.

[5] Münter, M.W. et al. *Heavy ion radiotherapy during pregnancy*. Fertil Steril, 94(6):2329 e5–7, 2010.

[6] *Strahlenschutzverordnung (StrlSchV) of 1976*. as accessed on 02/05/2015 10.00AM, available at http://www.gesetze-im-internet.de/strlschv_2001/index.html.

[7] Jablon, S. and Kato, H. *Childhood cancer in relation to prenatal exposure to atomic-bomb radiation*. Lancet, 2(7681):1000–1003, 1970.

[8] Brent, R.L. et al. *Preconception and Prenatal Radiation Exposure: Health Effects and Protective Guidance*. NCRP Report No. 174, 2013.

[9] Streffer, C. et al. *Biological effects after prenatal irradiation (embryo and fetus). A report of the International Commission on Radiological Protection*. Ann ICRP, 33(1-2):5–206, 2003.

[10] Hall, E. and Giaccia, A. *Radiobiology for the Radiologist*. Lippincott Williams and Wilkins, 2006.

[11] Scholz, M. *Effects of Ion Radiation on Cells and Tissues*, volume 162 of *Advances in Polymer Science*, chapter 4, pp. 95–155. Springer Berlin Heidelberg, 2003.

[12] Pawlik, T.M. and Keyomarsi, K. *Role of cell cycle in mediating sensitivity to radiotherapy*. Int J Radiat Oncol Biol Phys, 59(4):928–942, 2004.

[13] Goodarzi, A.A. and Jeggo, P.A. *The repair and signaling responses to DNA double-strand breaks*. Adv Genet, 82:1–45, 2013.

[14] Cornforth, M.N. *Analyzing radiation-induced complex chromosome rearrangements by combinatorial painting*. Radiat Res, 155(5):643–659, 2001.

[15] Pinto, M.M. et al. *Current status of biodosimetry based on standard cytogenetic methods*. Radiat Environ Biophys, 49(4):567–581, 2010.

[16] Haeckel, E. *Anthropogenie: Entwicklungsgeschichte des Menschen*. Wilhelm Engelmann, Leipzig, 1874.

[17] Haeckel, E. *Natürliche Schöpfungsgeschichte*. Georg Reimer, Berlin, 1888.

[18] Weismann, A. *Essays upon heredity and kindred biological problems*, volume 1. Clarendon Press, Oxford, 1889.

[19] Weismann, A. *The germ-plasm: A theory of heredity*. Charles Scribner's sons, New York, 1893.

[20] *The Nobel Prize in Physiology or Medicine 2007 - Press Release*. Nobel Media AB, as accessed on 02/05/2015 10.00AM, available at http://www.nobelprize.org/nobel_prizes/medicine/laureates/2007.

[21] Evans, M.J. and Kaufman, M.H. *Establishment in culture of pluripotential cells from mouse embryos*. Nature, 292(5819):154–156, 1981.

[22] Martin, G.R. *Isolation of a pluripotent cell line from early mouse embryos cultured in medium conditioned by teratocarcinoma stem cells*. Proc Natl Acad Sci U S A, 78(12):7634–7638, 1981.

[23] Thomson, J.A. et al. *Embryonic stem cell lines derived from human blastocysts*. Science, 282(5391):1145–1147, 1998.

[24] Takahashi, K. et al. *Induction of pluripotent stem cells from adult human fibroblasts by defined factors*. Cell, 131(5):861–872, 2007.

[25] Sullivan, G.J. et al. *Induced pluripotent stem cells: epigenetic memories and practical implications*. Mol Hum Reprod, 16(12):880–885, 2010.

[26] *The Nobel Prize in Physiology or Medicine 2012 - Press Release*. Nobel Media AB, as accessed on 02/05/2015 10.00AM, available at http://www.nobelprize.org/nobel_prizes/medicine/laureates/2012/press.html.

[27] Jaenisch, R. and Young, R. *Stem cells, the molecular circuitry of pluripotency and nuclear reprogramming*. Cell, 132(4):567–582, 2008.

[28] Pera, M.F. and Trounson, A.O. *Human embryonic stem cells: prospects for development*. Development, 131(22):5515–5525, 2004.

[29] Rossant, J. *Stem cells and early lineage development*. Cell, 132(4):527–531, 2008.

[30] Nichols, J. and Smith, A. *Naive and primed pluripotent states*. Cell Stem Cell, 4(6):487–492, 2009.

[31] *Stammzellgesetz (StZG) of 2002*. as accessed on 02/05/2015 10.00AM, available at http://www.gesetze-im-internet.de/stzg/.

[32] *Embryonenschutzgesetz (ESchG) of 1990*. as accessed on 02/05/2015 10.00AM, available at http://www.gesetze-im-internet.de/eschg/.

[33] Schnerch, A. et al. *Distinguishing between mouse and human pluripotent stem cell regulation: the best laid plans of mice and men*. Stem Cells, 28(3):419–430, 2010.

[34] Yeo, J.C. and Ng, H.H. *The transcriptional regulation of pluripotency*. Cell Res, 23(1):20–32, 2013.

[35] Pera, M.F. and Tam, P.P. *Extrinsic regulation of pluripotent stem cells*. Nature, 465(7299):713–720, 2010.

[36] Lanner, F. and Rossant, J. *The role of FGF/Erk signaling in pluripotent cells*. Development, 137(20):3351–3360, 2010.

[37] Kuhl, S.J. and Kuhl, M. *On the role of Wnt/beta-catenin signaling in stem cells*. Biochim Biophys Acta, 1830(2):2297–2306, 2013.

[38] Beyer, T.A. et al. *The TGF beta superfamily in stem cell biology and early mammalian embryonic development*. Biochim Biophys Acta, 1830(2):2268–2279, 2013.

[39] Xiao, L. et al. *Activin A maintains self-renewal and regulates fibroblast growth factor, Wnt, and bone morphogenic protein pathways in human embryonic stem cells*. Stem Cells, 24(6):1476–1486, 2006.

[40] D'Amour, K.A. et al. *Efficient differentiation of human embryonic stem cells to definitive endoderm*. Nat Biotechnol, 23(12):1534–1541, 2005.

[41] Touboul, T. et al. *Generation of functional hepatocytes from human embryonic stem cells under chemically defined conditions that recapitulate liver development*. Hepatology, 51(5):1754–1765, 2010.

[42] Amit, M. et al. *Clonally derived human embryonic stem cell lines maintain pluripotency and proliferative potential for prolonged periods of culture*. Dev Biol, 227(2):271–278, 2000.

[43] Singh, A.M. et al. *Signaling network crosstalk in human pluripotent cells: a Smad2/3-regulated switch that controls the balance between self-renewal and differentiation*. Cell Stem Cell, 10(3):312–326, 2012.

[44] Chen, Y.G. et al. *Where PI3K/Akt meets Smads: The crosstalk determines human embryonic stem cell fate*. Cell Stem Cell, 10(3):231–232, 2012.

[45] Sui, L. et al. *Signaling pathways during maintenance and definitive endoderm differentiation of embryonic stem cells*. Int J Dev Biol, 57(1):1–12, 2013.

[46] Goke, J. et al. *Genome-wide kinase-chromatin interactions reveal the regulatory network of ERK signaling in human embryonic stem cells*. Mol Cell, 50(6):844–855, 2013.

[47] Wang, X. et al. *Inhibition of caspase-mediated anoikis is critical for basic fibroblast growth factor-sustained culture of human pluripotent stem cells*. J Biol Chem, 284(49):34054–34064, 2009.

[48] Saito-Diaz, K. et al. *The way Wnt works: Components and mechanism*. Growth Factors, 31(1):1–31, 2013.

[49] Wray, J. and Hartmann, C. *WNTing embryonic stem cells*. Trends Cell Biol, 22(3):159–168, 2012.

[50] Jerabek, S. et al. *OCT4: Dynamic DNA binding pioneers stem cell pluripotency*. Biochim Biophys Acta, 1839(3):138–154, 2014.

[51] Chambers, I. and Tomlinson, S.R. *The transcriptional foundation of pluripotency*. Development, 136(14):2311–2322, 2009.

[52] Na, J. et al. *Molecular mechanisms of pluripotency and reprogramming*. Stem Cell Res Ther, 1(4):33, 2010.

[53] Wang, X. and Dai, J. *Concise review: Isoforms of OCT4 contribute to the confusing diversity in stem cell biology*. Stem Cells, 28(5):885–893, 2010.

[54] Saunders, A. et al. *Concise review: Pursuing self-renewal and pluripotency with the stem cell factor Nanog*. Stem Cells, 31(7):1227–1236, 2013.

[55] Boyer, L.A. et al. *Core transcriptional regulatory circuitry in human embryonic stem cells*. Cell, 122(6):947–956, 2005.

[56] Takahashi, K. and Yamanaka, S. *Induction of pluripotent stem cells from mouse embryonic and adult fibroblast cultures by defined factors*. Cell, 126(4):663–676, 2006.

[57] Simon, M.C. and Keith, B. *The role of oxygen availability in embryonic development and stem cell function*. Nat Rev Mol Cell Biol, 9(4):285–296, 2008.

[58] Dumollard, R. et al. *Mitochondrial function and redox state in mammalian embryos*. Semin Cell Dev Biol, 20(3):346–353, 2009.

[59] Armstrong, L. et al. *Human induced pluripotent stem cell lines show stress defense mechanisms and mitochondrial regulation similar to those of human embryonic stem cells*. Stem Cells, 28(4):661–673, 2010.

[60] Becker, K.A. et al. *Self-renewal of human embryonic stem cells is supported by a shortened G1 cell cycle phase*. J Cell Physiol, 209(3):883–893, 2006.

[61] Amps, K. et al. *Screening ethnically diverse human embryonic stem cells identifies a chromosome 20 minimal amplicon conferring growth advantage*. Nat Biotechnol, 29(12):1132–1144, 2011.

[62] Nagaria, P. et al. *DNA double-strand break response in stem cells: Mechanisms to maintain genomic integrity*. Biochim Biophys Acta, 1830(2):2345–2353, 2013.

[63] Barta, T. et al. *Cell cycle regulation in human embryonic stem cells: Links to adaptation to cell culture*. Exp Biol Med (Maywood), 238(3):271–275, 2013.

[64] Neganova, I. et al. *Expression and functional analysis of G1 to S regulatory components reveals an important role for CDK2 in cell cycle regulation in human embryonic stem cells*. Oncogene, 28(1):20–30, 2009.

[65] Neganova, I. et al. *An important role for CDK2 in G1 to S checkpoint activation and DNA damage response in human embryonic stem cells*. Stem Cells, 29(4):651–659, 2011.

[66] Pauklin, S. and Vallier, L. *The cell-cycle state of stem cells determines cell fate propensity*. Cell, 155(1):135–147, 2013.

[67] Kapinas, K. et al. *The abbreviated pluripotent cell cycle*. J Cell Physiol, 228(1):9–20, 2013.

[68] Vanneste, E. et al. *Chromosome instability is common in human cleavage-stage embryos*. Nat Med, 15(5):577–583, 2009.

[69] Stambrook, P.J. *An ageing question: Do embryonic stem cells protect their genomes?* Mech Ageing Dev, 128(1):31–35, 2007.

[70] Nguyen, H.T. et al. *Genetic and epigenetic instability in human pluripotent stem cells*. Hum Reprod Update, 19(2):187–205, 2013.

[71] Peterson, S.E. and Loring, J.F. *Genomic instability in pluripotent stem cells: Implications for clinical applications*. J Biol Chem, 289(8):4578–4584, 2014.

[72] Liu, J.C. et al. *Stem cells: Balancing resistance and sensitivity to DNA damage*. Trends Cell Biol, 24(5):268–274, 2014.

[73] Dumitru, R. et al. *Human embryonic stem cells have constitutively active Bax at the Golgi and are primed to undergo rapid apoptosis*. Mol Cell, 46(5):573–583, 2012.

[74] Qin, H. et al. *Regulation of apoptosis and differentiation by p53 in human embryonic stem cells*. J Biol Chem, 282(8):5842–5852, 2007.

[75] Liu, J.C. et al. *High mitochondrial priming sensitizes hESCs to DNA-damage-induced apoptosis*. Cell Stem Cell, 13(4):483–491, 2013.

[76] Valentijn, A.J. et al. *Anoikis*. Biochem Soc Trans, 32(Pt3):421–425, 2004.

[77] Sokolov, M. and Neumann, R. *Lessons learned about human stem cell responses to ionizing radiation exposures: A long road still ahead of us*. Int J Mol Sci, 14(8):15695–15723, 2013.

[78] Momcilovic, O. et al. *Ionizing radiation induces ataxia telangiectasia mutated-dependent checkpoint signaling and G(2) but not G(1) cell cycle arrest in pluripotent human embryonic stem cells*. Stem Cells, 27(8):1822–1835, 2009.

[79] Filion, T.M. et al. *Survival responses of human embryonic stem cells to DNA damage*. J Cell Physiol, 220(3):586–592, 2009.

[80] Wilson, K.D. et al. *Effects of ionizing radiation on self-renewal and pluripotency of human embryonic stem cells*. Cancer Res, 70(13):5539–5548, 2010.

[81] Frosina, G. *The bright and the dark sides of DNA repair in stem cells*. J Biomed Biotechnol, 2010:845396, 2010.

[82] Maynard, S. et al. *Human embryonic stem cells have enhanced repair of multiple forms of DNA damage*. Stem Cells, 26(9):2266–2274, 2008.

[83] Adams, B.R. et al. *Dynamic dependence on ATR and ATM for double-strand break repair in human embryonic stem cells and neural descendants*. PLoS One, 5(4):e10001, 2010.

[84] Bogomazova, A.N. et al. *Error-prone nonhomologous end joining repair operates in human pluripotent stem cells during late G2*. Aging (Albany NY), 3(6):584–596, 2011.

[85] Sokolov, M.V. et al. *Expression of pluripotency-associated genes in the surviving fraction of cultured human embryonic stem cells is not significantly affected by ionizing radiation*. Gene, 455(1-2):8–15, 2010.

[86] Zou, Y. et al. *Responses of human embryonic stem cells and their differentiated progeny to ionizing radiation*. Biochem Biophys Res Commun, 426(1):100–105, 2012.

[87] Sokolov, M.V. et al. *Dynamics of the transcriptome response of cultured human embryonic stem cells to ionizing radiation exposure*. Mutat Res, 709-710:40–48, 2011.

[88] Sokolov, M. and Neumann, R. *Effects of low doses of ionizing radiation exposures on stress-responsive gene expression in human embryonic stem cells*. Int J Mol Sci, 15(1):588–604, 2014.

[89] Sokolov, M.V. and Neumann, R.D. *Radiation-induced bystander effects in cultured human stem cells*. PLoS One, 5(12):e14195, 2010.

[90] Gilbert, S. *Developmental Biology*. Sinauer Associates, Sunderland (MA), 2000.

[91] Grapin-Botton, A. *Endoderm specification*. The Stem Cell Research Community, Cambridge MA, 2008.

[92] Tanaka, C. et al. *Long-range action of Nodal requires interaction with GDF1*. Genes Dev, 21(24):3272–3282, 2007.

[93] Engert, S. et al. *Wnt/beta-catenin signalling regulates Sox17 expression and is essential for organizer and endoderm formation in the mouse*. Development, 140(15):3128–3138, 2013.

[94] Kanai-Azuma, M. et al. *Depletion of definitive gut endoderm in Sox17-null mutant mice*. Development, 129(10):2367–2379, 2002.

[95] McLean, A.B. et al. *Activin a efficiently specifies definitive endoderm from human embryonic stem cells only when phosphatidylinositol 3-kinase signaling is suppressed*. Stem Cells, 25(1):29–38, 2007.

[96] Clift, D. and Schuh, M. *Restarting life: Fertilization and the transition from meiosis to mitosis*. Nat Rev Mol Cell Biol, 14(9):549–562, 2013.

[97] Luft, S. et al. *Fate of D3 mouse embryonic stem cells exposed to X-rays or carbon ions*. Mutat Res Genet Toxicol Environ Mutagen, 760:56–63, 2014.

[98] De Santis, M. et al. *Radiation effects on development*. Birth Defects Res C Embryo Today, 81(3):177–182, 2007.

[99] Haberer, T. et al. *Magnetic scanning system for heavy ion therapy*. Nuclear Instruments and Methods in Physics Research Section A: Accelerators, Spectrometers, Detectors and Associated Equipment, 330(1-2):296–305, 1993.

[100] Speicher, M.R. et al. *Karyotyping human chromosomes by combinatorial multi-fluor FISH*. Nat Genet, 12(4):368–375, 1996.

[101] Savage, J.R. and Simpson, P.J. *FISH "painting" patterns resulting from complex exchanges*. Mutat Res, 312(1):51–60, 1994.

[102] Mummery, C.L. et al. *Differentiation of human embryonic stem cells and induced pluripotent stem cells to cardiomyocytes: A methods overview*. Circ Res, 111(3):344–358, 2012.

[103] Muguruma, K. and Sasai, Y. *In vitro recapitulation of neural development using embryonic stem cells: From neurogenesis to histogenesis*. Dev Growth Differ, 54(3):349–357, 2012.

[104] Seiler, A.E. and Spielmann, H. *The validated embryonic stem cell test to predict embryotoxicity in vitro*. Nat Protoc, 6(7):961–978, 2011.

[105] Hong, E.J. and Jeung, E.B. *Assessment of Developmental Toxicants using Human Embryonic Stem Cells*. Toxicol Res, 29(4):221–227, 2013.

[106] Cervantes, R.B. et al. *Embryonic stem cells and somatic cells differ in mutation frequency and type*. Proc Natl Acad Sci U S A, 99(6):3586–3590, 2002.

[107] Gotoh, E. and Durante, M. *Chromosome condensation outside of mitosis: Mechanisms and new tools*. J Cell Physiol, 209(2):297–304, 2006.

[108] Ritter, S. and Durante, M. *Heavy-ion induced chromosomal aberrations: a review*. Mutat Res, 701(1):38–46, 2010.

[109] Gudowska-Nowak, E. et al. *Effect of LET and track structure on the statistical distribution of chromosome aberrations*. Advances in Space Research, 39(6):1070–1075, 2007.

[110] Weissenborn, U. and Streffer, C. *The one-cell mouse embryo: cell cycle-dependent radiosensitivity and development of chromosomal anomalies in postradiation cell cycles*. Int J Radiat Biol, 54(4):659–674, 1988.

[111] Streffer, C. *Genetic predisposition and genomic instability in preimplantation mouse embryos*. Effects of in utero exposure to ionising radiation during the early phases of pregnancy, pp. 4–16, 2002.

[112] Carreras Puigvert, J. et al. *Systems biology approach identifies the kinase Csnk1a1 as a regulator of the DNA damage response in embryonic stem cells*. Sci Signal, 6(259):ra5, 2013.

[113] Lee, K.H. et al. *A genomewide study identifies the Wnt signaling pathway as a major target of p53 in murine embryonic stem cells*. Proc Natl Acad Sci U S A, 107(1):69–74, 2010.

[114] Osafune, K. et al. *Marked differences in differentiation propensity among human embryonic stem cell lines*. Nat Biotechnol, 26(3):313–315, 2008.

Appendix

Table 4.1: Cell culture material

Type (and composition if applicable)	Manufacturer
DMEM liquid medium with stable glutamine	Biochrom
DMEM/F-12, no glutamine, no HEPES	Thermo Fisher Scientific
RPMI 1640	Thermo Fisher Scientific
KnockOut™DMEM	Thermo Fisher Scientific
KnockOut™Serum Replacement	Thermo Fisher Scientific
Non-essential amino acids (NEA)	Biochrom
L-alanyl-L-glutamine	Biochrom
1 M HEPES buffer (50x)	Biochrom
Recombinant Human FGF-basic (in 5 mM Tris, 0.01 % BSA, pH 7.6)	Peprotech
Fetal Bovine Serum (FBS or FCS)	Merck Milipore
Trypsin 0,05 %/EDTA 0,1 % in PBS without Ca^{2+} and Mg^{2+}	PAN-Biotech
PBS solution without Ca^{2+}, Mg^{2+} ($PBS^{-/-}$)	Merck Milipore
PBS-solution with Ca^{2+}, Mg^{2+} ($PBS^{+/+}$)	Merck Milipore
Gelatine (0.1 % in $PBS^{-/-}$)	neoLab
Matrigel growth factor reduced	BD
Dispase	BD
Recombinant Human Activin A	Peprotech
Recombinant Mouse Wnt-3a	Peprotech
DMSO	Roth
β-Mercaptoethanol	Roth
Tris ultrapure	Applichem
BSA	Sigma
Penicillin/Streptomycin	Biochrom

Table 4.2: H9-medium for enzymatic passaging

H9-medium for enzymatic passaging
DMEM/F12 + 25 % Knockout Serum Replacement + 1.875 % HEPES + 1.25 % L-Glutamin + 1.25 % Non essential amino acids + β-mercaptoethanol 100 µM final concentration + 0.5 % Penicilllin/Streptomycin

Table 4.3: H9-medium for manual passaging

H9-medium for manual passaging
Knockout DMEM + 25.7 % Knockout Serum Replacement + 0.64 % L-Glutamin + 1.29 % Non essential amino acids + β-mercaptoethanol 100 μM final concentration + 0.64 % Penicilllin/Streptomycin

Table 4.4: MEF-medium

MEF medium
DMEM FG0445 + 10 % FCS F + 1 % Penicilllin/Streptomycin

Table 4.5: Freezing-medium

Freezing-medium
90 % FCS F + 10 % DMSO

Table 4.6: DE-medium

DE-medium
RPMI + 50 % KO DMEM + 1.53 % L-Glu + 100 ng/ml ActA + 0.76 % Penicilllin/Streptomycin

Table 4.7: Chemicals and RNA

Type	Composition (optional)	Manufacturer
EDTA		Roth
Ethanol		ROTH
Formaldehyde solution 37 %		Merck
Triton-X-100		Merck
Vectashield		Vector Laboratories
Colcemid		Roche
KCl (0.075 M in H2O)		Merck
Methanol		Roth
Acetic Acid		Merck
Immersion oil		Zeiss Sybr green
RNAse and DNAse free water		Qiagen
DAPI		Roth
Hoechst 33342		Sigma-Aldrich
5x HOT FIREPol® EvaGreen® qPCR Mix Plus (ROX)		Solis Biodyne
human fetal liver whole tissue RNA		Clontech

Table 4.8: Primer for individual mRNA expression analysis

Gene	Oligo	Sequence	Manufacturer
POU5F1	sense	5'-ACC CAC ACT GCA GCA GAT CA-3'	biomers.net
POU5F1	antisense	5'-CAC ACT CGG ACC ACA TCC TTC T-3'	biomers.net
SOX2	sense	5'-CAC TGC CCC TCT CAC ACA TG-3'	biomers.net
SOX2	antisense	5'-CCC ATT TCC CTC GTT TTT CTT-3'	biomers.net
SOX17	sense	5'-CCA GAG GCT TTT TGG ATG TTT T-3'	biomers.net
SOX17	antisense	5'-AGG TAA ACT GAA TGT CGA GGA GTG T-3'	biomers.net
SDF1	sense	5'-CGT CAA GCA TCT CAA AAT TCT CA-3'	biomers.net
SDF1	antisense	5'-CAG CCG GGC TAC AAT CTG A-3'	biomers.net
AFP	sense	5'-CTG CAA ACT GAC CAC GCT-3'	biomers.net
AFP	antisense	5'-TGA GAC AGC AAG CTG AGG AT-3'	biomers.net

Table 4.9: List of primer sets in the stem cell signaling qPCR array

Pluripotency maintenance pathway
Receptors: IL6ST (GP130), LIF
Transcription Factor: STAT3

FGF signaling pathway
Receptors: FGFR1, FGFR2, FGFR3, FGFR4
Transcription Factor: CDX2

Hedgehog signaling pathway
Receptors and co-receptors: PTCH1, PTCHD2, SMO
Transcription factors and co-factors: GLI1, GLI2, GLI3, SUFU

Notch signaling pathway
Receptors and co-receptors: NCSTN, NOTCH1, NOTCH2, NOTCH3, NOTCH4, PSENEN, PSEN1, PSEN2
Transcription factor: RBPJL

TGF β superfamiliy signaling pathway
Receptors and co-receptors: ACVRL1, ACVR1, ACVR1B, ACVR1C, ACVR2A, ACVR2B, AMHR2, BMPR1A, BMPR1B, BMPR2, ENG, LTBP1, LTBP2, LTBP3, LTBP4, RGMA, TGFBR1, TGFBR2, TGFBR3, TGFBRAP1
Transcription factors and co-factors: EP300, SMAD1, SMAD2, SMAD3, SMAD4, SMAD5, SMAD6, SMAD7, SMAD9, CREBBP, E2F5, RBL1, RBL2, SP1, ZEB2

Wnt signaling pathway
Receptors: FZD1, FZD2, FZD3, FZD4, FZD5, FZD6, FZD7, FZD8, FZD9, LRP5, LRP6, VANGL2
Transcription factors and co-factors: BCL9, BCL9L, CTNNB1, LEF1, NFAT5, NFATC1, NFATC2, NFATC3, NFATC4, PYGO2, TCF7L1, TCF7L2, TCF7

Housekeeping Genes
ACTB, B2M, GAPDH, HPRT1, RPLP0

Table 4.10: Kits

Type	Manufacturer
MasterPure™RNA Purification Kit	epicentre
RT^2 First Strand Kit (12)	Qiagen
Human Stem Cell Signaling PCR Array PAHS047Z	Qiagen
RevertAid RT Kit	Thermo Fisher Scientific
Click-it EdU Alexa 488 Flow Cytometry Kit	Invitrogen
FITC Active Caspase-3 Apoptosis Kit	BD
BD Stemflow Human and Mouse Pluripotent Stem Cell Analysis Kit	BD
24xCyte Human Multicolor FISH Probe Kit	Metasystems
RNase-Free DNase Set (50)	Qiagen

Table 4.11: Devices

Type	Manufacturer
Flowcytometer FACSCanto II	BD
Microscope Axio Imager Z1	Zeiss
Thermocycler Primus 96 advanced	Peqlab
StepOnePlus™Real-Time PCR System	ABI
Cell Counter Casy™1	Schärfe System
Cell Counter TC20™automated	BIORAD
Colibri microvolume spectrophotometer	Titertek Berthold
X-ray tube Isovolt DS1	Seifert
Dosimeter SN4	PTW
Stereo microscope SMZ-171	Motic
Inverted Light Microscope Eclipse TS100	Nikon
Inverted Light Microscope DM IL	Leica

Table 4.12: Software

Type	Manufacturer
Metafer4 V3.8.9	Metasystems
Isis V5.5.5	Metasystems
FLOWJO V7.6.5 and V10	FLOWJO, LLC
FACSDiva V7.0	BD
Primer Express V3.0	Thermo Fisher Scientific
StepOne™Software V2.3	ABI

Ehrenwörtliche Erklärung

Ich erkläre hiermit ehrenwörtlich, dass ich die vorliegende Arbeit entsprechend den Regeln guter wissenschaftlicher Praxis selbstständig und ohne unzulässige Hilfe Dritter angefertigt habe.

Sämtliche aus fremden Quellen direkt oder indirekt übernommenen Gedanken sowie sämtliche von Anderen direkt oder indirekt übernommenen Daten, Techniken und Materialien sind als solche kenntlich gemacht. Die Arbeit wurde bisher bei keiner anderen Hochschule zu Prüfungszwecken eingereicht.

Weiterstadt, den

_____

(Sabine Luft)

Curriculum Vitae

Personal Data

Contact	Sabine Luft Taunusstraße 7 64331 Weiterstadt Germany
Date of birth	10/21/1984 in Darmstadt

Education

10/2011 - present	PhD student at GSI Helmholtzcentre for Heavy Ion Research, Department of Biophysics enrolled at the Technical University of Darmstadt
09/2006-07/2011	Diploma, Biology, at GSI Helmholtzcentre for Heavy Ion Research, Department of Biophysics enrolled at the Technical University of Darmstadt
09/2004-07/2006	Commercial training in insurance sales
06/2004	Abitur, Justus-Liebig-Schule in Darmstadt

Publications

Peer reviewed

03/2014	The effect of X-rays and C-ions on pluripotent embryonic stem cells; Luft S., Pignalosa D., Arrizabalaga O., Nasonova E., Helm A., Durante M., Ritter S.; in Journal of Radiation Research 55(Suppl 1):i55, 2014; doi: 10.1093/jrr/rrt175
01/2014	Fate of D3 mouse embryonic stem cells exposed to X-rays or carbon ions; Luft S., Pignalosa D., Nasonova E., Arrizabalaga O., Helm A., Durante M., Ritter S.; in Mutation Research - Genetic Toxicology and Environmental Mutagenesis 760:56, 2014; doi: 10.1016/j.mrgentox.2013.12.004

Scientific reports

10/2014	Preparatory experiments to investigate the radiosessitivity of human embryonic stem cells; Luft S., Schroeder I., Hessel P., Arrizabalaga O., Layer P. G., Durante M., Ritter S.; GSI Scientific Report 2013
05/2013	Influence of ionizing radiation on the potency state of murine embryonic stem cells; Luft S., Helm A., Hessel P., Pignalosa D., Brons S., Layer P.G., Durante M., Ritter S.; GSI Scientific Report 2012
05/2012	Radiation response of pluripotent stem cells derived from early mouse embryos; Luft S., Helm A., Pignalosa D., Hessel P., Durante M., Layer P.G., Ritter S.; GSI Scientific Report 2011

Contributions to international conferences

09/2013 Poster	Radiation effects on early embryonic development: Emphasis on gene expression; Gesellschaft fuer Biologische Strahlenforschung, Jahrestagung 2013 in Darmstadt, Germany
05/2013 Oral presentation	The effect of X-rays and C-ions on pluripotent embryonic stem cells; Heavy Ions in Therapy and Space Radiation Symposium 2013 in Chiba, Japan
04/2013 Poster	Early and late effects of densely ionizing radiation on mouse embryonic stem cells; 7th International Meeting des Kompetenznetzwerk Stammzellforschung NRW 2013 in Koeln, Germany
10/2012 Oral presentation	Impact of X-ray and C-ion exposure on mouse embryonic stem cells; 10th International Symposium on Chromosomal Aberrations 2012 in Amalfi, Italy

Danksagung

Für die Unterstützung während meiner Doktorarbeit möchte ich mich recht herzlich bedanken, besonders bei folgenden Personen.

Prof. Dr. Marco Durante danke ich für die Aufnahme als Doktorandin in seiner Abteilung, sowie für seine Unterstützung und sein Interesse an meiner Arbeit. Danke für die vielen wertvollen Ratschläge.

Prof. Dr. Paul G. Layer vom Fachbereich Biologie danke ich für die Übernahme des Koreferats, sowie für die stets sehr hilfreichen Besprechungen von Versuchsplanungen und Datanenalysen.

Dr. Sylvia Ritter danke ich herzlich für die Aufnahme in der Gruppe der Chromosomen- und Stammzellfreunde und für Ihre Unterstützung und Ihr Vertrauen in meine Arbeit.

Prof. Dr. Suzanne Kadereit danke ich für die freundliche Anleitung und das Teilhaben lassen an Ihrer Expertise während der ersten Schritte in der Stammzellkultivierung, sowie für wertvolle Diskussionen von Experimenten und Ergebnissen.

Dr. Diana Pignalosa und Dr. Insa Schröder danke ich herzlich für die hervorragende Betreuung und Unterstützung. Ich habe viel von ihnen gelernt.

Petra Hessel, Dr. Elena Nasonova, Dr. Onetsine Arrizabalaga und Dr. Nerea Paz danke ich für die starke Unterstützung und Expertise beim Durchführen von Experimenten und Chromosomenanalysen.

Dr. Alexander Helm danke ich für seine Offenheit und Freundschaft, und seine wertvollen Ratschläge.

Dr. Thomas Friedrich danke ich für die Unterstützung (inklusive dem Entgegenehmen und Weiterreichen von wichtigen Telefonanrufen) bei Strahlzeiten, sowie für das Teilen seiner Expertise beispielsweise bei der Berechnung von Fluenzen, Apoptosedaten und Fehlerberechnungen.

Ireen Kuhlish, Giorgia Ciliberti und Simon Frank danke ich für den tollen Einsatz während der Durchführung sowie Vor- und Nachbereitung von Strahlzeiten.

Anna, Andreas, Till, Maren, Zhan, Walter, Uli, Anke, Bernadette und Francesco danke ich für ihre Hilfe bei Fachfragen und ihre Freundschaft.

Paul Görgen und Stefan Schulz danke ich herzlich für ihren Einsatz beim Retten meiner LaTeX-Dateien.

Ich möchte mich bei allen Mitgliedern der Abteilung Biophysik für die freundliche Aufnahme und Unterstützung bedanken.

Bei HGS-HiRE und FIAS bedanke ich mich für die finanzielle Unterstützung. Diese Arbeit wurde im Rahmen des Verbundprojektes mit dem Förderkennzeichen 02NUK025 durch das Bundesministerium für Bildung und Forschung gefördert.